MEASUREMENT AND ASSESSMENT OF TRANSIENT TORQUES IN A THREE-PHASE SQUIRREL CAGE INDUCTION MOTOR

L. NIGRINI

MEASUREMENT AND ASSESSMENT OF TRANSIENT TORQUES IN A THREE-PHASE SQUIRREL CAGE INDUCTION MOTOR

Lucas Nigrini

Dissertation submitted in compliance with the requirements for the Master's Diploma in Technology in the Faculty of Engineering at the Technikon O.F.S

Bloemfontein, 1993

Supervisor : Prof. C.F. Landy
Co-supervisor : Mr. G.D. Jordaan

ACKNOWLEDGMENTS

I wish to express my special gratitude to the following people:

Prof. J.P. Reynders for giving me the opportunity to be exposed to a research environment.

Prof. C.F. Landy whose never ending dedication to his subject was a real motivating force.

The Power Engineering Workshop Team: Harry, Eddy and Trevor, in no specific order, for their assistance.

Mr. G.D. Jordaan for his continued support and unconditional friendship.

The Foundation for Research and Development for the grant received.

Finally, I wish to express my appreciation to my wife, Nicolette, and my two sons, Walter and Dirk, for their patience and encouragement.

SYNOPSIS

The objectives of this research were to:

- obtain significant correlation between measured and simulated results of the transient starting- and reswitching torque and speed characteristics of a 75 kW three-phase squirrel cage induction motor with **deep rotor bars**;

- compare similar measurements on an identical machine with a broken rotor bar with measurements taken from the machine with the "healthy" rotor to investigate the possibility that a broken rotor bar may be detected without dismantling the motor.

Computer models are available which simulate the transient torque characteristics of induction motors during starting and reswitching. These models make use of the fixed parameter model where the rotor time constant does not vary as the frequency of the induced rotor voltage changes. A simulation package (**CASED**) has been developed at the UNIVERSITY OF THE WITWATERSRAND which takes the deep rotor bars of a motor into account when simulating transient conditions.

Simulated results of both the fixed parameter model and the deep bar model are shown for comparison. It is mentioned that the accuracy of the simulation depends on the exactness of the data obtained for the induction motor parameters from the design sheet and measurements.

The transient torque- and speed characteristics were obtained by using a measurement system which is suitable for measuring both slow and fast changes in rotational speed. The system was reasonably noisy and digital filtering was used to improve analysis.

Comparison of the measured and simulated starting and reswitching (positive and negative) transient torque signals are shown. The difference in the magnitudes between the measured and simulated results of the starting and reswitching transients is less than 3%. This difference is negligible for all practical purposes. Simulating the start-up, positive- and negative reswitching transients of the induction motor shows that the deep bar model in the CASED software package gives a very close correlation with the measured values.

The measurements on the induction motor with the broken bar show that the transient behaviour of this motor is related to the condition of the cage. It is beyond the scope of this project to investigate this more fully but the author is convinced that this is an area for future meaningful research. It is anticipated that if these differences can be quantified, this type of transient measurement may become a successful tool to be used in assessing the state of the cage of a large squirrel cage induction motor.

UITTREKSEL

Die doel van hierdie navorsing was:

- om sinvolle korrelasie tussen die gemete en gesimuleerde resultate van die oorgangs- en heraanskakel draaimoment en spoed karakteristieke van 'n 75 kW drie-fase kou-rotor induksiemotor met **diep rotorgeleiers** te verkry;

- om soortgelyke metings op 'n identiese motor met 'n gebreekte rotorgeleier te neem en dit te vergelyk met die metings geneem op die diensbare motor. 'n Beduidende verskil tussen die twee stelle gemete resultate sou dui op die moontlike diagnosering van 'n gebreekte rotorgeleier in 'n motor - sonder om die motor uitmekaar te haal.

Rekenaarsagteware is beskikbaar om die aanskakel en heraanskakel oorgangs draaimomente van 'n induksie motor te simuleer. Hierdie sagteware maak gebruik van die tradisionele model waar die rotor tydkonstante onveranderd bly gedurende 'n oorgangstydperk. 'n Sagtewarepakket (**CASED**), is egter ook by die UNIVERSITEIT VAN DIE WITWATERSRAND ontwikkel en neem die veranderende rotor tydkonstante (die diep rotorgeleier effek) in ag gedurende 'n oorgangstydperk.

Gesimuleerde resultate van beide die tradisionele model en die diep rotorgeleier model is vergelyk. Daar is gevind dat die geldigheid van die simulasie afhanklik is van die akkuraatheid van die motorparameters verkry vanaf die ontwerpers en tydens die uitvoer van metings.

Die oorgangskoppels en snelhede is verkry deur gebruik te maak van 'n meetstelsel wat pasgemaak is om klein veranderings teen beide lae en hoë rotasiesnelhede waar te neem. Die elektroniese geraas in die stelsel is veminder deur van 'n digitale filter gebruik te maak.

Gemete en gesimuleerde resultate van aanskakel en heraanskakel draaimomente (positief en negatief) is vergelyk en die amplitudes van die seine korreleer met meer as 97%. Hierdie korrelasie is aanvaarbaar vir alle praktiese doeleindes en bewys die geldigheid van die diep rotorgeleier model in die CASED sagteware pakket vir motors van hierdie grootte.

Metings op die induksiemotor met die gebreekte rotorgeleier toon aan dat daar 'n verband is tussen die oorgangskarakteristieke van hierdie motor en die kondisie van die rotorgeleiers. Hierdie verband sal deur verdere intensiewe navorsing geverifieer moet word. Positiewe resultate sal aandui dat hierdie 'n effektiewe metode kan word om die toestand van die rotor van 'n groot induksie motors te bepaal sonder om die motor uitmekaar the haal.

Central University of Technology, Free State

CONTENTS

LIST OF SYMBOLS

F	magneto-motive force
T	torque
β	angle between stator and rotor axis
θ	angle between stator and rotor axis
M	mutual inductance (H)
i	current (A)
[i]	vector of two-axes currents
[*G*]	rotational inductance matrix
N	number of turns
R	resistance (Ω)
[*R*]	resistance matrix
V	voltage (V)
[V]	vector of two-axes voltages
t	time (seconds)
λ	flux linkage
L	self inductance (H)
[*L*]	inductance matrix
ρ	time rate of change
c	constant
k	constant
ω	rotational speed
J	rotational moment of inertia
D	damping constant
P	number of pole pairs

Subscripts

s	stator
r	rotor
e	electromagnetic
a, b, c	three phase stator and rotor winding subscripts
D	stator direct axis
Q	stator quadrature axis
O	stator zero axis
d	rotor direct axis
q	rotor quadrature axis
o	rotor zero axis
x, y	axes to which three phase *a, b, c* system is actively transformed to
L	load

Superscripts

T	matrix transposition
'	rotor value referred to the stator

LIST OF FIGURES

CHAPTER 2

CHAPTER 3

CHAPTER 4

CHAPTER 5

Central University of Technology, Free State

LIST OF TABLES

CHAPTER 5

CHAPTER 1

INTRODUCTION

Computer simulation models have been developed to predict the magnitude of transient torques when starting and reswitching induction motors (De Sarkar & Berg, 1970:1031, Ghani, 1988:106 and Krause & Thomas, 1965:1038). In these models the starting or running parameters are used so that the squirrel cage induction motor has been represented by its single cage model and the effects of deep rotor bars have not been considered.

During transient conditions, in an induction machine with deep bars, the deep bar effect can significantly influence the rotor time constant of the machine, which is an important parameter during reswitching operations.

A model was developed by McCulloch, Landy, Levy & MacLeod that accommodates the change in rotor resistance and leakage inductance as the rotor speed changes and it takes into account the effect of saturating the stator and rotor leakage reactances.

During the implementation of the research project the motor dynamic equations have been simulated using the CASED (**C**omputer **A**nalysis and **S**imulation of **E**lectric **D**rives) software package developed by McCulloch **et al** for the simulation of the dynamic performance of motors with the addition of variable speed drive systems. It allows one to predict behavior with or without the improved bar models. The equations are formulated in the direct - quadrature axis form.

Similar models have been developed (Klingshirn & Jordan, 1970 : 1038,

Lipo & Consoli, 1984 : 180, Smith, 1990 : 48 and Slemon, 1992 : 412) but more experimental measurements where required to validate the models.

This would mean developing and using methods to measure the transient characteristics of the motor. Therefore, the measuring system forms a vital part of this work.

Successful measurements were achieved of starting and restarting transients on a 75 kW induction motor. The very acceptable correlation obtained between measured and predicted results, using the deep bar model, was very encouraging and without any doubt shows the advantage of using these improved models when predicting performance.

This research project has met its objectives by showing how important it is to use the improved model. It is shown in chapter 3 that if the fixed parameter model is used the correlation between measured and predicted results is very poor.

When starting a loaded induction motor direct on line, its rotor windings are subjected to mechanical and thermal stresses due the sudden inrush of current. The performance of the rotor windings, under these conditions, is affected if the motor has loose or broken rotor bars. Techniques have been developed to detect rotor winding malfunctions i.e. broken rotor bars (Tavner & Penman, 1987:259).

During completion of the project there was an opportunity to assess whether a broken bar in the cage of the motor affects the transient behaviour. If a deviation in the transient behaviour of the motor indicates the presence of broken rotor bar(s), the torque measurement system can be economically

used as a diagnostic tool to detect broken rotor bars. For this reason, measurements on an identical machine having a broken cage where taken.

These results are also shown in this thesis and it is interesting to note that it was found that the position of the broken bar affected the transient torque developed by the motor during run-up. Although no reason for this is offered in this work, the author believes that this finding can form the basis for further intensive research.

In the project the background information on the equations used for the simulation of the dynamic performance of a squirrel cage induction machine and the CASED computer simulation package are discussed. A method used to measure the torque-speed curve of the motors is also described. The simulated and measured results of the transient starting- and reswitching torque on the healthy motor are discussed. The reswitching transient torques on the healthy motor and the motor with the broken rotor bar are compared. Finally, the measured results of the starting torque on the motor with the broken rotor bar are shown and evaluated.

BACKGROUND THEORY:

Deriving the two-axes differential equations of an induction motor.

2.1 Torque in a uniform air gap machine.

When three phase voltages are applied to the stator windings, balanced three phase currents flow in the phase windings. These currents set up a sinusoidally distributed Magneto-Motive Force field $\mathbf{F_1}$ in the air gap, travelling at a speed proportional to the frequency of the supply and number of machine poles (synchronous speed). If the rotor speed is different from the speed of this rotating MMF, balanced three phase currents will be induced in the short circuited windings of the rotor. A second sinusoidally distributed rotating MMF field $\mathbf{F_2}$, with its magnetic poles on the surface of the rotor, is produced by the induced rotor currents. Both MMF fields rotate at synchronous speed and are separated by an angle β_{sr}, stationary with respect to each other as shown in Figure 2.1-1.

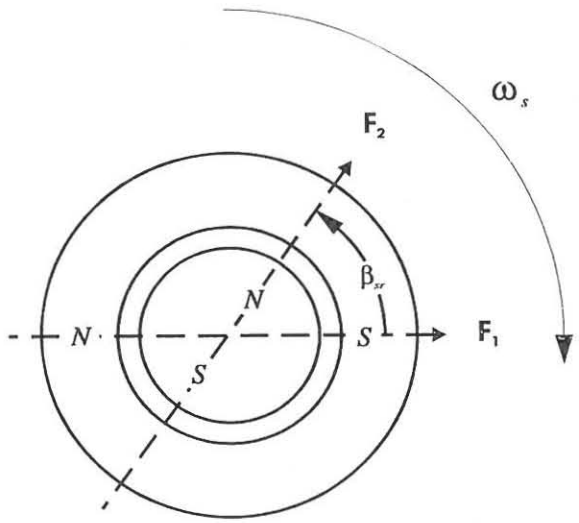

Figure 2.1-1 : Torque produced in an elementary, rotating, smooth air gap machine.

Power is transferred from the stator to the rotor by these interacting magnetic fields developed in the air gap.

The torque in the air gap T_e is proportional to the product of the instantaneous rotor and stator currents and the mutual inductance linking them.

$$T_e \propto M_{sr} i_s i_r \sin\beta_{sr} \qquad (2.1)$$

where β_{sr} is the angle between $\mathbf{F_1}$ and $\mathbf{F_2}$ in electrical degrees. For a constant load on the rotor shaft (steady state conditions) the instantaneous values of the currents in the stator - and rotor - phase windings vary sinusoidally, and the angle β_{sr} stays constant.

During transient conditions the above mentioned currents do not vary sinusoidally. The rotor oscillates relative to the rotating stator field so that the flux linking the stator and the rotor changes with time. Additional " transient " currents are induced in each of the stator and rotor windings and the angle β_{sr} changes continuously as the rotor accelerates and decelerates. The transient torque, developed in the air gap of the machine, is determined by the instantaneous value of each of these currents. The response of these currents is the solution of the induction motor voltage equations.

2.2 Induction motor voltage equations

In Figure 2.2-1 equal stator winding turns ($N_{sa} = N_{sb} = N_{sc} = N_s$), and equal rotor winding turns ($N_{ra} = N_{rb} = N_{rc} = N_r$) are assumed. The physical configuration of the machine is balanced. The stator- and rotor resistances are equal: $R_{sa} = R_{sb} = R_{sc} = R_s$ and $R_{ra} = R_{rb} = R_{rc} = R_r$. Stator and rotor voltages, currents and the air gap flux are assumed to vary sinusoidally in time and space.

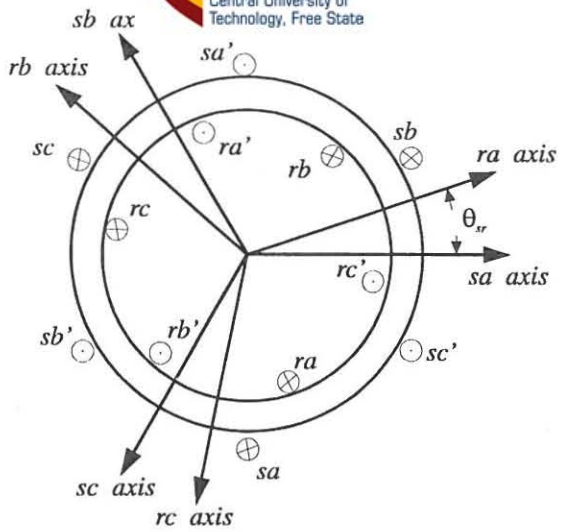

Figure 2.2-1 : Three - phase, 2-pole, star - connected, slipring induction motor.

Instantaneous values of the stator and rotor currents can be obtained by simultaneously solving the three - phase stator and rotor voltage equations which can be expressed as:

$$V_{sa} = R_s i_{sa} + \frac{d\lambda_{sa}}{dt}$$

$$V_{sb} = R_s i_{sb} + \frac{d\lambda_{sb}}{dt} \qquad (2.2)$$

$$V_{sc} = R_s i_{sc} + \frac{d\lambda_{sc}}{dt}$$

in a stationary reference frame and

$$V_{ra} = R_r i_{ra} + \frac{d\lambda_{ra}}{dt}$$

$$V_{rb} = R_r i_{rb} + \frac{d\lambda_{rb}}{dt} \qquad (2.3)$$

$$V_{rc} = R_r i_{rc} + \frac{d\lambda_{rc}}{dt}$$

in a reference frame fixed to the rotor.

Since each stator and rotor phase winding has its own resistance, self - inductance and mutual inductance, the flux linkage terms in each of these equations are expanded to express the mutual magnetic coupling of the relevant phase winding with each of the other two stator windings and the three rotor windings e.g.

$$\lambda_{sa} = L_{sasa} i_{sa} + M_{sasb} i_{sb} + M_{sasc} i_{sc} + M_{sard} i_{ra} + M_{sarb} i_{rb} + M_{sarc} i_{rc} \qquad (2.4)$$

where

λ_{sa} = flux cutting the stator a-phase winding due to currents flowing in the three stator- and rotor phase windings.

L_{sasa} = inductance due to the flux produced by the stator a-phase winding linking with the stator a-phase winding i.e. self inductance.

M_{sasb} = inductance due to the flux produced by the stator a-phase winding linking with the stator b-phase winding i.e. mutual inductance.

M_{sasc} = inductance due to the flux produced by the stator a-phase winding linking with the stator c-phase winding i.e. mutual inductance.

M_{sara} = inductance due to the flux produced by the stator a-phase winding linking with the rotor a-phase winding i.e. mutual inductance.

M_{sarb} = inductance due to the flux produced by the stator a-phase winding linking with the rotor b-phase winding i.e. mutual inductance.

M_{sarc} = inductance due to the flux produced by the stator a-phase winding linking with the rotor c-phase winding i.e. mutual inductance.

Since the air gap is constant and the machine is assumed to be symmetrical, the stator self inductances are equal

$L_{sasa} = L_{sbsb} = L_{scsc}$ and can be expressed as L_s.

Similarly the rotor self inductances are equal

$L_{rara} = L_{rbrb} = L_{rcrc}$ and can be given as L_r where

L_{rara} = inductance due to the flux produced by the rotor a-phase winding linking with the rotor a-phase winding i.e. self inductance.

The mutual inductance between any two stator windings are equal

$M_{sasb} = M_{sasc} = M_{scsb}$ and can be written as M_s where

M_{sasb} = inductance due to the flux produced by the stator a-phase winding linking with the stator b-phase winding i.e. mutual inductance.

Similarly, the mutual inductances between any two rotor windings are equal

$M_{rarb} = M_{rarc} = M_{rbrc}$ and becomes M_r where

M_{rarb} = inductance due to the flux produced by the rotor a-phase winding linking with the rotor b-phase winding i.e. mutual inductance.

The mutual inductances between the following stator and rotor windings M_{sara}, M_{sbrb} and M_{scrc} are equal and may be written as $M_{sr}\cos\theta_{sr}$ where θ_{sr} is the angle shown in Figure 2.2-1.

Also, $M_{sarb} = M_{scrb} = M_{scra}$ are equal and can be expressed as $M_{sr}\cos(\theta_{sr} + 120°)$.

In conclusion $M_{sarc} = M_{sbra} = M_{scrb}$ and may be written as $M_{sr}\cos(\theta_{sr} + 240°)$.

If $\theta_{sr} = \theta$, $\theta_{sr} + 120° = \theta_1$, $\theta_{sr} + 240° = \theta_2$ and $\rho = \frac{d}{dt}$, the stator and rotor voltage equations can be combined as:

$$\begin{bmatrix} V_{sa} \\ V_{sb} \\ V_{sc} \\ V_{ra} \\ V_{rb} \\ V_{rc} \end{bmatrix} = \begin{bmatrix} R_s + \rho L_s & \rho M_s & \rho M_s & \rho M_{sr}\cos\theta & \rho M_{sr}\cos\theta_1 & \rho M_{sr}\cos\theta_2 \\ \vdots & \vdots & \vdots & \vdots & \vdots & \vdots \\ \vdots & \vdots & \vdots & \vdots & \vdots & \vdots \\ \vdots & \vdots & \vdots & \vdots & \vdots & \vdots \\ \vdots & \vdots & \vdots & \vdots & \vdots & \vdots \\ \rho M_{sr}\cos\theta_2 & \rho M_{sr}\cos\theta_1 & \rho M_{sr}\cos\theta & \rho M_r & \rho M_r & R_r + \rho L_r \end{bmatrix} \begin{bmatrix} i_{sa} \\ i_{sb} \\ i_{sc} \\ i_{ra} \\ i_{rb} \\ i_{rc} \end{bmatrix}$$

(2.5)

In the impedance matrix, $\rho = \frac{d}{dt}$ operates on the inductances during transient conditions when the angle θ_{sr} varies with time as the rotor accelerates and decelerates.

These time dependent inductances can be eliminated by transforming the three phase stator - and rotor variables (the voltages, currents and flux linkages) to their two phase equivalents (Levy, 1990 : 95), by assuming that :

1. The current produced in any stator or rotor circuit sets up a sinusoidally distributed flux pattern in the air gap.

2. The effects of saturation, eddy currents and hysteresis are neglected.

2.3 Transforming the three - phase induction motor voltage equations to a two - phase reference frame, rotating at an arbitrary speed

Utilizing the fact that the supply system is a balanced 3 - wire system and the neutral point on the rotor and stator is isolated, the zero - sequence voltage and current components can be set to zero. This facilitates the original group of 6 voltage equations to be transformed into an equivalent group of 4 voltage equations.

For example, the stator phase voltages V_{sa}, V_{sb} and V_{sc} are replaced by a set of three transformed quantities, the direct - axis component V_D , the quadrature - axis component V_Q and a zero - sequence component $V_O = 0$. Likewise, the rotor phase voltages V_{ra}, V_{rb} and V_{rc} are replaced by the transformed quantities V_d, V_q and $V_o = 0$ shown in Figure 2.3 -1 .

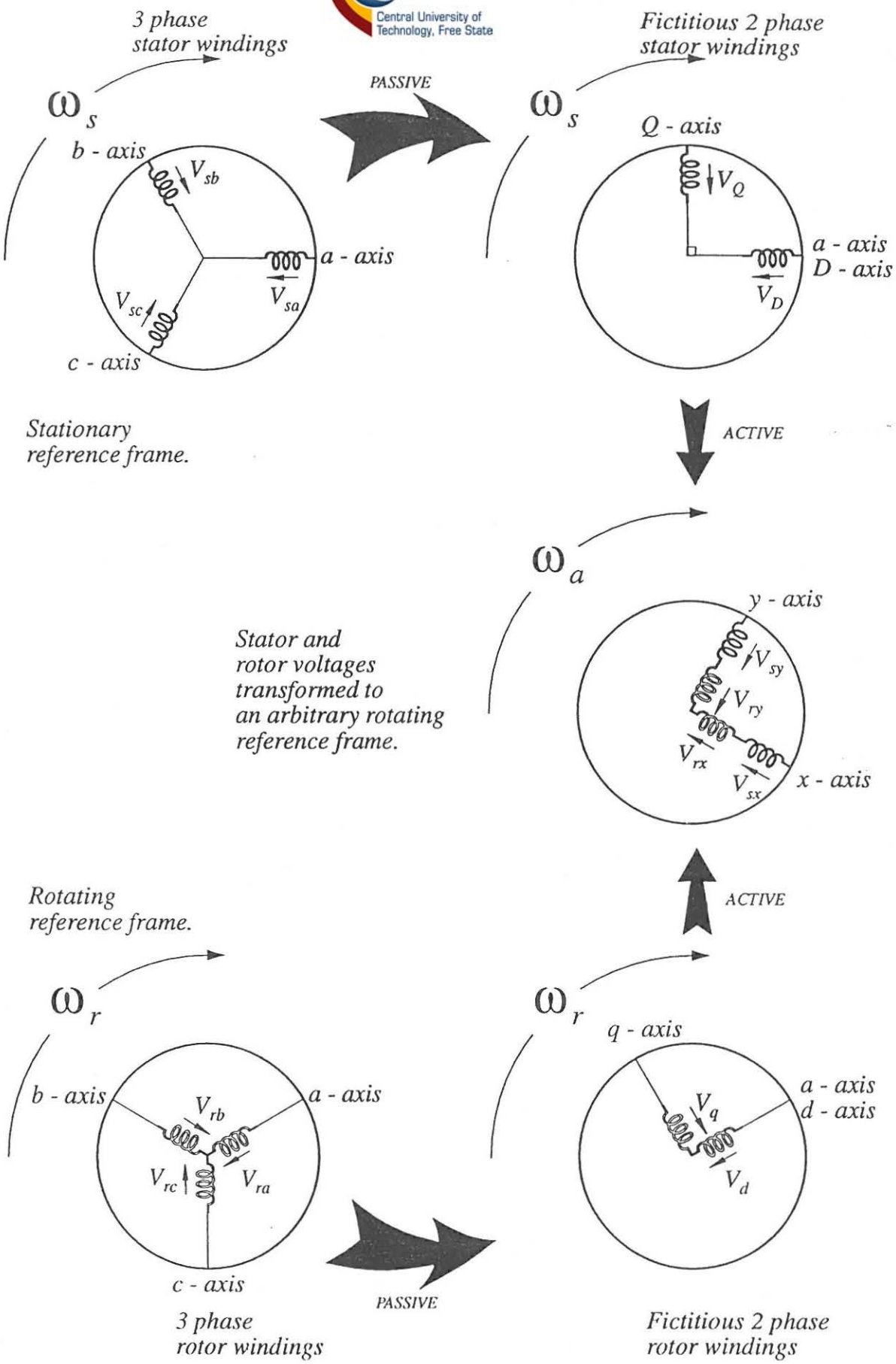

Figure 2.3 -1 : Transforming the three - phase stator and rotor variables to a common reference frame, rotating at an arbitrary speed.

2.3.1 Obtaining a coefficient matrix for the transformation between the existing stationary three phase windings and the fictitious two phase windings

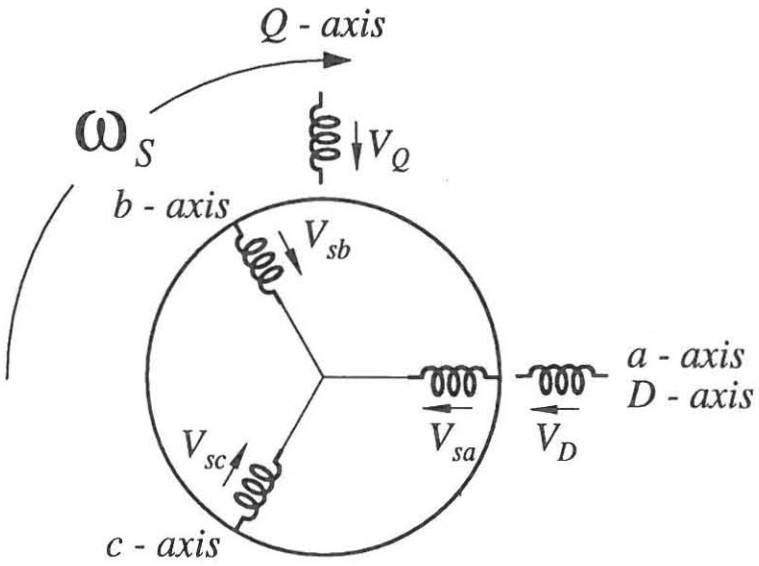

Figure 2.3 -2 : Trigonometric relationship between the stator three - phase winding and the two - phase winding.

The following transformation relationship exists between V_D, V_Q and V_{sa}, V_{sb}, V_{sc} shown in Figure 2.3 -2 :

$$V_D = V_{sa} + V_{sb}\cos(+120°) + V_{sc}\cos(-120°)$$

$$V_Q = 0 + V_{sb}\sin(+120°) + V_{sc}\sin(-120°) \qquad (2.6)$$

To represent V_D and V_Q in terms of V_{sa}, V_{sb} and V_{sc} and vice versa, an additional equation must be added to construct a "square" matrix . As mentioned earlier $V_0 = 0$. This can be written as $V_O = 0 = c(V_{sa} + V_{sb} + V_{sc})$ where the constant c can be adjusted to a value so that the coefficient matrix becomes orthogonal .

If $c = \frac{1}{\sqrt{2}}$ then $V_O = 0 = (\frac{1}{\sqrt{2}}V_{sa} + \frac{1}{\sqrt{2}}V_{sb} + \frac{1}{\sqrt{2}}V_{sc})$ and from (2.6)

$$\begin{bmatrix} V_D \\ V_Q \\ V_O \end{bmatrix} = \begin{bmatrix} 1 & -\frac{1}{2} & -\frac{1}{2} \\ 0 & \frac{\sqrt{3}}{2} & -\frac{\sqrt{3}}{2} \\ \frac{1}{\sqrt{2}} & \frac{1}{\sqrt{2}} & \frac{1}{\sqrt{2}} \end{bmatrix} \begin{bmatrix} V_{sa} \\ V_{sb} \\ V_{sc} \end{bmatrix} \tag{2.7}$$

So that

$$[\mathbf{V}_{DQO}] = [\mathbf{A}] \cdot [\mathbf{V}_{sabc}] \quad \text{and} \quad [\mathbf{V}_{sabc}] = [\mathbf{A}]^{-1} \cdot [\mathbf{V}_{DQO}] \tag{2.8}$$

Now if

$$[\mathbf{A}] = \sqrt{\frac{3}{2}} \cdot \sqrt{\frac{2}{3}} \begin{bmatrix} 1 & -\frac{1}{2} & -\frac{1}{2} \\ 0 & \frac{\sqrt{3}}{2} & -\frac{\sqrt{3}}{2} \\ \frac{1}{\sqrt{2}} & \frac{1}{\sqrt{2}} & \frac{1}{\sqrt{2}} \end{bmatrix} = \sqrt{\frac{3}{2}} \cdot [\mathbf{B}] \tag{2.9}$$

and $$[\mathbf{A}]^{-1} = \left| \sqrt{\frac{3}{2}} [\mathbf{B}] \right|^{-1} = \sqrt{\frac{2}{3}} [\mathbf{B}]^{-1} \tag{2.10}$$

Then

$$[\mathbf{A}]^{-1} = \sqrt{\frac{2}{3}}\sqrt{\frac{3}{2}}\begin{bmatrix} 1 & 0 & \frac{1}{\sqrt{2}} \\ -\frac{1}{2} & \frac{\sqrt{3}}{2} & \frac{1}{\sqrt{2}} \\ -\frac{1}{2} & -\frac{\sqrt{3}}{2} & \frac{1}{\sqrt{2}} \end{bmatrix} = \sqrt{\frac{2}{3}}[\mathbf{B}]^{T} \qquad (2.11)$$

and so $[\mathbf{B}]^{-1} = [\mathbf{B}]^{T}$

where $[\mathbf{B}]$ is an orthogonal matrix and is now possible to solve.

That is:

$$[\mathbf{V}_{DQO}] = \sqrt{\frac{3}{2}}[\mathbf{B}] \cdot [\mathbf{V}_{sabc}] \qquad \text{and} \qquad [\mathbf{V}_{sabc}] = \sqrt{\frac{2}{3}}[\mathbf{B}]^{T} \cdot [\mathbf{V}_{DQO}] \qquad (2.12)$$

2.3.2 Obtaining a coefficient matrix to transform the fictitious two phase windings to two phase windings rotating in an arbitrary reference frame.

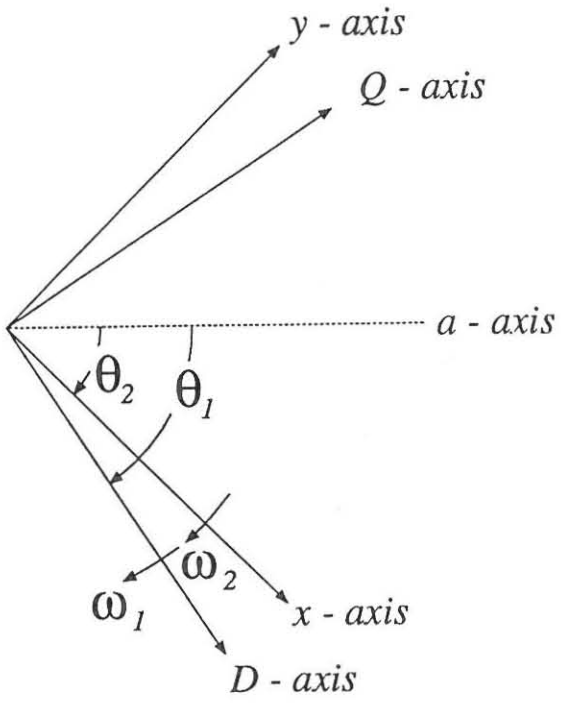

Figure 2.3 -3 : Trigonometric relationship between two reference frames rotating at two different velocities.

In Figure 2.3 - 3 the two sets of orthogonal quantities represent two frames of reference; The xy reference frame rotating at an arbitrary speed ω_1 and the DQ reference frame rotating at a speed ω_2. The stator variables are transformed from the stationary DQ reference frame to the xy reference frame and the rotor variables are transformed from the rotating dq reference frame to the xy reference frame. The transformed stator and rotor variables are now stationary with respect to each other in the xy reference frame so that the magnetic coupling between the rotor and stator windings stays "constant ", i.e. the angle θ_{sr} stays constant.

Using the stator voltages as an example again:

At $t = 0$, the initial displacement of the stator phase a- axis, the transformed quantity V_D and the arbitrary rotating quantity V_x is set to zero. The trigonometric relationship between the two sets of rotating quantities after some time t is :

$$V_x = V_D \cos(\theta_1 - \theta_2) + V_Q \sin(\theta_1 - \theta_2)$$

$$V_y = -V_D \sin(\theta_1 - \theta_2) + V_Q \cos(\theta_1 - \theta_2) \qquad (2.13)$$

$$V_O = V_O$$

and the zero phase sequence component is again included to present a square, orthogonal coefficient matrix :

$$\begin{bmatrix} V_x \\ V_y \\ V_O \end{bmatrix} = \begin{bmatrix} \cos(\theta_1 - \theta_2) & \sin(\theta_1 - \theta_2) & 0 \\ -\sin(\theta_1 - \theta_2) & \cos(\theta_1 - \theta_2) & 0 \\ 0 & 0 & 1 \end{bmatrix} \cdot \begin{bmatrix} V_D \\ V_Q \\ V_O \end{bmatrix} \qquad (2.14)$$

from which the inverse is

$$\begin{bmatrix} V_D \\ V_Q \\ V_O \end{bmatrix} = \begin{bmatrix} \cos(\theta_1 - \theta_2) & -\sin(\theta_1 - \theta_2) & 0 \\ \sin(\theta_1 - \theta_2) & \cos(\theta_1 - \theta_2) & 0 \\ 0 & 0 & 1 \end{bmatrix} \cdot \begin{bmatrix} V_x \\ V_y \\ V_O \end{bmatrix} \qquad (2.15)$$

and again the inverse reduces to the transpose so that

$$[\mathbf{V}_{xyO}] = [\mathbf{S}] \cdot [\mathbf{V}_{DQO}] \quad \text{and} \quad [\mathbf{V}_{DQO}] = [\mathbf{S}]^{\mathrm{T}} \cdot [\mathbf{V}_{xyO}] \qquad (2.16)$$

where $$[\mathbf{S}]=\begin{bmatrix}\cos(\theta_1-\theta_2) & \sin(\theta_1-\theta_2) & 0\\ -\sin(\theta_1-\theta_2) & \cos(\theta_1-\theta_2) & 0\\ 0 & 0 & 1\end{bmatrix} \quad (2.17)$$

The desired transformation matrix, $[\mathbf{C}_s]$, from the stationary V_{sabc} axes to the arbitrary rotating V_{sxyO} axes, is obtained by combining equations (2.12) with equations (2.16) :

$$[\mathbf{V}_{sabc}]=\sqrt{\frac{2}{3}}[\mathbf{B}]^{\mathrm{T}}\cdot[\mathbf{V}_{DQO}] \quad \text{and} \quad [\mathbf{V}_{DQO}]=[\mathbf{S}]^{\mathrm{T}}\cdot[\mathbf{V}_{sxyO}]$$

$$\therefore \quad [\mathbf{V}_{sabc}]=\sqrt{\frac{2}{3}}[\mathbf{B}]^{\mathrm{T}}\cdot[\mathbf{S}]^{\mathrm{T}}\cdot[\mathbf{V}_{sxyO}] \quad (2.18)$$

$$[\mathbf{V}_{sxyO}]=[\mathbf{S}]\cdot[\mathbf{V}_{DQO}] \quad \text{and} \quad [\mathbf{V}_{DQO}]=\sqrt{\frac{3}{2}}[\mathbf{B}]\cdot[\mathbf{V}_{sabc}]$$

$$\therefore \quad [\mathbf{V}_{sxyO}]=[\mathbf{S}]\cdot\sqrt{\frac{3}{2}}[\mathbf{B}]\cdot[\mathbf{V}_{sabc}]=\sqrt{\frac{3}{2}}[\mathbf{S}]\cdot[\mathbf{B}]\cdot[\mathbf{V}_{sabc}] \quad (2.19)$$

from (2.9) and (2.17) let

$$[\mathbf{C}_s]=[\mathbf{S}]\cdot[\mathbf{B}]=\sqrt{\frac{2}{3}}\begin{bmatrix}\cos(\theta_1-\theta_2) & \cos(\theta_1-\theta_2-120°) & \cos(\theta_1-\theta_2+120°)\\ -\sin(\theta_1-\theta_2) & -\sin(\theta_1-\theta_2-120°) & -\sin(\theta_1-\theta_2+120°)\\ \frac{1}{\sqrt{2}} & \frac{1}{\sqrt{2}} & \frac{1}{\sqrt{2}}\end{bmatrix}$$

(2.20)

$$\text{and } [\mathbf{C}_s]^T = [\mathbf{S}]^T \cdot [\mathbf{B}]^T = \sqrt{\frac{2}{3}} \begin{bmatrix} \cos(\theta_1 - \theta_2) & -\sin(\theta_1 - \theta_2) & \frac{1}{\sqrt{2}} \\ \cos(\theta_1 - \theta_2 - 120°) & -\sin(\theta_1 - \theta_2 - 120°) & \frac{1}{\sqrt{2}} \\ \cos(\theta_1 - \theta_2 + 120°) & -\sin(\theta_1 - \theta_2 + 120°) & \frac{1}{\sqrt{2}} \end{bmatrix} \tag{2.21}$$

then finally :

$$[\mathbf{V}_{sxyO}] = \sqrt{\frac{3}{2}}[\mathbf{C}_s] \cdot [\mathbf{V}_{sabc}] \quad \text{and} \quad [\mathbf{V}_{sabc}] = \sqrt{\frac{2}{3}}[\mathbf{C}_s]^T \cdot [\mathbf{V}_{sxyO}] \tag{2.22}$$

2.3.3 Stationary stator voltage equations transformed to an arbitrary rotating reference frame

The stator voltage equations (2.2) can be written as:

$$\begin{bmatrix} V_{sa} \\ V_{sb} \\ V_{sc} \end{bmatrix} = R_s \cdot \begin{bmatrix} I_{sa} \\ I_{sb} \\ I_{sc} \end{bmatrix} + \frac{d}{dt} \begin{bmatrix} \lambda_{sa} \\ \lambda_{sb} \\ \lambda_{sc} \end{bmatrix} \tag{2.23}$$

in a stationary reference frame.

When applying the transformation matrix $[\mathbf{C}_s]^T$ in (2.21) to the stator variables, the angular velocities ω_1 and ω_2 in Figure 2.3-3 must be adjusted to $\omega_1 = \omega$ and

$\omega_2 = 0$ so that

$$[\mathbf{C}_s]^{\mathrm{T}} = \sqrt{\frac{2}{3}} \begin{bmatrix} \cos(\theta) & -\sin(\theta) & \frac{1}{\sqrt{2}} \\ \cos(\theta - 120°) & -\sin(\theta - 120°) & \frac{1}{\sqrt{2}} \\ \cos(\theta + 120°) & -\sin(\theta + 120°) & \frac{1}{\sqrt{2}} \end{bmatrix} \tag{2.24}$$

Consequently

$$[V_{sabc}] = [\mathbf{C}_s]^{\mathrm{T}} \cdot [V_{sxyO}] \tag{2.25}$$

$$[i_{sabc}] = [\mathbf{C}_s]^{\mathrm{T}} \cdot [i_{sxyO}] \tag{2.26}$$

$$\frac{d}{dt}\lambda_{sabc} = \frac{d}{dt}\left([\mathbf{C}_s]^{\mathrm{T}} \cdot \lambda_{sxyO}\right) \tag{2.27}$$

The angle θ in the transformation matrix $[\mathbf{C}_s]^{\mathrm{T}}$ is a time varying quantity.

Equation (2.27) is then expanded to :

$$\frac{d}{dt}\begin{bmatrix} \lambda_{sa} \\ \lambda_{sb} \\ \lambda_{sc} \end{bmatrix} = \frac{d}{dt}\left(\sqrt{\frac{2}{3}} \begin{bmatrix} \cos(\theta) & -\sin(\theta) & \frac{1}{\sqrt{2}} \\ \cos(\theta - 120°) & -\sin(\theta - 120°) & \frac{1}{\sqrt{2}} \\ \cos(\theta + 120°) & -\sin(\theta + 120°) & \frac{1}{\sqrt{2}} \end{bmatrix} \cdot \begin{bmatrix} \lambda_{sx} \\ \lambda_{sy} \\ \lambda_{sO} \end{bmatrix} \right) \tag{2.28}$$

$$= \sqrt{\frac{2}{3}} \begin{bmatrix} -\sin(\theta) & -\cos(\theta) & 0 \\ -\sin(\theta-120°) & -\cos(\theta-120°) & 0 \\ -\sin(\theta+120°) & -\cos(\theta+120°) & 0 \end{bmatrix} \cdot \begin{bmatrix} \lambda_{sx} \\ \lambda_{sy} \\ \lambda_{sO} \end{bmatrix} \frac{d\theta}{dt} + \sqrt{\frac{2}{3}} \begin{bmatrix} \cos(\theta) & -\sin(\theta) & \frac{1}{\sqrt{2}} \\ \cos(\theta-120°) & -\sin(\theta-120°) & \frac{1}{\sqrt{2}} \\ \cos(\theta+120°) & -\sin(\theta+120°) & \frac{1}{\sqrt{2}} \end{bmatrix} \frac{d}{dt} \begin{bmatrix} \lambda_{sx} \\ \lambda_{sy} \\ \lambda_{sO} \end{bmatrix}$$

(2.29)

where $\frac{d\theta}{dt} = \omega$

so that the result is:

$$\frac{d}{dt}\lambda_{sabc} = \sqrt{\frac{2}{3}} \begin{bmatrix} \lambda_{sx} \\ \lambda_{sy} \\ \lambda_{sO} \end{bmatrix} \cdot \begin{bmatrix} \frac{d}{dt}\lambda_{sx} - \omega\lambda_{sy} \\ \frac{d}{dt}\lambda_{sy} + \omega\lambda_{sx} \\ \frac{d}{dt}\lambda_{sO} + 0 \end{bmatrix} = [\mathbf{C}_s]^{\mathrm{T}} \left(\frac{d}{dt} \begin{bmatrix} \lambda_{sx} \\ \lambda_{sy} \\ \lambda_{sO} \end{bmatrix} + \omega \begin{bmatrix} -\lambda_{sy} \\ \lambda_{sx} \\ 0 \end{bmatrix} \right) \qquad (2.30)$$

Inserting equations (2.25, 2.26 and 2.30) into equation (2.23) gives the complete transformed stator voltage equations as :

$$[\mathbf{C}_s]^{\mathrm{T}} \cdot \begin{bmatrix} V_{sx} \\ V_{sy} \\ V_{sO} \end{bmatrix} = R_s \cdot [\mathbf{C}_s]^{\mathrm{T}} \cdot \begin{bmatrix} i_{sx} \\ i_{sy} \\ i_{sO} \end{bmatrix} + [\mathbf{C}_s]^{\mathrm{T}} \left(\frac{d}{dt} \begin{bmatrix} \lambda_{sx} \\ \lambda_{sy} \\ \lambda_{sO} \end{bmatrix} + \omega \begin{bmatrix} -\lambda_{sy} \\ \lambda_{sx} \\ 0 \end{bmatrix} \right) \qquad (2.31)$$

or

$$\begin{bmatrix} V_{sx} \\ V_{sy} \\ V_{sO} \end{bmatrix} = R_s \cdot \begin{bmatrix} i_{sx} \\ i_{sy} \\ i_{sO} \end{bmatrix} + \frac{d}{dt} \begin{bmatrix} \lambda_{sx} \\ \lambda_{sy} \\ \lambda_{sO} \end{bmatrix} + \omega \cdot \begin{bmatrix} -\lambda_{sy} \\ \lambda_{sx} \\ 0 \end{bmatrix} \qquad (2.32)$$

2.3.4 Rotating rotor voltage equations transformed to an arbitrary rotating reference frame

The rotor voltage equations in (2.3) can be written as :

$$\begin{bmatrix} V'_{ra} \\ V'_{rb} \\ V'_{rc} \end{bmatrix} = R'_r \cdot \begin{bmatrix} i'_{ra} \\ i'_{rb} \\ i'_{rc} \end{bmatrix} + \frac{d}{dt} \begin{bmatrix} \lambda'_{ra} \\ \lambda'_{rb} \\ \lambda'_{rc} \end{bmatrix} \tag{2.33}$$

where the rotor voltages, currents and flux-linkages are referred to the stator winding and are represented by a reference frame fixed to a point on the moving rotor.

Adjusting the angular velocities in Figure 2.3-3 to $\omega_1 = \omega$ and $\omega_2 = \omega_r$, equation (2.33) is transformed by

$$[\mathbf{C}_r]^{\mathrm{T}} = \sqrt{\frac{2}{3}} \begin{bmatrix} \cos(\theta - \theta_r) & -\sin(\theta - \theta_r) & \frac{1}{\sqrt{2}} \\ \cos(\theta - \theta_r - 120°) & -\sin(\theta - \theta_r - 120°) & \frac{1}{\sqrt{2}} \\ \cos(\theta - \theta_r + 120°) & -\sin(\theta - \theta_r + 120°) & \frac{1}{\sqrt{2}} \end{bmatrix} \tag{2.34}$$

from the rotor abc axis, first to a fictitious dq axis rotating with the rotor and then to the arbitrary rotating xy axis in Figure 2.3-1. The transformed equations are :

$$[\mathbf{C}_r]^{\mathrm{T}} \cdot \begin{bmatrix} V'_{rx} \\ V'_{ry} \\ V'_{ro} \end{bmatrix} = R'_r \cdot [\mathbf{C}_r]^{\mathrm{T}} \cdot \begin{bmatrix} i'_{rx} \\ i'_{ry} \\ i'_{ro} \end{bmatrix} + [\mathbf{C}_r]^{\mathrm{T}} \cdot \left(\frac{d}{dt} \begin{bmatrix} \lambda'_{rx} \\ \lambda'_{ry} \\ \lambda'_{ro} \end{bmatrix} + (\omega - \omega_r) \cdot \begin{bmatrix} -\lambda'_{ry} \\ \lambda'_{rx} \\ 0 \end{bmatrix} \right) \tag{2.35}$$

or

$$\begin{bmatrix} V'_{rx} \\ V'_{ry} \\ V'_{ro} \end{bmatrix} = R'_r \cdot \begin{bmatrix} i'_{rx} \\ i'_{ry} \\ i'_{ro} \end{bmatrix} + \frac{d}{dt} \begin{bmatrix} \lambda'_{rx} \\ \lambda'_{ry} \\ \lambda'_{ro} \end{bmatrix} + (\omega - \omega_r) \cdot \begin{bmatrix} -\lambda'_{ry} \\ \lambda'_{rx} \\ 0 \end{bmatrix} \tag{2.36}$$

2.3.5 Stator and rotor voltage equations in the arbitrary xy reference frame variables

The induction motor is symmetric, so that :

- the air gap is uniform and the direct axis inductance is equal to the quadrature axis inductance $L_x = L_y$ i.e. no reluctance torque is developed.

- the stator and rotor resistances and inductances are equal.

$$R_{sa} = R_{sb} = R_{sc} = R_s,$$
$$R_{ra} = R_{rb} = R_{rc} = R_r,$$
$$L_{sa} = L_{sb} = L_{sc} = L_s$$

and $L_{ra} = L_{rb} = L_{rc} = L_r$.

- zero phase sequence components are discarded.

The arbitrary reference frame stator and rotor flux linkages can now be written as:

$$\begin{aligned}
\lambda_{sx} &= L_s i_{sx} + M_{sr} i'_{rx} \\
\lambda_{sy} &= L_s i_{sy} + M_{sr} i'_{ry} \\
\lambda'_{rx} &= L'_r i'_{rx} + M_{sr} i_{sx} \\
\lambda'_{ry} &= L'_r i'_{ry} + M_{sr} i_{sy}
\end{aligned} \tag{2.37}$$

and inserting equations (2.37) into (2.32) and (2.36) gives the complete voltage equations transformed to the arbitrary reference frame :

$$\begin{aligned}
V_{sx} &= R_s i_{sx} + L_s \frac{d}{dt} i_{sx} + M_{sr} \frac{d}{dt} i'_{rx} - \omega L_s i_{sy} - \omega M_{sr} i'_{ry} \\
V_{sy} &= R_s i_{sy} + L_s \frac{d}{dt} i_{sy} + M_{sr} \frac{d}{dt} i'_{ry} - \omega L_s i_{sx} - \omega M_{sr} i'_{rx} \\
V'_{rx} = 0 &= R'_r i'_{rx} + L'_r \frac{d}{dt} i'_{rx} + M_{sr} \frac{d}{dt} i_{sx} - (\omega - \omega_r) L'_r i'_{ry} - (\omega - \omega_r) M_{sr} i_{sy} \\
V'_{ry} = 0 &= R'_r i'_{ry} + L'_r \frac{d}{dt} i'_{ry} + M_{sr} \frac{d}{dt} i_{sy} - (\omega - \omega_r) L'_r i'_{rx} - (\omega - \omega_r) M_{sr} i_{sx}
\end{aligned} \tag{2.38}$$

Putting $V'_{rx} = V'_{ry} = 0$ is only valid for the squirrel cage induction motor because the rotor is short circuited.

The voltage equations can be constructed as:

$$\begin{bmatrix} V_{sx} \\ V_{sy} \\ 0 \\ 0 \end{bmatrix} = \begin{bmatrix} R_s + L_s\frac{d}{dt} & -\omega L_s & M_{sr}\frac{d}{dt} & -\omega M_{sr} \\ \omega L_s & R_s + L_s\frac{d}{dt} & \omega M_{sr} & M_{sr}\frac{d}{dt} \\ M_{sr}\frac{d}{dt} & -(\omega-\omega_r)M_{sr} & R'_r + L'_r\frac{d}{dt} & -(\omega-\omega_r)L'_r \\ (\omega-\omega_r)M_{sr} & M_{sr}\frac{d}{dt} & (\omega-\omega_r)L'_r & R'_r + L'_r\frac{d}{dt} \end{bmatrix} \cdot \begin{bmatrix} i_{sx} \\ i_{sy} \\ i'_{rx} \\ i'_{ry} \end{bmatrix} \quad (2.39)$$

The transformed impedance matrix contains only 16 terms which is a significant reduction when compared with equation (2.5) where the original impedance matrix contains 36 terms. A further reduction in the impedance terms can be achieved by setting $\omega = 0$. This means that the state of the electric system is observed from a stationary stator - fixed frame of reference and that there are now only 12 terms in the impedance matrix to evaluate. The stator - fixed frame of reference is then a most efficient method to model these linear differential equations.

Equation (2.39) can be expressed as:

$$[\mathbf{V}] = [\mathbf{R}]\cdot[\mathbf{i}] + [\mathbf{L}]\frac{d}{dt}[\mathbf{i}] + [\mathbf{G}]\cdot[\mathbf{i}] \quad (2.40)$$

where

$$[\mathbf{V}] = \begin{bmatrix} V_{sD} \\ V_{sQ} \\ 0 \\ 0 \end{bmatrix} \quad (2.41)$$

$$[\mathbf{i}] = \begin{bmatrix} i_{sD} \\ i_{sQ} \\ i'_{rd} \\ i'_{rq} \end{bmatrix} \tag{2.42}$$

$$[\mathbf{R}] = \begin{bmatrix} R_s & 0 & 0 & 0 \\ 0 & R_s & 0 & 0 \\ 0 & 0 & R'_r & 0 \\ 0 & 0 & 0 & R'_r \end{bmatrix} \tag{2.43}$$

$$[\mathbf{L}] = \begin{bmatrix} L_s & 0 & M_{sr} & 0 \\ 0 & L_s & 0 & M_{sr} \\ M_{sr} & 0 & L'_r & 0 \\ 0 & M_{sr} & 0 & L'_r \end{bmatrix} \tag{2.44}$$

$$[\mathbf{G}] = \begin{bmatrix} 0 & -\omega L_s & 0 & -\omega M_{sr} \\ \omega L_s & 0 & \omega M_{sr} & 0 \\ 0 & -(\omega - \omega_r) M_{sr} & 0 & -(\omega - \omega_r) L'_r \\ (\omega - \omega_r) M_{sr} & 0 & (\omega - \omega_r) L'_r & 0 \end{bmatrix} \tag{2.45}$$

The voltage equations can be solved in other reference frames, depending on the choice of ω for that specific reference frame. For example :

1. $\omega = \omega_r$: This reference frame is fixed to a point on the rotating rotor.

2. $\omega = \omega_a$: The speed of this frame of reference can be adjusted to rotate arbitrarily, relative to the rotor speed.

2.3.6 Air gap torque expressed in the arbitrary xy reference frame variables.

The air gap torque, in terms of the arbitrary reference frame, can be given as:

$$T_e = k(\lambda'_{ry} i'_{rx} - \lambda'_{rx} i'_{ry}) \tag{2.46}$$

where the constant k is adjusted to accommodate the physical considerations of each individual machine. By substituting for the rotor flux linkages from equations (2.37), equation (2.46) becomes :

$$\begin{aligned} T_e &= k(L'_r i'_{ry} i'_{rx} + M_{sr} i_{sy} i'_{rx} - L'_r i'_{rx} i'_{ry} - M_{sr} i_{sx} i'_{ry}) \\ &= k M_{sr}(i_{sy} i'_{rx} - i_{sx} i'_{ry}) \end{aligned} \tag{2.47}$$

The torque in equation (2.1) can now be expressed in terms of the transformed currents as:

$$T_e \propto M_{sr}(i_{sy} i'_{rx} - i_{sx} i'_{ry}) \tag{2.48}$$

and the mutual inductance term M_{sr} is still a constant.

Neglecting non - linear effects, the performance of the induction motor during transient conditions can now be determined using equation (2.40) together with the equation of motion of the mechanical system, as given below :

$$T_e = J\frac{d\omega_r}{dt} + D\omega_r + T_L \tag{2.49}$$

where T_L is the load torque,

$D\omega_r$ is the damping torque.

The damping constant D describes the friction and windage losses.

$J\omega_r$ is the inertia constant where

J represents the rotor inertia during free acceleration.

$\omega_r = \frac{d\theta_r}{dt}$ is the angular velocity of the rotor.

The angle θ_r is in electrical degrees and it is related to the angle θ_{sr} in Figure 2.2-1 as follows :

$$\theta_r = P\theta_{sr} \tag{2.50}$$

where θ_{sr} is the angle in mechanical degrees and P is the number of pole pairs of the machine.

2.4 Summary

In this chapter the air gap torque and the stator and rotor voltage equations that describe the transient performance of an induction motor, are discussed. The air gap torque is proportional to the instantaneous values of the stator and rotor currents and the mutual inductance between the stator and the rotor.

The differential voltage equations which contains these currents and time varying mutual inductances are reduced by transforming the three-phase (three-axes) stator and rotor voltages to two sets of two-axes variables where the:

- stator and rotor mutual inductances are independent of time;
- six voltage equations are reduced to four voltage equations.

The three stator voltages from the stationary stator winding are passively transformed to a fictitious two phase stator winding and then actively transformed to a arbitrarily rotating two phase winding. The rotating rotor voltages are transformed to the same arbitrarily rotating winding. The reduced differential voltage equations together with the equation of motion can be used to simulate the transient behaviour of an induction motor.

CHAPTER 3

SIMULATION AND PREDICTED PERFORMANCE

3.1 The CASED package

The equations discussed in the previous chapter are built into the CASED package (**C**omputer **A**nalysis and **S**imulation of **E**lectric **D**rives), developed by McCulloch **et al**. It forms the basis from which machine simulation takes place and allows you to either use the fixed parameter model or the deep bar model when predicting the performance of induction motors. The program is executed by making use of the following modules :

1. CREATE which reads in the electrical supply environment, motor variables, shaft load-characteristics, simulation reswitching- and end time. The state - space technique is then used to model this system mathematically.

2. SIM uses an initialization routine to read the system files compiled by the CREATE module. The prepared data is then passed to the event scheduler ⇔ equation solver part of the program. The function of the event scheduler is to record and process any change in events as stipulated in the CREATE module, i.e. sending output variables to the screen or to the disk and to end the simulation.

Equation (2.40) is re - arranged as:

$$\frac{d}{dt}[\mathbf{i}] = [\mathbf{L}]^{-1} \cdot \{ [\mathbf{V}] - [\mathbf{R}] \cdot [\mathbf{i}] - [\mathbf{G}] \cdot [\mathbf{i}] \} \qquad (3.1)$$

for the differential equation solver which uses the Runge - Kutta - Fehlberg Method (RKF45) with adaptive stepsize control to obtain a solution. The basic inputs and outputs for this system are shown in Figure 3.1-1.

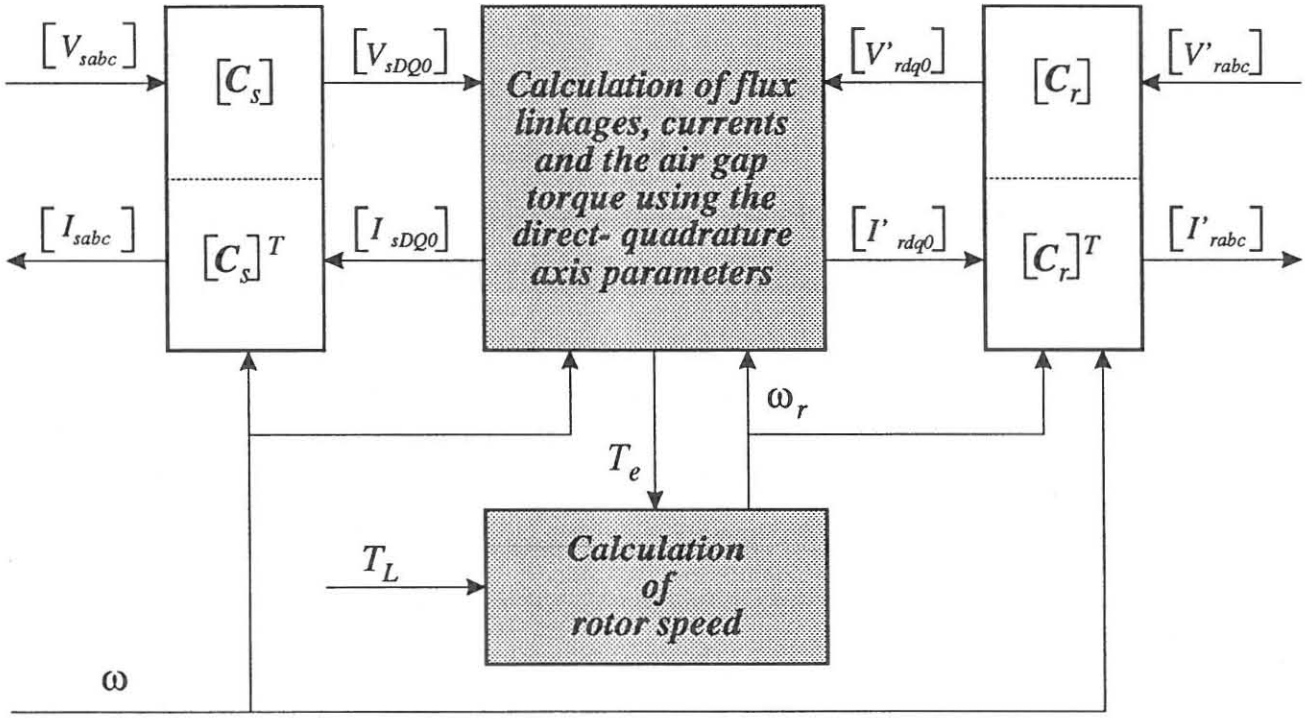

Figure 3.1-1 : A simplified block diagram showing the simulation of a three - phase induction motor in the arbitrary reference frame.

3. GRAPH is used to evaluate the simulated results. The data files generated by the SIM module can be exported to a spreadsheet or word - processor.

3.2 Factors influencing the accuracy of the simulation

The work of several authors on the computer simulation of the dynamic response of electric motors have been published. Simulated results of the transient torque of industrial rated induction motors, developed during the initial run - up period, are graphed (Smith,1990:44) and (Krause,1987:190).

Functions describing the effects of saturation (Krause,1987:461) and deep rotor bars (Smith,1990:52) are mentioned in these publications, but they are not accounted for in the simulated results. The influence of these phenomena on the motor during transient conditions will briefly be discussed below.

3.2.1 Saturation effects

The iron parts of electrical machines are usually designed to transport as much magnetic flux as possible, using the minimum amount of ferromagnetic material (Krause,1987:9). This is obvious from an economic and sometimes, a transportation and size, point of view. Running at full load, an induction motor may operate at a flux level where its iron parts are close to, or slightly saturated.

The most likely place where saturation can occur is in the stator and rotor teeth, which forms a major part of the leakage flux paths of a machine. During transient conditions in an induction motor, the stator currents can increase to several times their full load value. The leakage flux paths will saturate so that the effect of leakage saturation should be included in the analysis of the machine's transient performance (Smith, 1990:48).

The effect of leakage saturation cannot readily be determined from measurements made at the machine terminals. Levy (1990:68) has tested and incorporated two methods in the CASED program, which makes use of machine dimensions, to estimate the effect of saturation.

3.2.2 Deep bar effects

The starting torque of an induction motor is dependent on the rotor resistance. A high rotor resistance results in a high starting torque and a low starting current, a phenomenon which is an advantage from a designer's point of view. However, at normal operating speeds the high resistance reduces the efficiency of the motor. Varying the rotor resistance with the motor speed solves this problem. In a squirrel cage induction motor a variable rotor resistance can only be produced by the use of deep rotor bars (Fitzgerald, Kingsley & Umans, 1985:447).

If the rotor conductors are designed to extend deep into the rotor iron, the leakage flux that crosses the rotor slots will be distributed as indicated in Figure 3.2-1a. The leakage flux density decreases considerably near the air gap because the flux does not like to be driven through an area of high reluctance. More leakage flux links the deeper part of the bar where the reluctance is lower, so that the magnitude of the leakage inductance L_r increases with the depth of the rotor conductor.

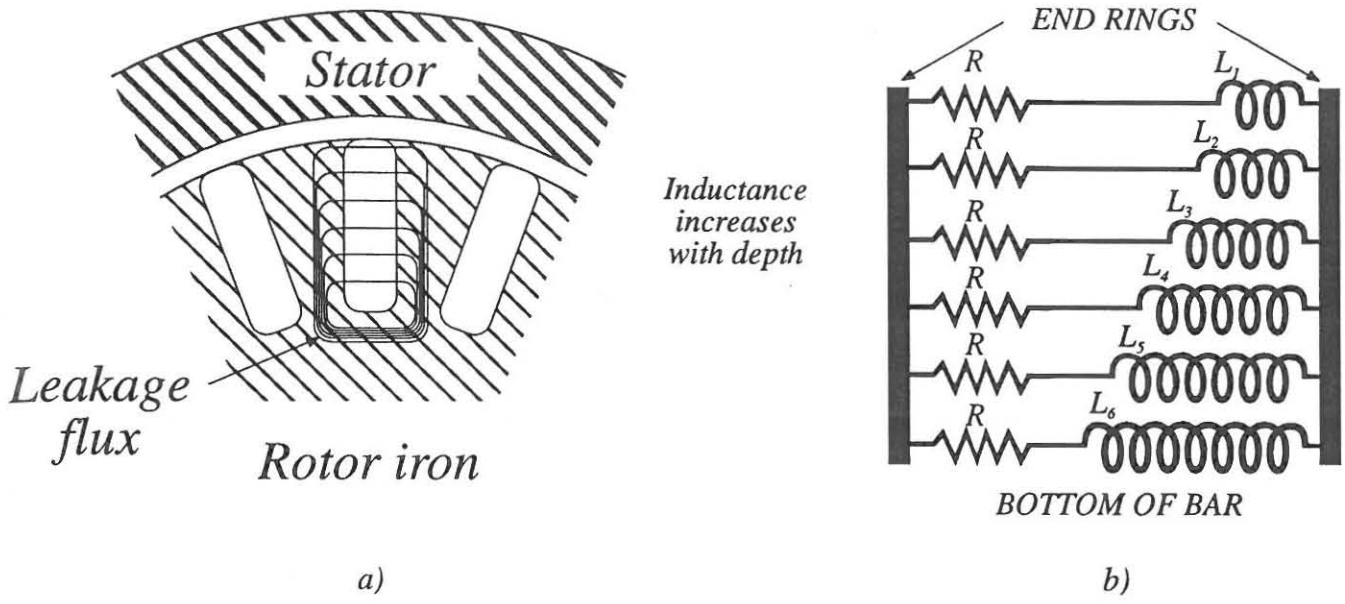

Figure 3.2-1 : Cross section of a deep rotor bar . (a) Concentration of the rotor - slot leakage flux near the bottom of the rotor conductor. (b) Equivalent circuit

Since inductive reactance is a function of frequency, the impedance of the rotor bar will vary with depth as the slip changes, particularly during the start - up period. At high slip (start - up), the large impedance in the lower part of the bar will force some of the induced current to move to the upper area where the reactance is lower. The high current density close to the air gap results in an increase of the effective resistance R_r of the bar, increasing the torque during start - up.

At low slip, the reactances of all the parallel paths in the bar, shown in Figure 3.2-1b, are small compared to their resistances. The magnitude of the impedances and currents at different depths are equal, resulting in a lower value for R_r and a higher efficiency at normal operating speeds.

It can be seen that the deep bar effect can only be utilized when the frequency of the rotor currents vary. The impedance matrix in equation (2.39) contains values of R_r and L_r which do not change as the frequency of the

rotor currents vary. An accurate simulation model of the deep bar effect has been developed by Levy (1990:12) in which the values of R_r and L_r are continuously computed as the rotor frequency changes. The torque - time graphs drawn in section 3.3 in this chapter, clearly shows the difference in simulated results when the effect of the deep bar model is included.

Most industrial rated squirrel - cage motors are designed with either a double cage or with a deep, solid rotor bar to achieve the advantages as mentioned above. By altering the shape of the cross-section of the rotor bar the designer can change the torque - speed curve of the motor to suit most applications. This model also makes provision for the most frequently used rotor bar cross-sections and it has a facility to simulate a "users defined" bar shape. Any range of supply frequencies can be included by the analyzer using CASED as a design tool.

3.2.3 Obtaining the induction motor parameters

To complement the precision of the simulation software, care must be taken when obtaining the machine parameters. The simulation program cannot be expected to predict the transient performance of the induction motor very accurately if the machine impedances are evaluated on the basis of the blocked rotor test.

The degree of similarity between the measured and the simulated results depends on the accuracy of the machine parameters, used for the simulation of the measured transient event.

The values of the stator and rotor leakage reactances, rotor conductor- and endring resistances are to be obtained from the motor designer's office.

The coefficient of friction and the moment of inertia J are measured using methods described by Landy (1970 : 26).

The accuracy of simulated results are therefore dependent on a combination of supplied and accurately measured machine variables.

3.3 Simulated results

Figure 3.3-1 shows the simulated results using the fixed parameter (or traditional) model with the 50 Hz rotor parameters obtained from the motor design sheet. It should be noted that the same set of random values for friction and inertia were used in these simulated results.

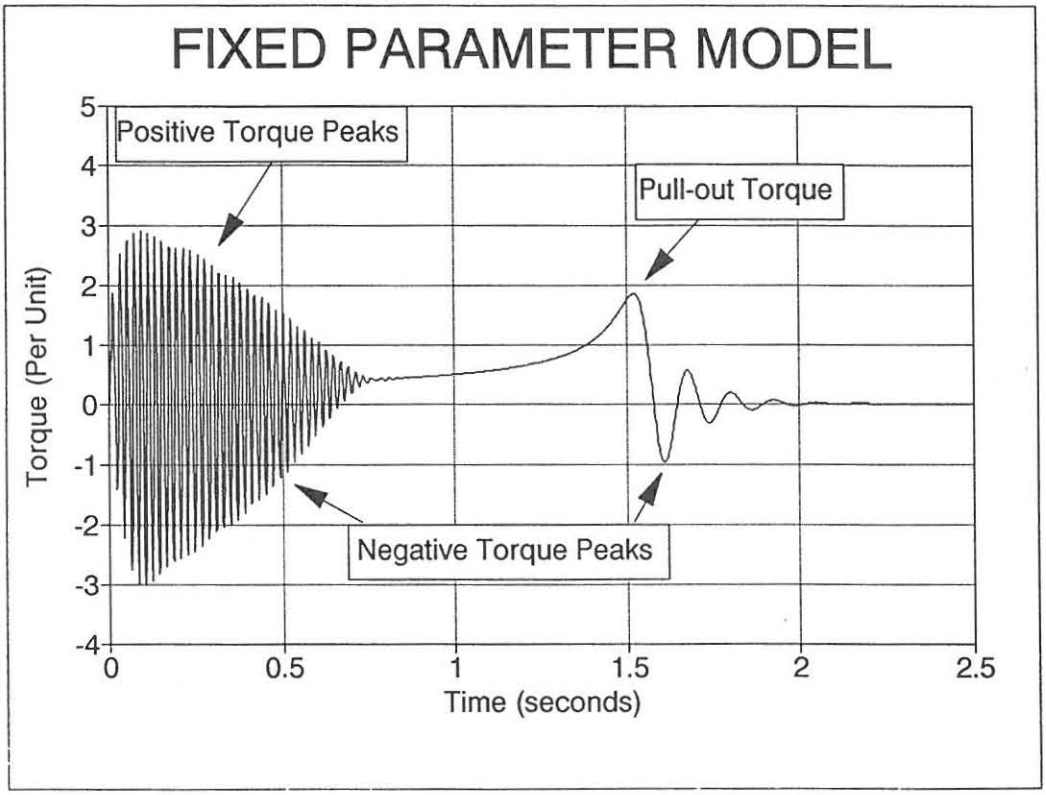

Figure 3.3-1 : Predicted starting torque curve of a 75 kW, 380 V, 6 pole induction motor using the fixed parameter model and the 50 Hz rotor parameters.

Figure 3.3-2 shows the simulated results using the deep bar model where the actual dimensions of the embedded rotor bar, also obtained from the manufacturers, were taken into account as the rotor time-constant changes continuously during the run-up period.

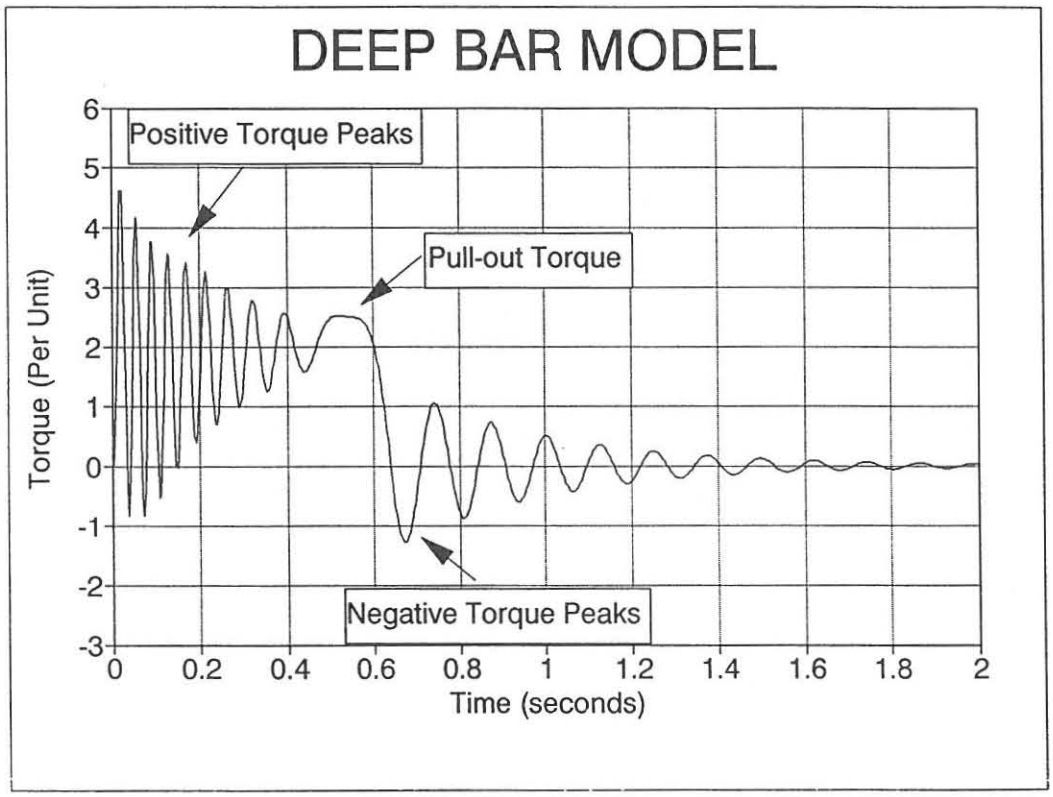

Figure 3.3-2 : Predicted starting torque curve of a 75 kW, 380 V, 6 pole induction motor with a T-shaped bar using the deep bar model .

Comparing the graphs in Figure 3.3-1 and Figure 3.3-2, the frequency of the torsional oscillations in Figure 3.3-1 are significantly higher and the magnitudes of the first positive torque cycle and the pull-out torque are lower than the similar magnitudes shown in Figure 3.3-2. It will be seen in Chapter 5 that the deep bar model is very successful when predicting the magnitude,

frequency and total transient time of a starting and reswitching torque transient event of an induction motor.

3.4 Summary

The CASED software package is briefly described and it is shown how the equations mentioned in chapter 2 are adapted to simulate the transient performance of an induction motor. The **accuracy** of the simulation is very dependent on effect of saturation, the deep bar effect and the correctness of the values used in computing the simulated model. When comparing the simulated results of the traditional model with the deep bar model, the traditional model does not adjust the rotor inductance and resistance according to the change in rotor frequency during transient conditions.

The simulation time of the traditional model is more than 10 times less than the time taken to simulate the deep bar model. The global accuracy of the differential equation solver also affect the simulation time. A value of 5% was used in the simulations and the results obtained were acceptable as will be seen in chapter 5.

CHAPTER 4

MEASUREMENT SYSTEM

4.1 The Speed and Torque Measuring system.

The motor is accelerated from standstill to its rated speed by supplying it with its rated r.m.s line to line voltage. Traces of acceleration measured during no-load conditions are proportional to the torque produced on the motor shaft because the inertia of the load is assumed to be equal to the inertia of the rotor (Krause, 1987:190).

To measure rotational transient events, a system with a high response time and a wide bandwidth is needed. Such a system must also be able to supply useful information at very low rotational speeds e.g. the starting and plugging of electric motors. The measuring system used overcomes these difficulties. It makes use of two non-transparent discs, each with 150 holes drilled through it and fitted as shown in Figure 4.1-1 . Sensitivity of the device may be adjusted by varying the :

- number of holes in the discs.

- speed of the reference motor (constant speed disc).

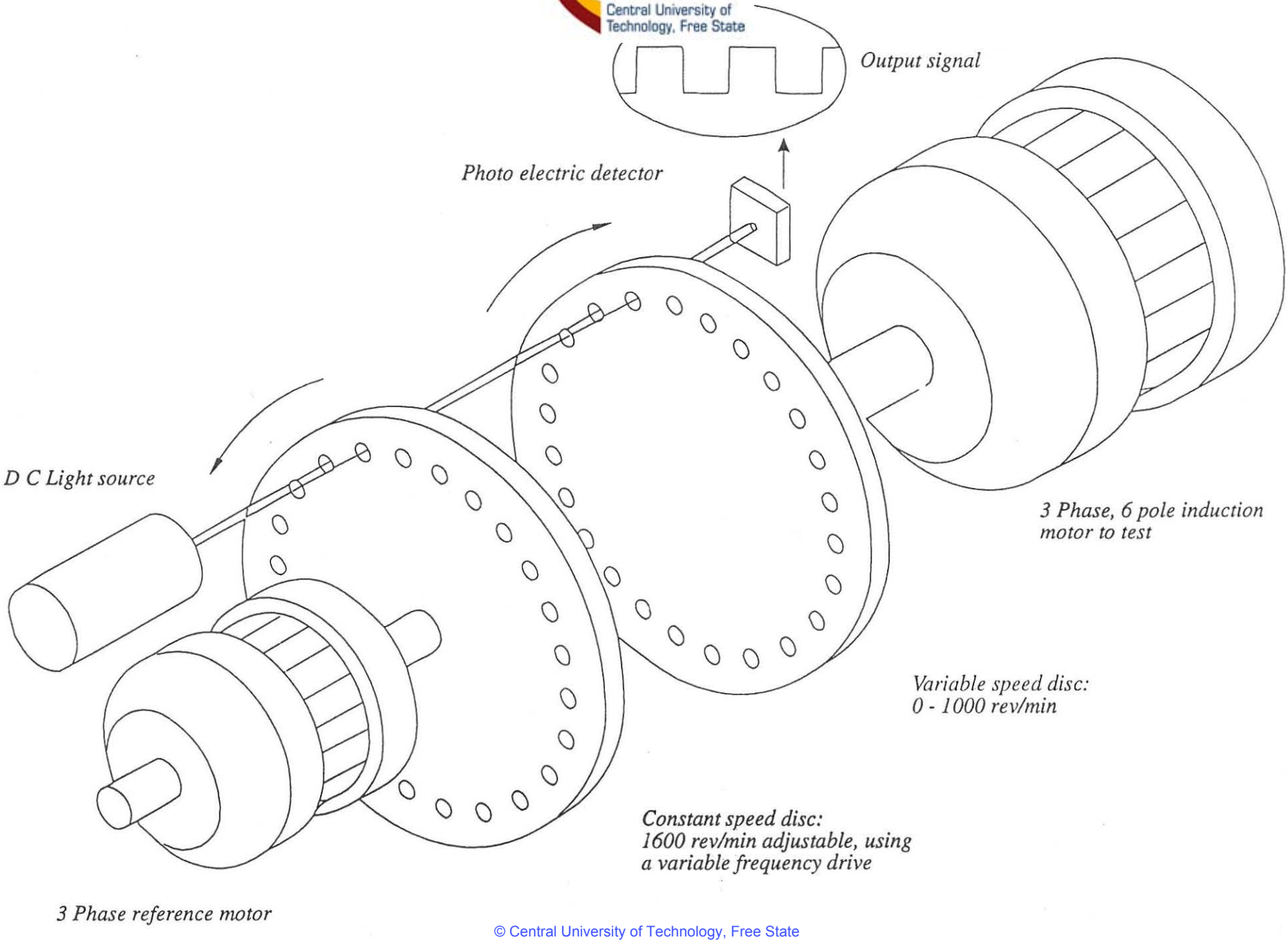

The constant speed disc can be rotated in either the same or the opposite direction as the disc connected to the shaft of the motor being tested. However, if the constant speed disc is rotated in the same direction as the variable speed disc, it must be done at a speed of at least twice that of the motors' speed under test. Additional electronic equipment will also be needed to invert the signal. For the sake of convenience the two discs were set up to rotate in opposite directions.

A set of optical lenses is used to focus the light beam on 5 - 6 holes as shown in figure 4.1-2 to improve the signal to noise ratio of the measured results.

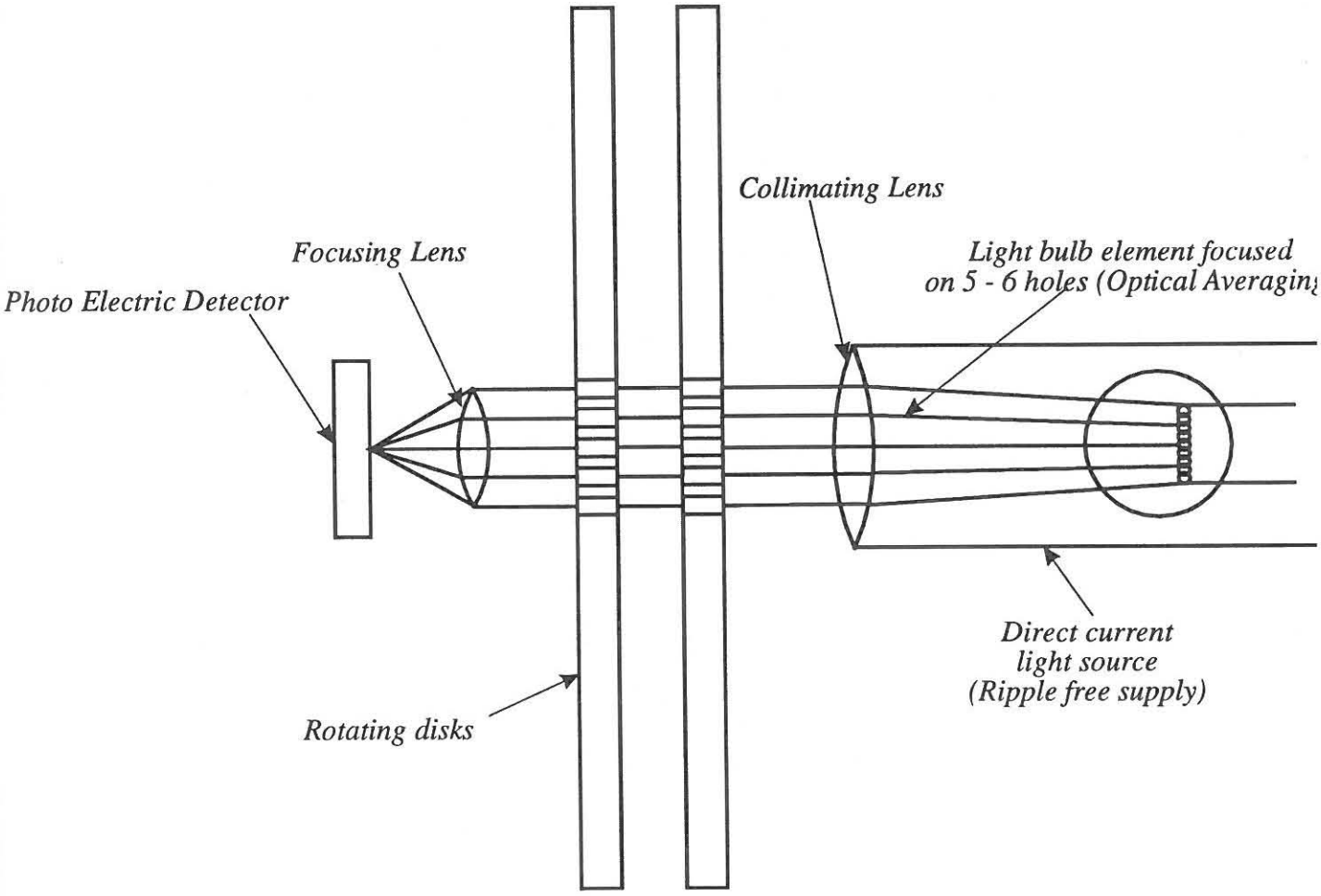

Figure 4.1-2 : The optical averaging system

As the discs rotate, light from the source is alternatively transmitted and stopped, thereby submitting a digital signal (pulse train) to a photo detector. The frequency of the pulse train is proportional to the relative speed of both motors.

Since each disc has N holes, the frequency of the pulses may be expressed as :

$$frequency = N(\omega_1 \pm \omega_2) \qquad (4.1)$$

where ω_1 and ω_2 are the motor velocities expressed in revolutions per second and the $\pm$ indicates the direction of rotation of the discs.

The constant speed disc was adjusted to rotate at approximately 1600 rev/min so that the frequency of the pulse train is 4 kHz when the other disc is stationary. This is the minimum frequency of transmission of the information.

If the test motor is accelerated to 1000 rev/min, assuming the slip to be negligible, the frequency of the pulse train increases to 6.5 kHz. The transmission band of the transient event is 2.5 kHz and the pulse from the photo-detector is used to trigger a monostable multivibrator.

The pulse width of the monostable multivibrator output signal is determined by the timing capacitor connected to the circuit and is constant irrespective of the relative speed of the motors. This avoids non - linearity in the speed signal (Stephenson, 1983:1969). This measuring system makes use of the fact that the duty cycle of this pulse (see Figure 4.1-3) is proportional to the speed of the test motor. The speed signal is then proportional to the average value (the dc

component) of the pulse train:- the more pulses per unit time, the higher the average voltage.

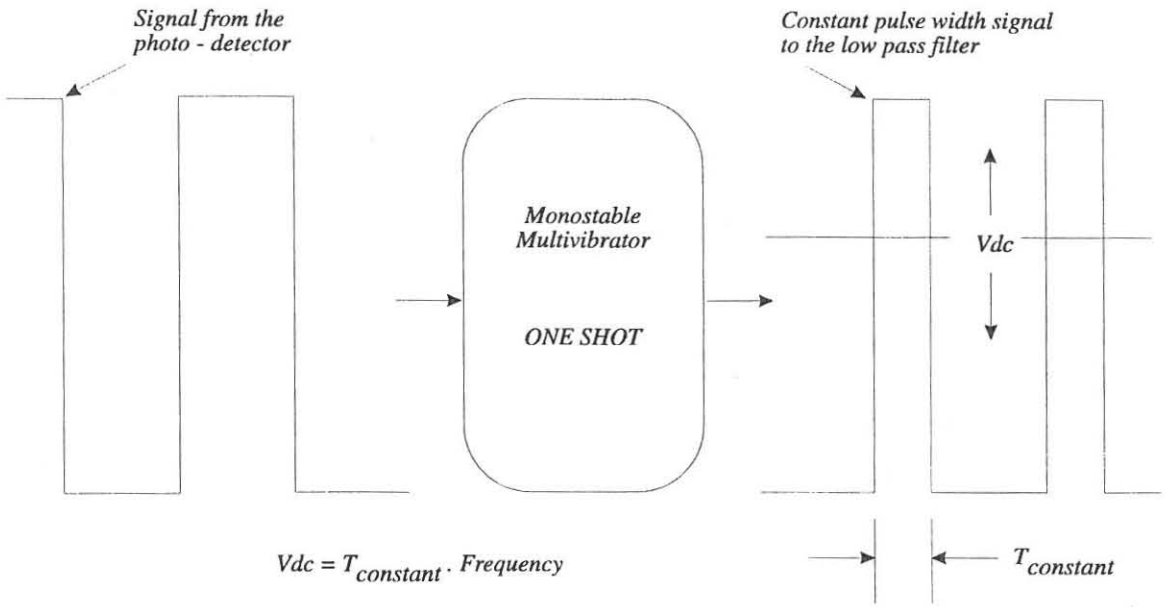

Figure 4.1-3 : A 74121 Monostable multivibrator "squares"' the signal from the photo transistor and the dc component of the voltage is proportional to the frequency of the signal.

A 4th order low pass Butterworth filter (see Figure 4.1-4) is used to remove the fundamental frequency and its higher frequency components, extracting a dc. voltage which is proportional to the speed of rotation of the motor under test. The speed signal is differentiated to give an acceleration signal which is proportional to the torque on the motor shaft.

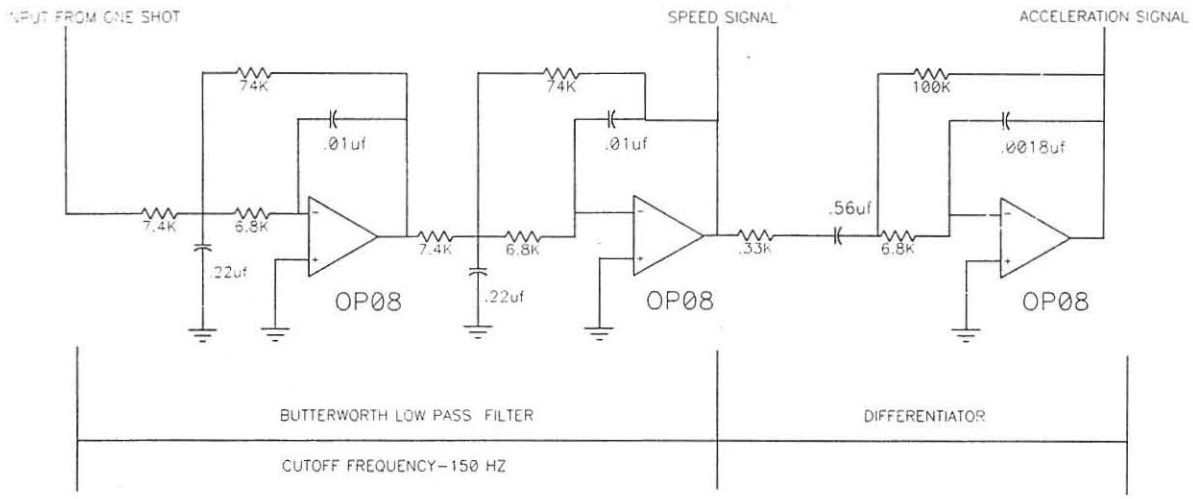

Figure 4.1-4 : The circuit diagram of the filter and differentiator used in the measuring system.

4.2 Noise

The discs were manufactured from TUFNOL™, a material similar in appearance to Bakelite. Previous measurement discs where machined on a milling machine and slots where cut into the disc periphery. This produced a very accurate, clean parallel slot, as the material is removed in one direction only. The advantage is a very low noise signal. The disadvantage of using this method is that the bottom of the tooth between two slots has a narrow "base" and the disc is subject to tooth breakage when transported between different motors.

A new, more rigid set of discs was manufactured by replacing the slots with drilled holes. This method produced a stronger disc, but due to the method of machining, the accuracy of the holes decreased. The hole diameter and the spacing between the holes were 3mm. A shadow graph was used to measure the percentage error in the hole diameter and some holes were found to be as much as 0.4 mm off-size. This severely increased the noise in the measured results. A sample of the measured noise is shown in Figure 4.2-1.

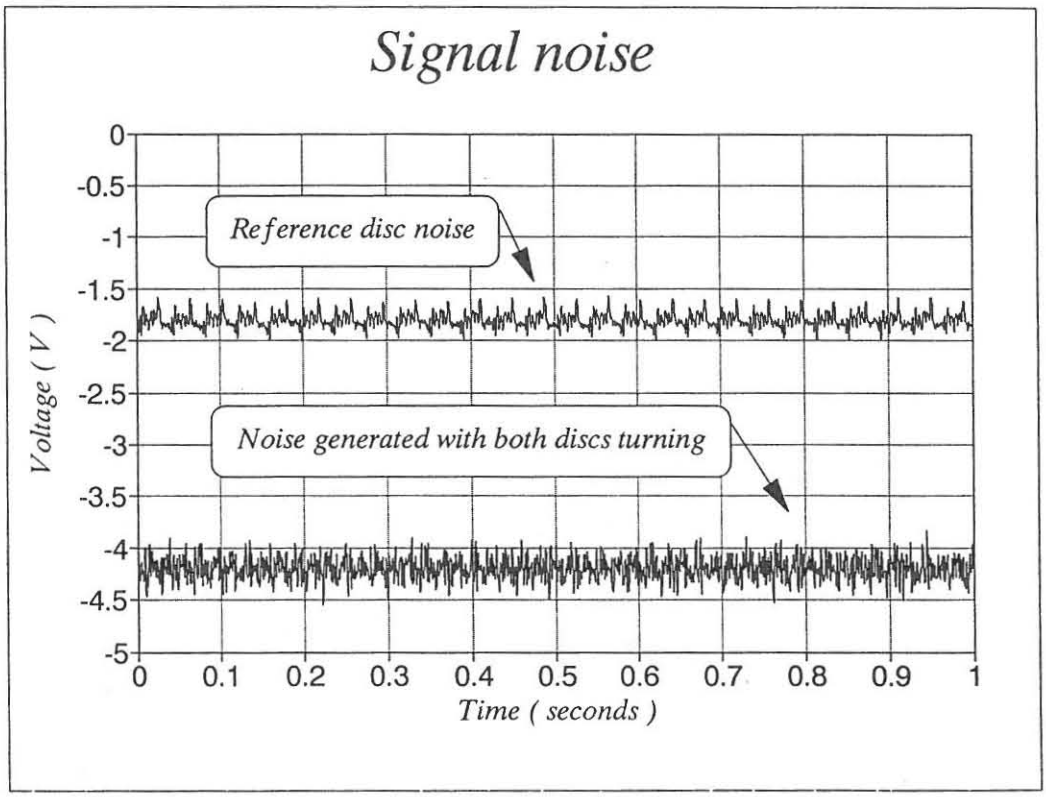

Figure 4.2-1 : A sample of the noise.

A second source of noise is introduced by the discs being mounted slightly eccentric. The noise generated is directly proportional to the speed of the discs and can be seen when a Fourier analysis is done on the noise. When the constant speed disc is running at 1600 rev/min the frequency spectrum of the noise shows that the fundamental component is situated at 26.7 Hz as shown in Figure 4.2-2. When the test motor was accelerated to its rated speed a frequency spectrum of the noise generated shows a component at approximately 52 Hz as shown in Figure 4.2-3.

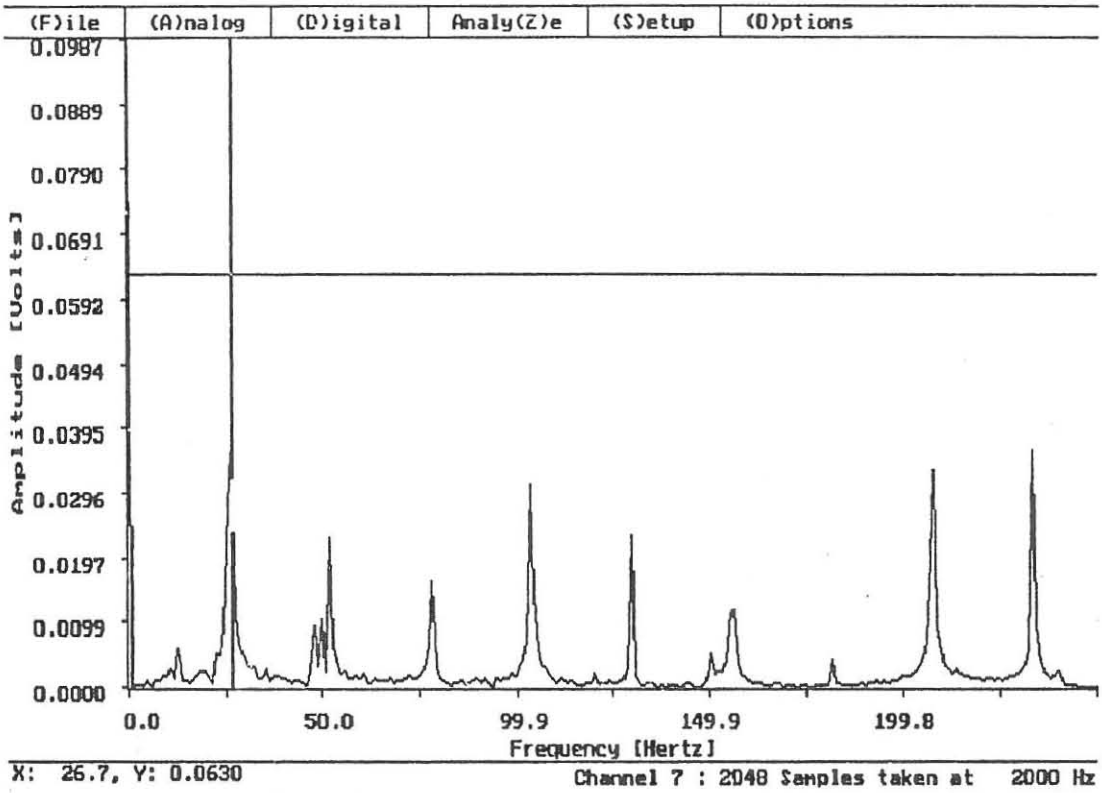

Figure 4.2-2 : A frequency spectrum of the noise generated by the disc on the reference motor.

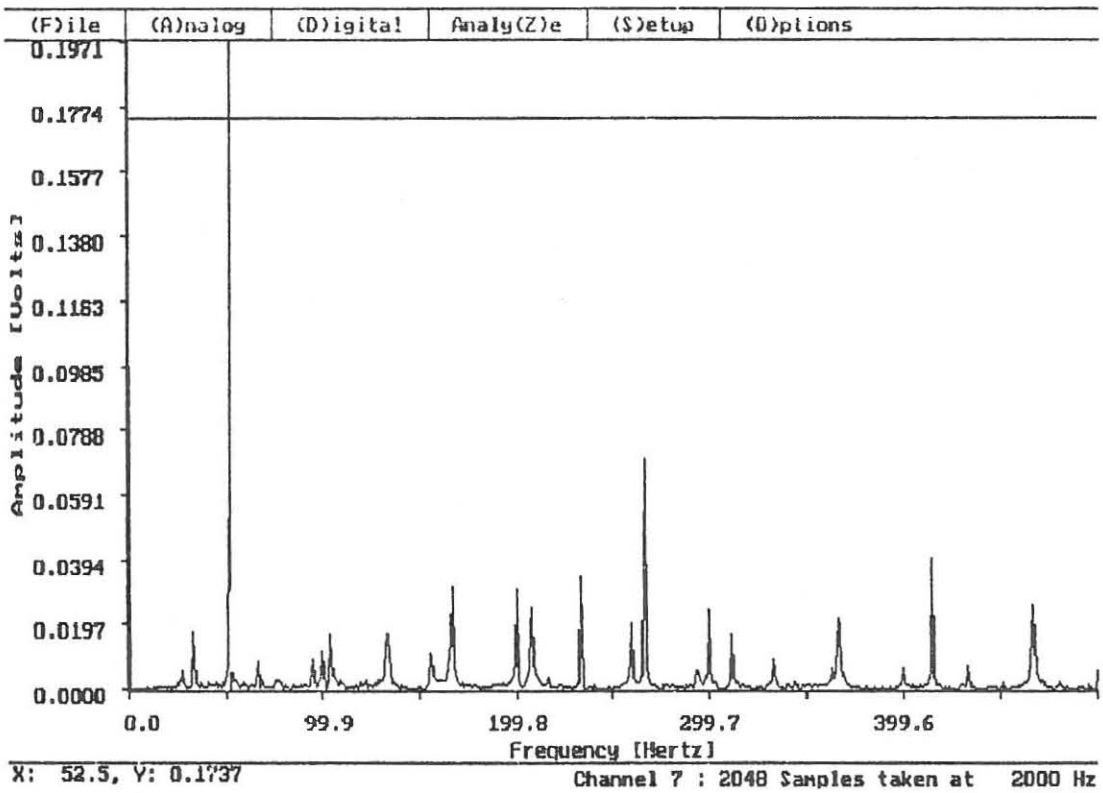

Figure 4.2-3 : A frequency spectrum of the noise generated when both discs are turning in opposite directions.

Initial measurements were taken using a storage oscilloscope. Due to the noise level generated by the discs, measurements were then taken using a data acquisition card and a PC. It was hoped that the noise could be filtered out mathematically if the data could be captured in an ASCII file.

4.3 The data acquisition package

Data from the speed, torque and voltage signals were collected using an analog-to-digital converter I/O card together with a menu-driven data acquisition package. A number of samples were obtained in powers of two so that it could be processed through the signal analysis software. The sampling rate varied from 512 Hz to 4096 Hz, depending on the number of channels sampled.

The length of the transient events recorded was typically less than 2 seconds. The accuracy of the event depended on the value of the BUS clock speed of the PC which had to be given each time when the software was loaded to record the transient event. As the actual clock speed of the XT-PC was not known a value of 12 MHz was assumed. This influenced the accuracy of the time-axis and the measured results was shown in a shorter time then it should have been. For instance, a recorded event took place in 3 seconds but it showed in the data file that it happened in 1.0 second. This problem was detected when all the measurements were completed and is taken into account when the measured and simulated results are compared.

A number of data files were generated of starting- and reswitching transient events. Some of these files were exported to a spreadsheet and a mathematical software package (MATHCAD®) for processing.

4.4 Digital filtering

The frequency spectrum of the acceleration signal and the noise correspond closely. This makes it difficult to extract all the noise from the signal as it will degenerate the shape of the signal severely. The measured results were improved with respect to noise if the higher frequencies are removed . This was done applying the FFT as a "brick-wall filter" as shown in Figure 4.4-1 and Figure 4.4-2 on the next pages. Acceptable results were obtained when the cut-off frequency of approximately 110 Hz, determined experimentally, was used.

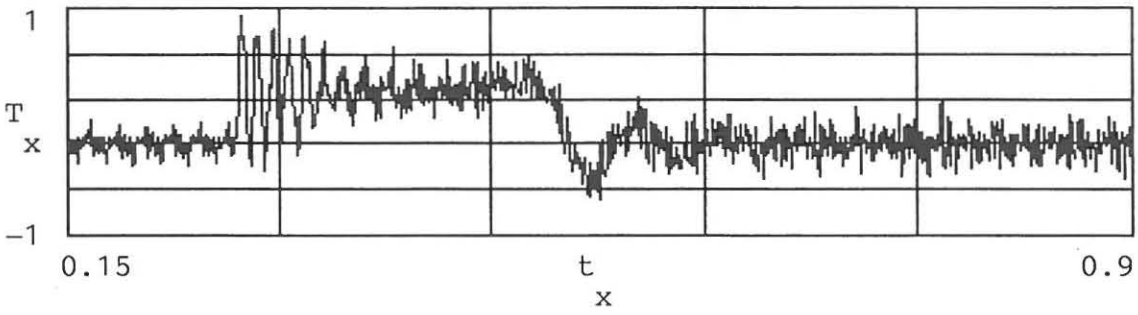

z := fft(T) y := 0 ..1024

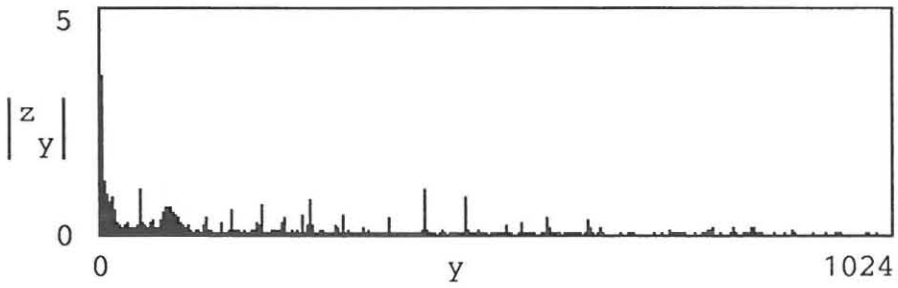

filter := 110 ..1024 z := 0 z := 0 z := 0
filter 53 64

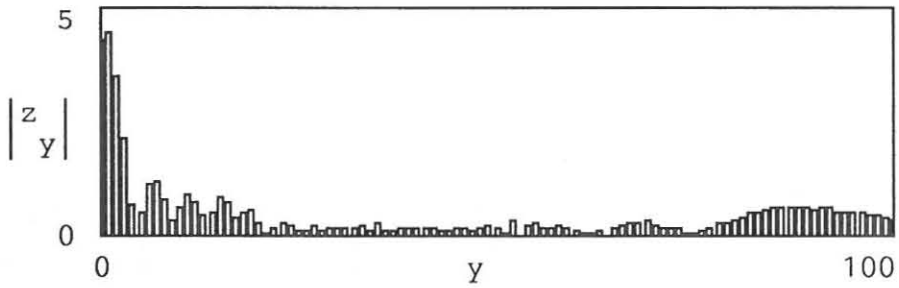

I := ifft(z)

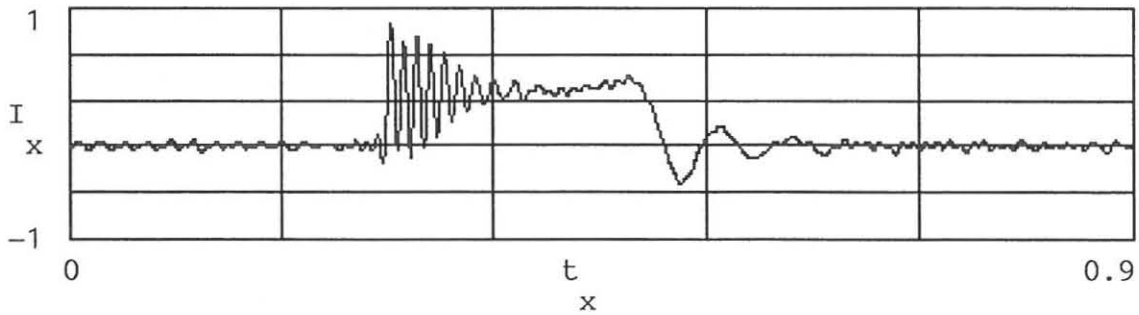

Figure 4.4-1 : Graphs of shaft acceleration during start - up showing the measured result , applying the brick wall filter.

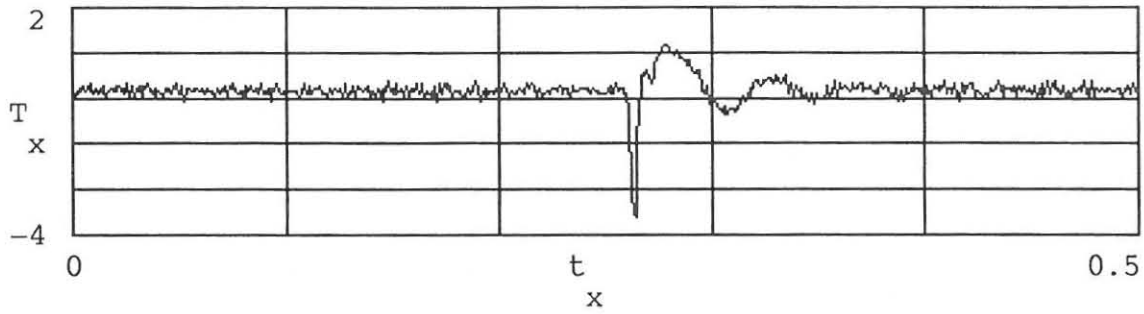

z := fft(T) y := 0 ..256

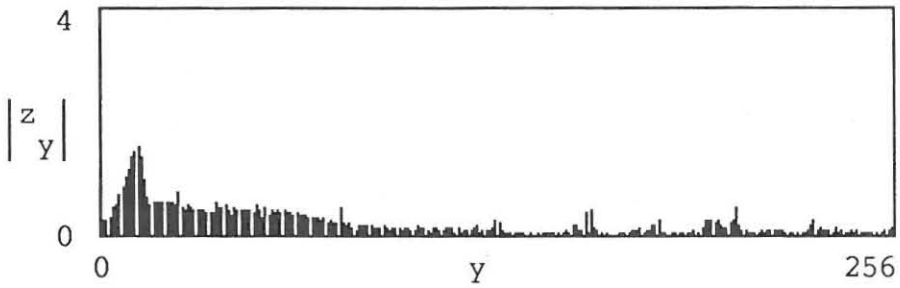

filter := 115 ..256 z := 0 z := 0 z := 0
filter 54 63

z := 0
29

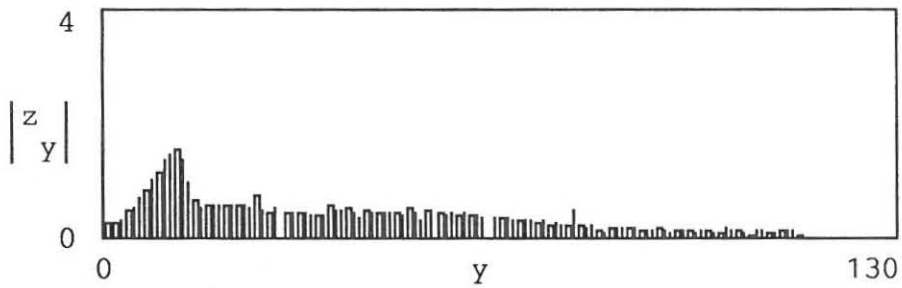

I := ifft(z)

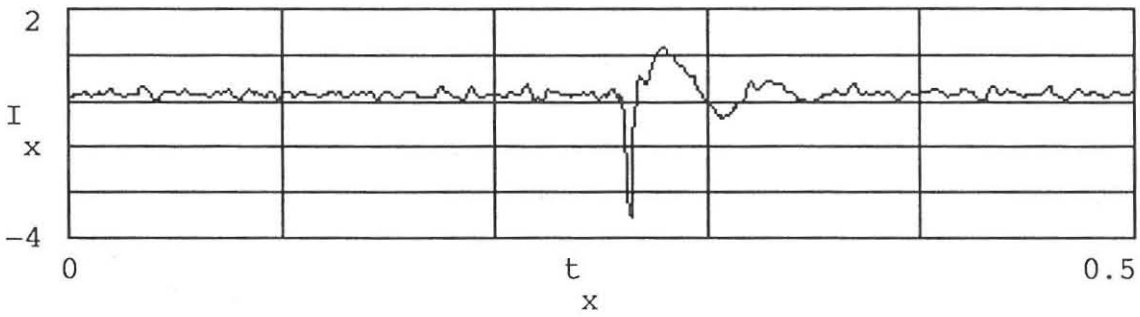

Figure 4.4-2 : Graphs of shaft acceleration during reswitching showing the measured result , applying the brick wall filter. The cut-off frequency was selected in such a way that the magnitudes of the positive and negative torque peaks were not affected by the filter.

4.5 Summary

A very innovative and fairly simple measuring system was used to measure the rotor shaft acceleration during transient conditions. It is especially suited to measure slow changes in rotational velocity. The drawback of this measuring system is that it takes time to set it up properly and it is electrically noisy. To reduce the noise the holes in the discs must be drilled very accurately and this can become a very expensive exercise.

A mathematical filter was used to reduce the influence of the noise on the signal and acceptable results were obtained. Thus the measured results can be compared with the simulated results.

CHAPTER 5

COMPARISON OF MEASURED AND PREDICTED RESULTS

Measurements were taken of the starting and reswitching transient acceleration (or torque) on a 75 kW, 6-pole, 380 V, three phase squirrel cage induction motor. The switching conditions were as follows: Direct On Line starting and restarting. All the run-up measurements were taken on no-load conditions. The details of the motor are recorded in appendix A.

5.1 STARTING TRANSIENTS

When starting an induction motor Direct On Line, the stator and rotor windings can absorb 5-8 times the full-load current, depending on the load inertia and the motor's torque characteristics. The effect of this inrush current can last for several seconds and the stator and rotor windings are subject to large mechanical and thermal stresses during this period.

Large squirrel cage induction motors are now being used to an increasing extent in the petrochemical-, steel manufacture-, mining and oil production industries. The system design engineer usually has to match these motors to the local supply system and to the mechanical load.

If the exact starting characteristics of the motor is known, i.e. the magnitude of the positive peak torque and the pull-out torque, the high frequency oscillatory component and the duration of the transient event, it could be of considerable benefit when a mechanical and/or electrical system is designed or modified.

5.1.1 COMPARISON OF MEASURED AND SIMULATED DATA.

Figure 5.1.1-1 and Figure 5.1.1-2 on the next page shows the measured and simulated starting transients for the motor. Measurements were taken for numerous such starts at different sampling rates and very little difference was observed in the startup transients.

It is clearly seen that there is very good agreement between the measured and predicted results. The duration for the motor to reach its negative torque peak (±0.75 seconds) is well predicted. Also, the magnitude and number of torque oscillations during run-up correlate very well. The most significant magnitudes are recorded in Table 5.1 below :

Table 5.1: Comparison of important torque magnitudes

	Positive torque peak (PU)	Pull-out torque (PU)	Negative torque peak (PU)
Measured	**4.9**	**2.6**	**-1.3**
Simulated	**4.8**	**2.68**	**-1.32**

The difference between the measured and predicted magnitudes can be attributed to the mechanical parameters of the motor (i.e. a small discrepancy in the measured- and the simulated values of the bearing-friction and the inertia of the rotor).

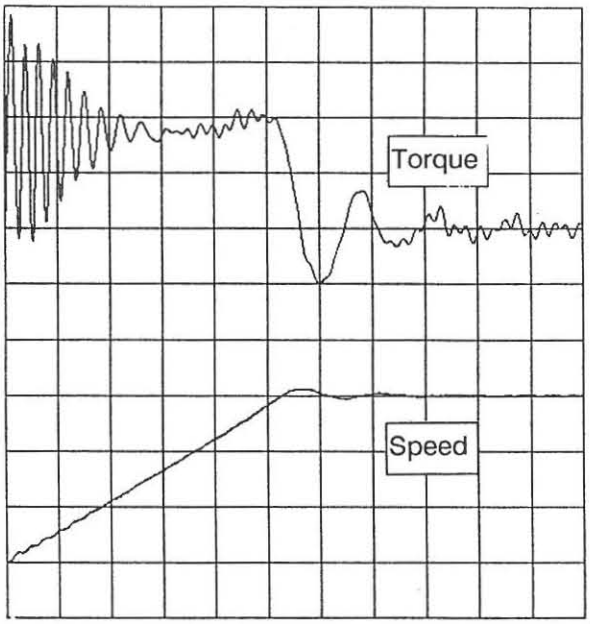

y-axis: torque = **1.3** PU/div. and speed = **0.333** PU/div.
x-axis: time = **0.125** sec/div

Figure 5.1-1: Measured torque and speed trace of the induction motor.

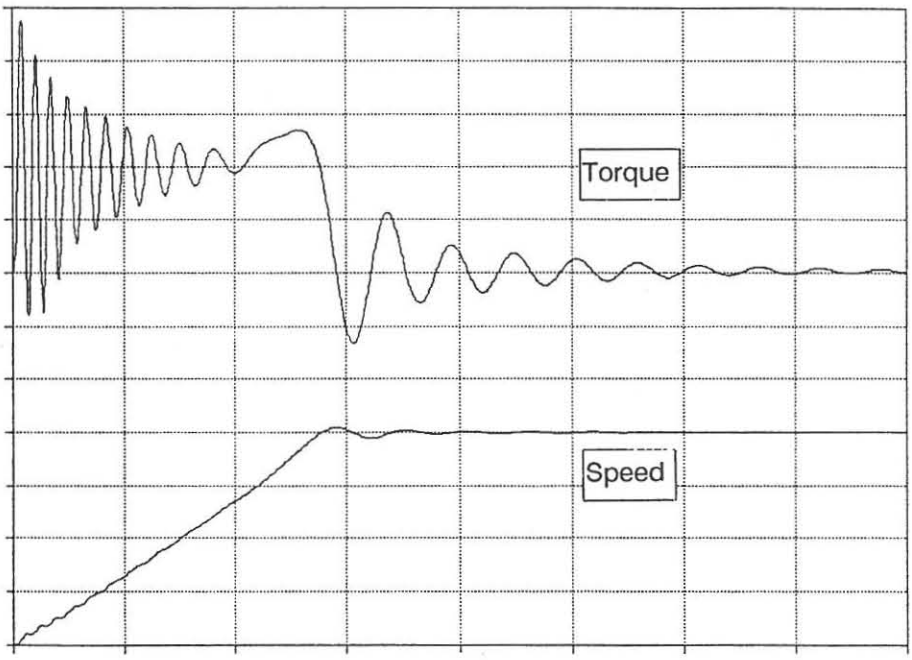

y-axis: torque = **1.0** PU/div. and speed = **0.25** PU/div.
x-axis: time = **0.25** sec/div.

Figure 5.1-2: Simulated torque and speed trace of the induction motor.

It is interesting to note that both the predicted and measured results show that the transient torque actually swings negative during the starting cycle. These values are small and should not be of any consequence to the motor's performance.

Figure 5.1-3 below shows the predicted transient torque speed curve with the typical steady state torque/speed curve superimposed. It can be seen that once the machine is operating close to pull-out torque it is following an almost steady state characteristic.

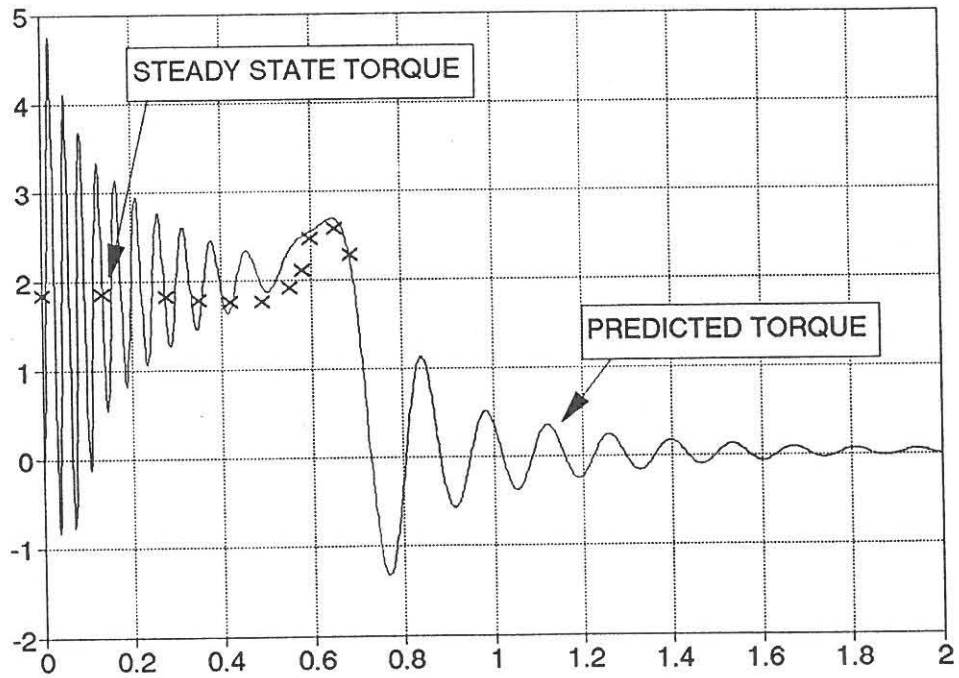

Figure 5.1-3: The steady state response super-imposed on the simulated run-up transient.

5.2 RESWITCHING TRANSIENTS

Reswitching transients occur when a motor has been disconnected and later reconnected to a supply while the rotor is still rotating. The instantaneous current and torque transients may reach several times their normal value. The size and the sign of the transient torque depends on the phase angle between the air gap voltage and the new supply voltage and the amplitude of the air gap voltage when reconnecting. The resulting peak transient torque can be either positive or negative depending on the conditions present at the instant of reconnection. These are the :

- duration of the supply interruption;
- rotor speed;
- load.

Although such an event lasts only for a few cycles, it can subject the mechanical drive system to severe torque imbalances. It is therefore important to accurately determine the amplitude of this torque before completing the design of the drive system.

5.2.1 COMPARISON OF MEASURED AND SIMULATED DATA.

Test data was collected of both positive and negative transient events. The reswitching transients were recorded by breaking and remaking the supply in an arbitrary fashion. Each measurement was taken after the motor was allowed to run up to rated, steady state speed and the rotor-shaft was slightly loaded before switch-off. Comparisons between measured and predicted results was made for a positive and a negative reswitching event.

5.2.1.1 POSITIVE TORQUE TRANSIENTS

The response of the torque and speed during test and simulation are shown in Figure 5.2.1-1 and Figure 5.2.1-2 on the next two pages. The two positive torque peaks shown in the measured results were thought to be the influence of the noise in the measuring system but it is shown in the simulated result in Figure 5.2.1-2 that these peaks are part of the inherent characteristics of the motor under test.

In both the measured and simulated results the first positive torque peaks have magnitudes in the excess of +5.5 PU which means that the motor has exerted a positive torque of more than twice the designed pull-out torque of 2.6 PU. The change in direction of the torque from +5.5 PU to -2.8 PU in 0.09 seconds is interrupted by secondary, smaller torque signals which in effect damp the effect of the sudden change from a positive to a negative direction. The first torque peak is in the same direction as the rotation of the shaft and has twice the magnitude of the negative torque peak so that there is no severe mechanical strain on the rotor shaft. The important magnitudes are compared in Table 5.2-1 below:

Table 5.2.1: Comparison of important reswitching torque magnitudes.

	Positive torque peak (PU)	Negative torque peak (PU)
Measured	**+5.6**	**-2.8**
Simulated	**+5.5**	**-2.8**

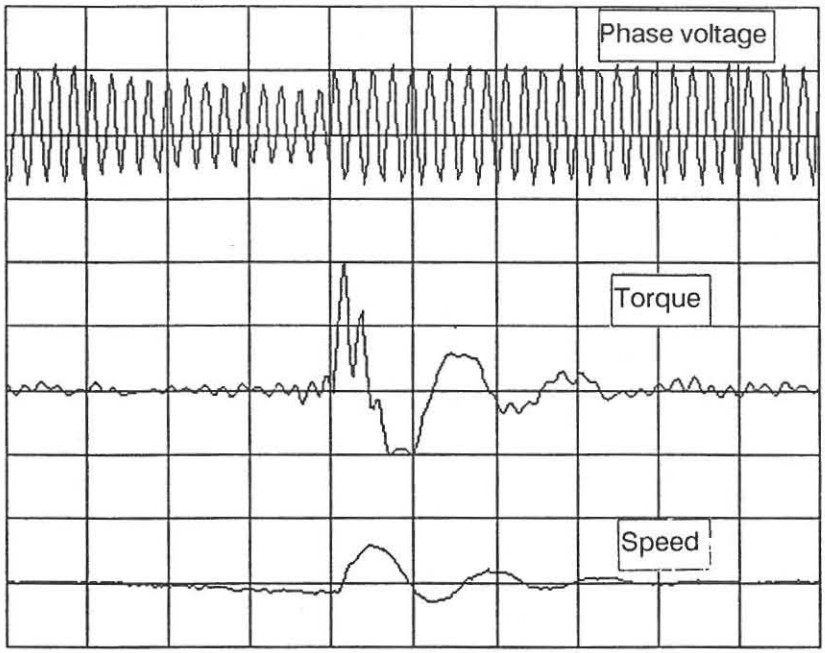

y-axis: torque = **2.8** PU/div. and speed = **0.125** PU/div.
x-axis: time = **0.08** sec/div. The supply was disconnected for 12.5 cycles (0.25 seconds) and then remade.

Figure 5.2.1-1: Measured torque and speed trace of the induction motor during reswitching of the supply.

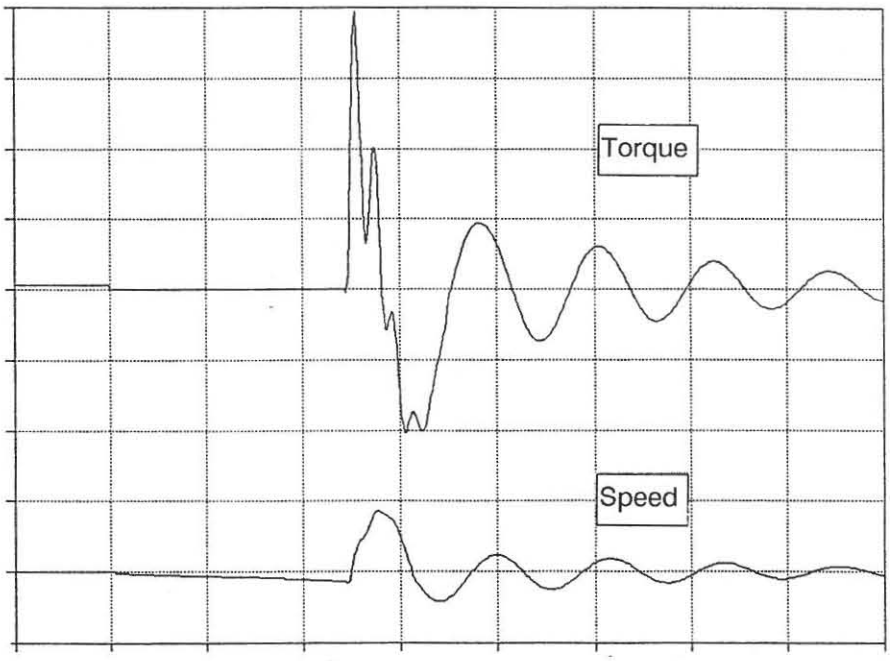

y-axis: torque = **1.4** PU/div. and speed = **0.09** PU/div.
x-axis: time = **0.1** sec/div. The supply was disconnected for 12.25 cycles (0.245 seconds) and then remade.

Figure 5.2.1-2: Simulated torque and speed trace of the induction motor during reswitching of the supply.

5.2.1.2 NEGATIVE TORQUE TRANSIENTS

The response of the torque and speed during test and simulation are shown in Figure 5.2.1-3 and Figure 5.2.1-4 on the next page. The noise in the pre-transient signal has the same shape and size as the small peaks in the negative and positive parts of the transient signal. It is therefore assumed that the transient torque peaks are slightly smaller than shown in the measured results. As shown in Figure 5.2.1-3 the switch-off duration was again measured in terms of the number of cycles of the supply reference voltage (±33 cycles). The measured and simulated results show a negative torque peak of -9 PU and the first positive torque peak of +3 PU. This gives a change in torque of 12 PU in approximately 3 cycles (0.06 seconds).

It is interesting to note that the direction and magnitude of the transient reswitching torque is very dependent on the instant of remake after switch-off. It has been recorded in the literature (Landy, 1970:71 and Say, 1978:339) that these negative torques are worst when the motor is reswitched with the supply voltage and rotor induced voltage being 180° out of phase. Important magnitudes are listed in Table 5.2.2.

Table 5.2.2: Comparison of important reswitching torque magnitudes.

	Positive torque peak (PU)	Negative torque peak (PU)
Measured	**3.0**	**-9.0**
Simulated	**3.0**	**-9.1**

The results again show that good correlation was achieved between measured and predicted transients.

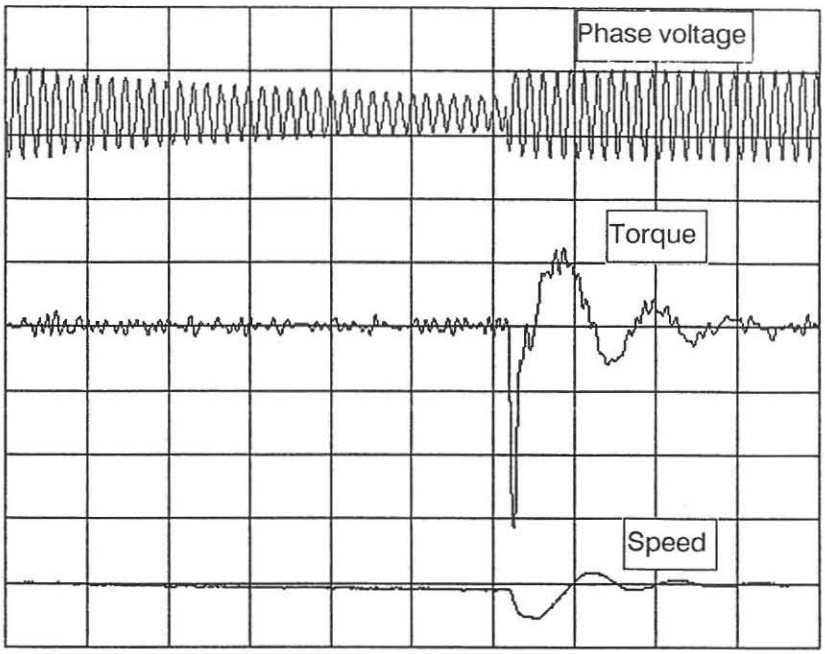

y-axis: torque = **3** PU/div. and speed = **0.24** PU/div.
x-axis: time = **0.12** sec/div. The supply was disconnected for 33 cycles (0.66 seconds) and then remade.

Figure 5.2.1-3: Measured torque and speed trace of the induction motor during reswitching of the supply.

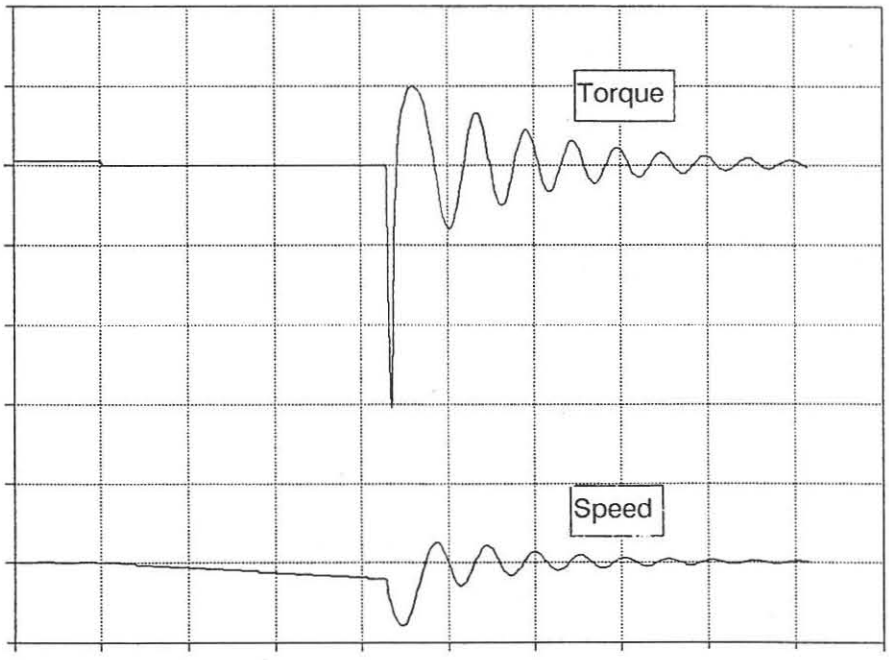

y-axis: torque = **3** PU/div. and speed = **0.16** PU/div.
x-axis: time = **0.2** sec/div.

Figure 5.2.1-4: Simulated torque and speed trace of the induction motor during reswitching of the supply.

5.3 BROKEN BAR MEASUREMENTS

Seeing that an identical machine having a broken rotor bar was available and that the transient measuring system had been developed, it was decided to take starting and reswitching measurements on the machine with the broken bar as well. The purpose of these measurements was merely to examine whether the presence of the broken bar produced any significant variation in the starting and reswitching transients.

5.3.1 STARTING TRANSIENTS

The starting transients where measured with the shaft in four different positions as shown in Figure 5.3-1. The slot in the shaft was used as a reference and it was rotated through 90 mechanical degrees for each new measurement.

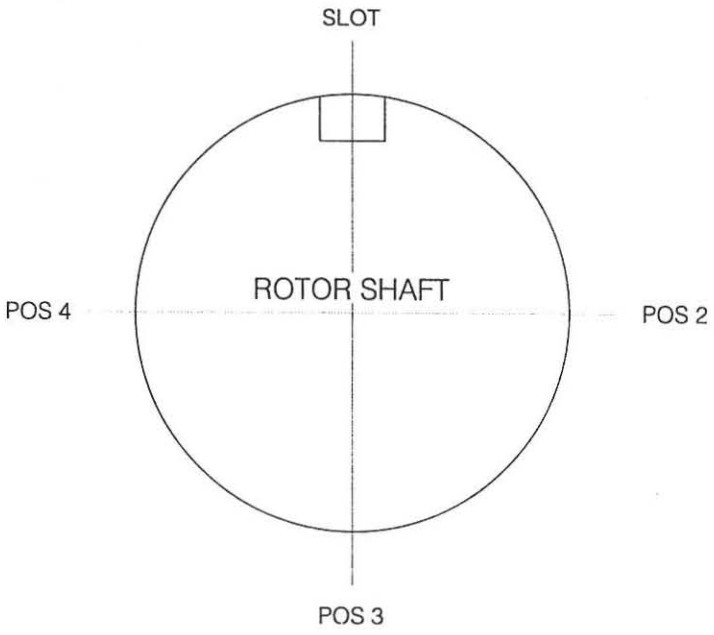

Figure 5.3-1: The different positions through which the slot was rotated.

All the measurements were taken within 1 hour and the supply voltage was constant at 385 V for the duration of the measuring period. The results of some of these measurements are shown in Figure 5.3-2 through to Figure 5.3-5.

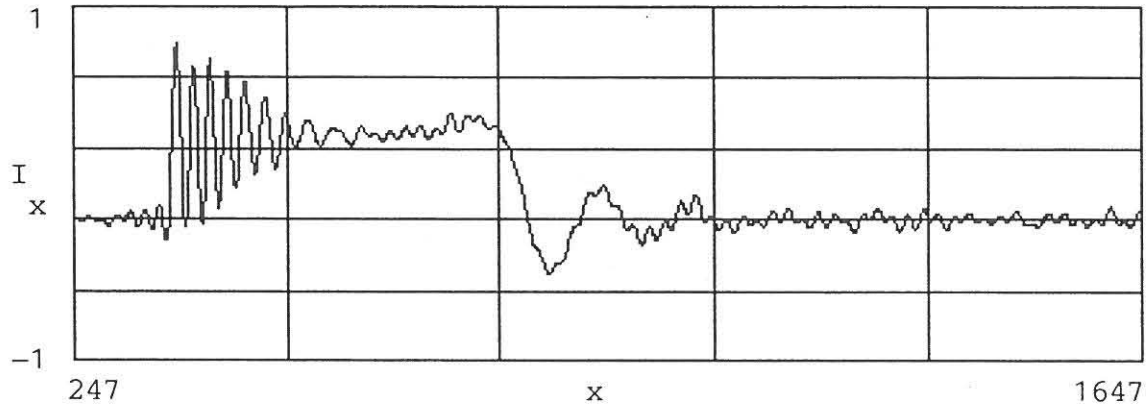

Figure 5.3-2: Starting transient measured with the slot in the top position.

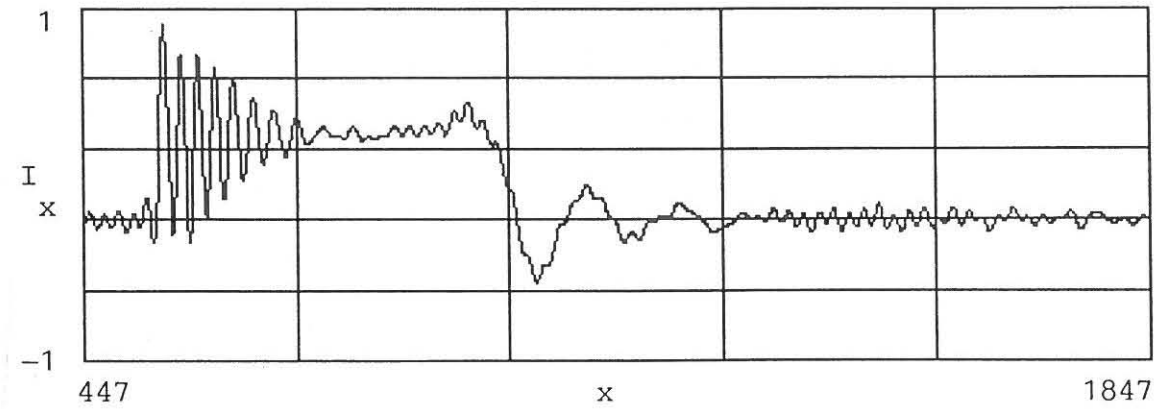

Figure 5.3-3: Starting transient measured with the slot in position 2.

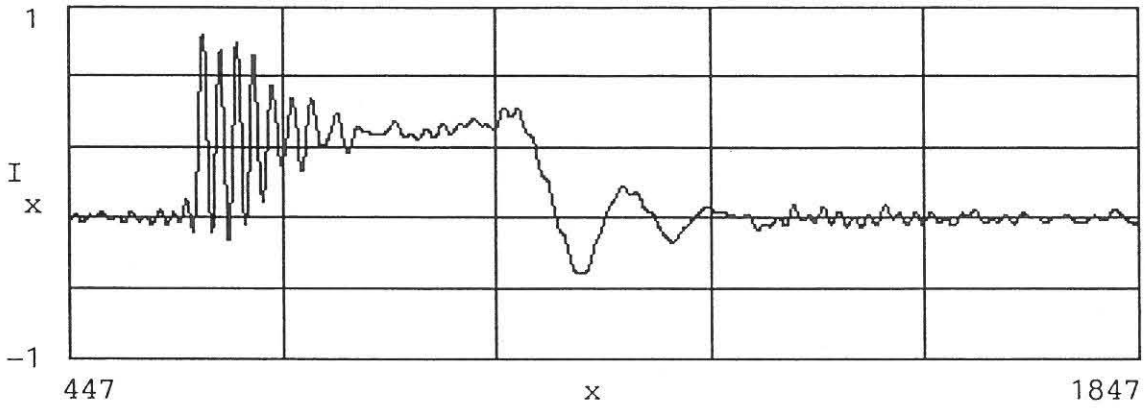

Figure 5.3-4: Starting transient measured with the slot in position 3

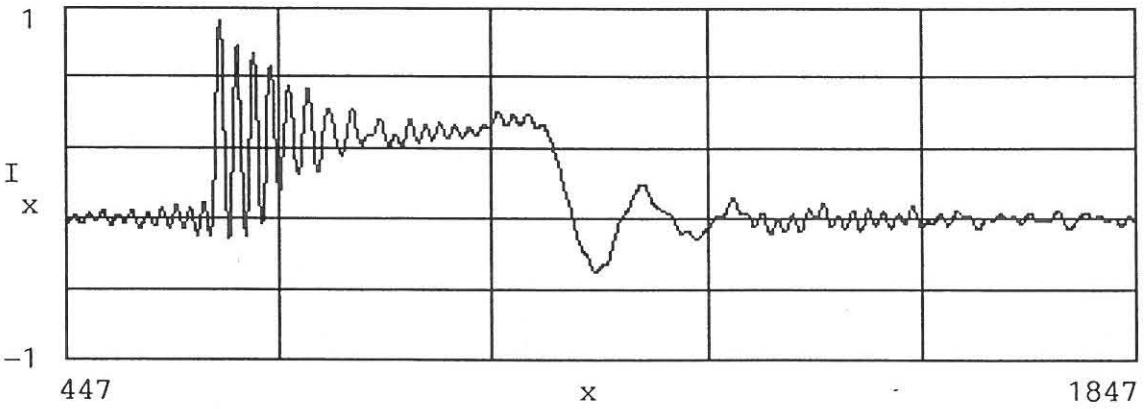

Figure 5.3-5: Starting transient measured with the slot in position 4.

It can be seen from Figure 5.3-2 through to Figure 5.3-5 that the shape of the starting transient was dependent on the physical position of the rotor at the time of starting. In contrast, the healthy cage machine could be started in any position and the shape of the transient torque would stay constant. Five run-up transients from the broken bar motor were recorded for each position and these measurements are shown in Appendix B for comparison.

5.3.2 RESWITCHING TRANSIENTS

Reswitching transients were measured of the broken rotor under the same conditions as stipulated in the first paragraph of section 5.2.1. Nevertheless, the measurements on the broken bar machine showed a greater tendency to produce large negative torque transients as shown in Figure 5.3-6 through to Figure 5.3-10. These negative peaks were all in the excess of -8 PU.

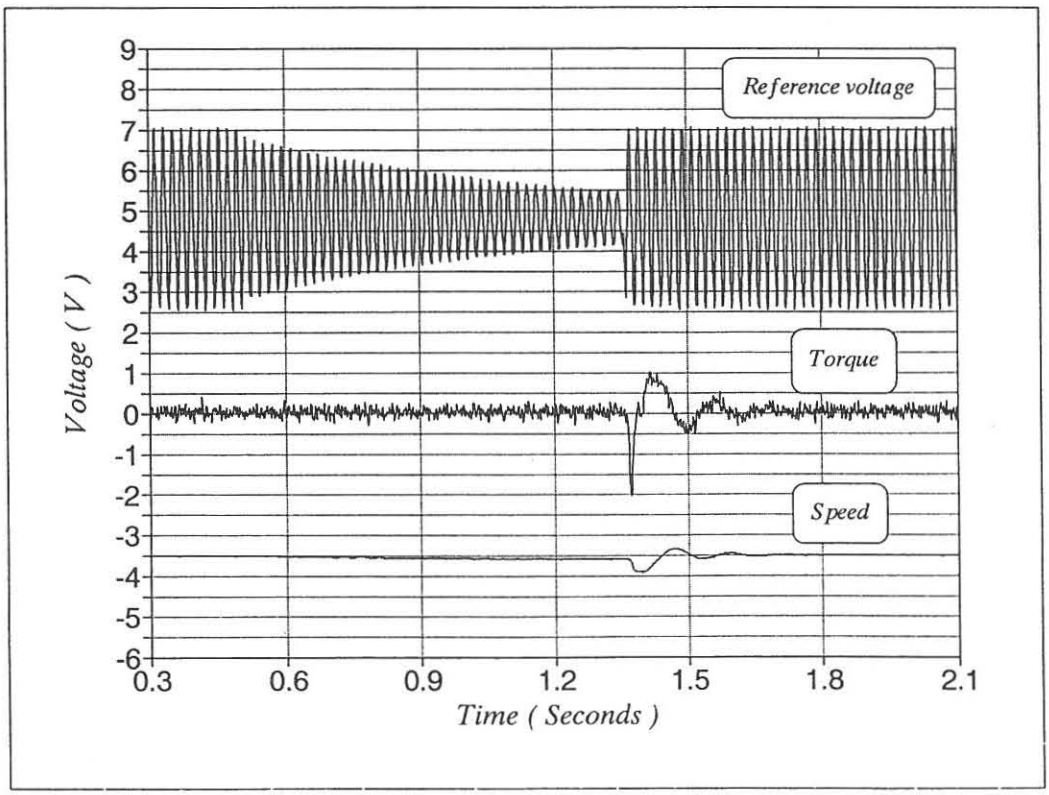

y-axis: torque = **4.2** PU/volt. Negative peak torque = ± **8.4** PU

Figure 5.3-6: A measured torque and speed trace of the induction motor with the **broken bar** neglecting the noise on the signal.

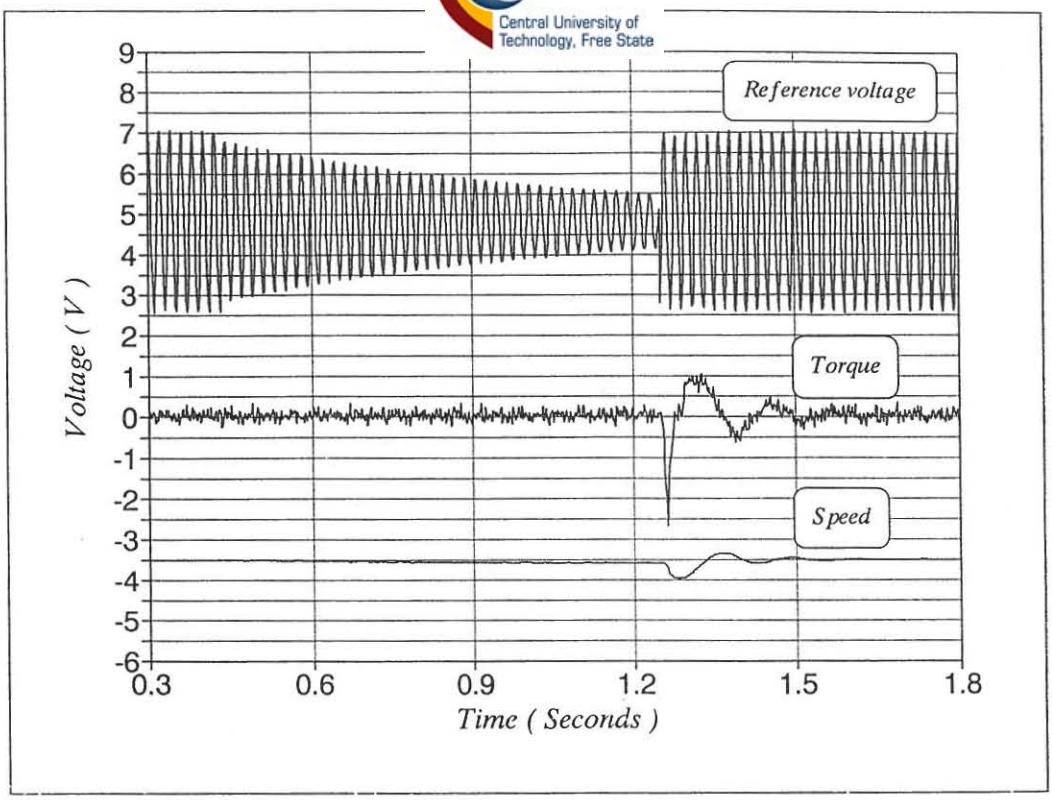

y-axis: torque = **4.2** PU/volt. Negative peak torque = ± **11** PU

Figure 5.3-7: A measured torque and speed trace of the induction motor with the **broken bar** neglecting the noise on the signal.

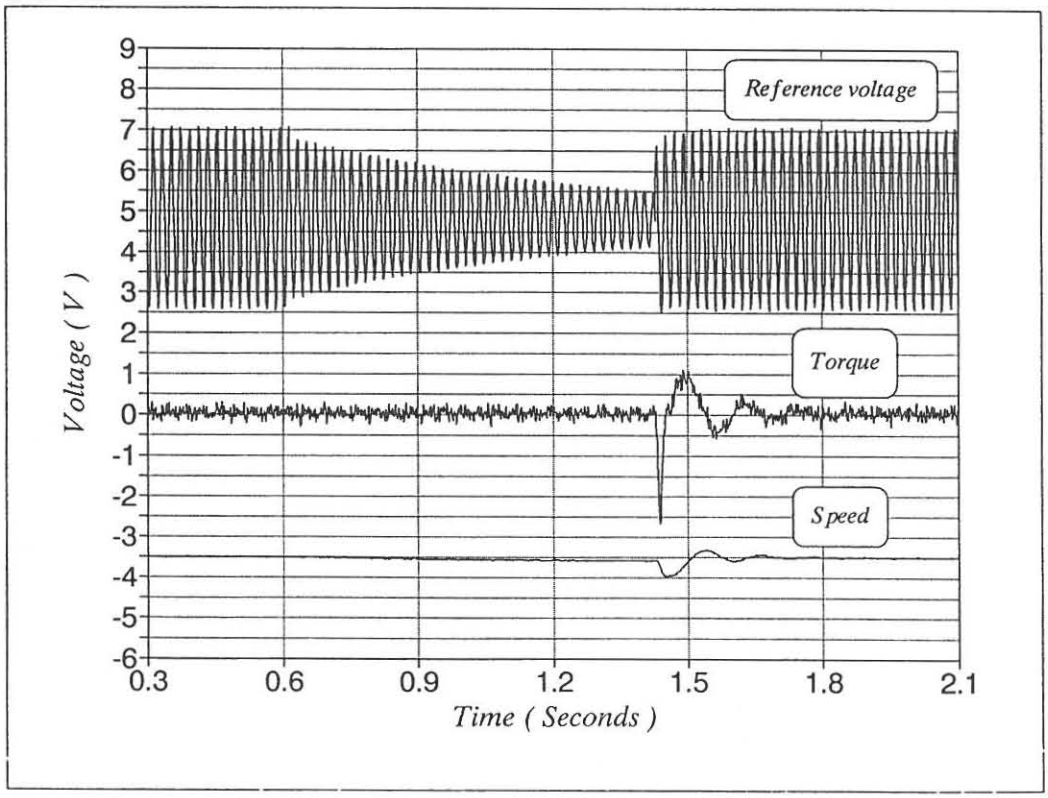

y-axis: torque = **4.2** PU/volt. Negative peak torque = ± **11** PU

Figure 5.3-8: A measured torque and speed trace of the induction motor with the **broken bar** neglecting the noise on the signal.

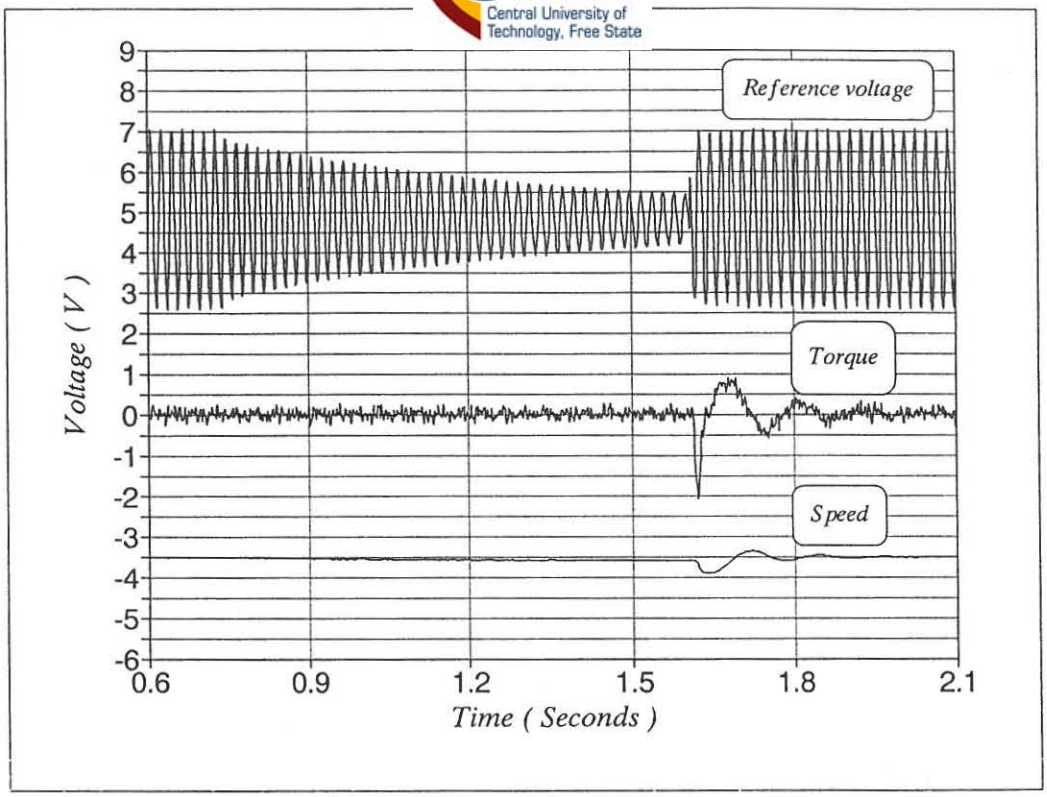

y-axis: torque = **4.2** PU/volt. Negative peak torque = ± **8.8** PU

Figure 5.3-9: A measured torque and speed trace of the induction motor with the **broken bar** neglecting the noise on the signal.

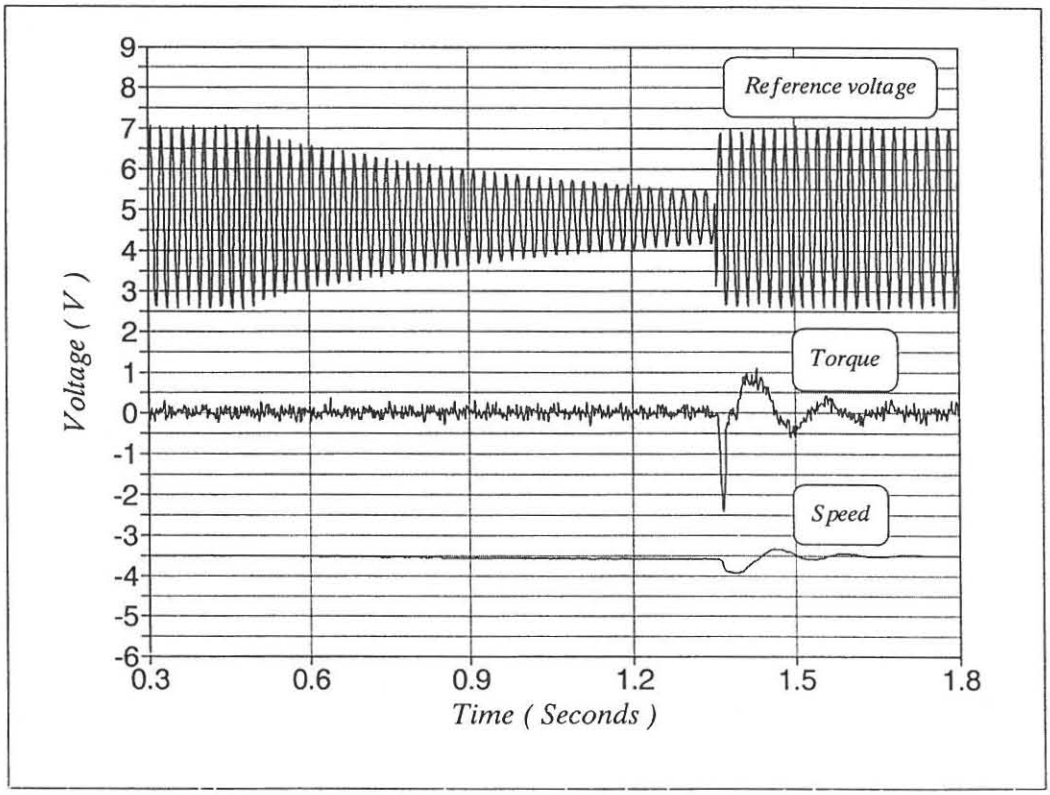

y-axis: torque = **4.2** PU/volt. Negative peak torque = ± **10** PU

Figure 5.3-10: A measured torque and speed trace of the induction motor with the **broken bar** neglecting the noise on the signal.

Figure 5.3-11 and Figure 5.3-12 shows the negative torque peaks produced by the motor with the "healthy" cage. The measurement of these torque peaks were not as consistent as the negative torque peaks obtained with measurements on the broken rotor.

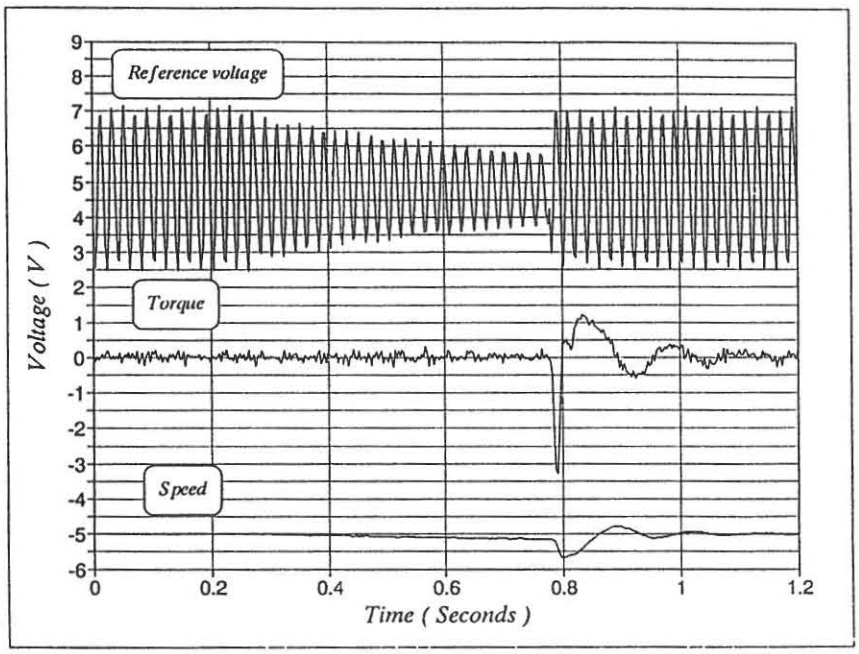

y-axis: torque = **4.2** PU/volt. Negative peak torque = ± **13.8** PU

Figure 5.3-11: A measured torque and speed trace of the induction motor with the **healthy cage** neglecting the noise on the signal.

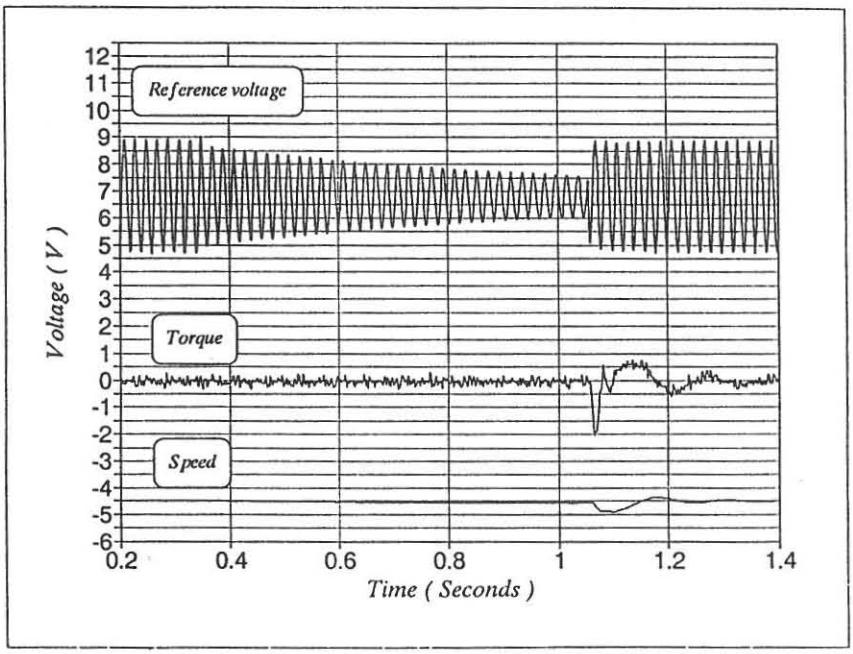

y-axis: torque = **4.2** PU/volt. Negative peak torque = ± **7.9** PU

Figure 5.3-12: A measured torque and speed trace of the induction motor with the **healthy cage** neglecting the noise on the signal.

5.4 Conclusion

The difference in the magnitudes between the measured and simulated results of the starting and reswitching transients varies by less than 3%. This difference is negligible for all practical purposes. Simulating the start-up, positive- and negative reswitching transients of the induction motor shows that the deep bar model in the CASED software package gives a very close correlation with the measured values. Smith (1990:68), Figure 3.13 also shows measured and predicted starting transients for a large squirrel cage motor. These results appear to be for a machine that displays very little deep bar properties and look similar to those shown in Figure 3.3-1 on page 35. Besides Smith's results (1990:68) there are very few measured results recorded in the literature. None of these show comparisons between measurement and simulation. The published results available are either measured (Wood, Flynn and Shanmugasundaram, 1965:1352) or simulated (Kraus and Thomas, 1965:1052) and (Ghani,1988:185).

It can be seen from Figure 5.2.1-1 and Figure 5.2.1-3 that the magnitude and sign of the reswitching transients are dependent on the time the circuit breaker takes to reclose. It is shown that the deep bar model can accurately predict these events (which depends on the mechanical system to which the motor is connected). It has the following benefits:

- The motor- and load shaft sizes and the coupling system can now be optimized during the design stage to reduce the effect of these reswitching transients on the mechanical system.

- The reclosing time of the supply circuit breaker to the induction motor can be adjusted so that the magnitude of a transient negative torque peak is kept to a minimum.

The measurements on the induction motor with the broken bar show that the transient behaviour of this motor is related to the condition of the cage. It is beyond the scope of this project to investigate this more fully but the author is convinced that this is an area for future meaningful research. It is anticipated that if these differences can be quantified, this type of transient measurement may become a successful tool to be used in assessing the state of the cage of a large squirrel cage induction motor.

CHAPTER 6

SUMMARY

Levy (1990:12) has developed and tested a deep bar model to predict the starting and reswitching transients of induction motors. The main objective of this project was to obtain additional measurements of transient behaviour of a large induction motor so that prediction of induction motor starting and reswitching characteristics using this deep bar model could be further substantiated. This could only be achieved if the measurement system was made to function correctly and if meaningful simulations of the machine tested were successfully completed. The correlation between the measured- and simulated results clearly demonstrates that this objective has been attained.

In chapter 2 the equations describing the transient behaviour of an induction motor are discussed and in chapter 3 the simulation software which incorporates these equations is described. Simulations comparing the deep bar model with the traditional model are shown.

The construction, advantages and disadvantages of the transient measurement system are discussed in chapter 4. The measurement system has a high response time, a wide bandwidth and is also able to supply useful information at very low rotational speeds e.g. the starting and plugging of electric motors. The noise on the signal, which is a distinct disadvantage has been overcome by careful digital filtering.

In chapter 5 the measured and simulated results are analysed. It is clear from the measured results achieved that this system is very suitable for the measurement of these torque and speed transients. The excellent correlation

achieved between the measured and simulated results shows that the CASED program has meaningful models of the machine system giving reliable simulated results. The validity of these predicted results could only be established because a highly successful measurement system was developed.

A new, compact measurement system with a very high signal to noise ratio was developed at the OFS Technikon. Using this system, transient torque measurements will be done on a serviceable 3 kW deep bar induction motor to confirm the results obtained in chapter 5. In this manner the validity of the deep bar model with regard to much smaller machines, will be verified.

Additional measurements taken on an identical 75 kW motor with a broken rotor bar are also shown in chapter 5. The additional research on the motor with the broken rotor bar was intended to be purely observational rather than qualitative. The shape and magnitude of the run-up transient torque measurements of the broken rotor are not consistent. A thorough investigation, using a measuring system with a very low electric noise level, needs to be done to confirm the findings shown in Appendix B. Similar results, on a range of induction motor with broken rotor bars, could lead to a very economical diagnostic tool to analyse the condition of the rotor cage in any squirrel cage induction motor.

APPENDIX A

Motor details

Power = 75 kW

Number of phases = 3

Connection = Delta (for all the measurements taken)

Supply frequency = 50 Hz

Supply line voltage = 385 V

Number of poles = 6

Speed = 990 rev/min.

Stator winding resistance = 0.04383 Ω per phase.

Stator leakage reactance = 0.26717 Ω per phase.

Rotor cage resistance = 0.05521 Ω per phase.

Rotor leakage reactance = 0.70716 Ω per phase.

Magnetising reactance = 10.6191 Ω per phase.

Inertia = 1.667 kg.m^2

Central University of Technology, Free State

APPENDIX B

Starting transients of the 75 kW induction motor with the broken rotor bar.

All the starting measurements on this motor were taken on the same day. The supply voltage was slightly imbalanced at 384 V, 385 V and 384 V per phase. The data sampling rate was kept constant at 2048 samples @ 2000 Hz. The highest signal frequency component in any data file was less than 40 Hz so that the sampling frequency was adequate and the filter frequency (see paragraph 4.4) was kept constant for all the data files.

Five measurements were taken for each of the four slot positions. The measurements are shown in Figure B-1 through to Figure B-20 on the next 20 pages. In Figure B-1 the first graph shows a sample of the noisy signal. The second graph shows all the frequency components of the signal. In the third graph the filtered components are shown and the last graph shows the filtered signal.

M := READPRN(slot2)

x := 0 ..2047

t := M⟨0⟩

T := M⟨2⟩

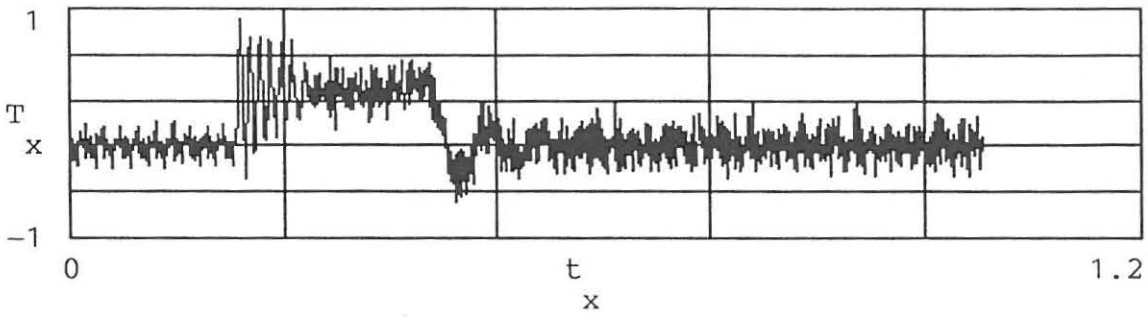

z := fft(T)

y := 0 ..1024

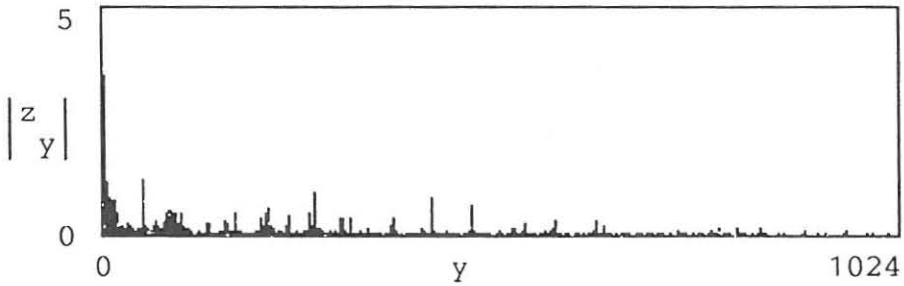

filter := 110 ..1024

z := 0
filter

z := 0
53

z := 0
64

I := ifft(z)

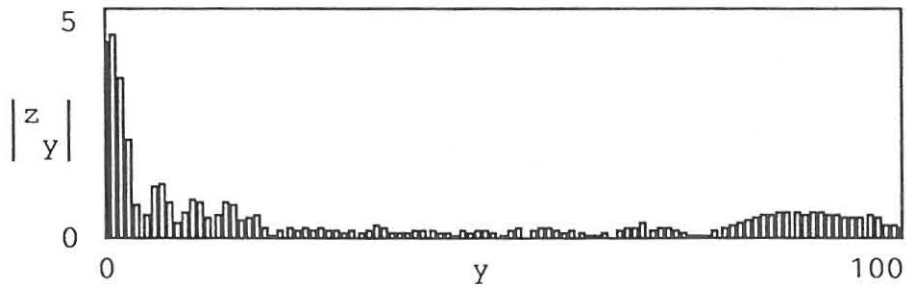

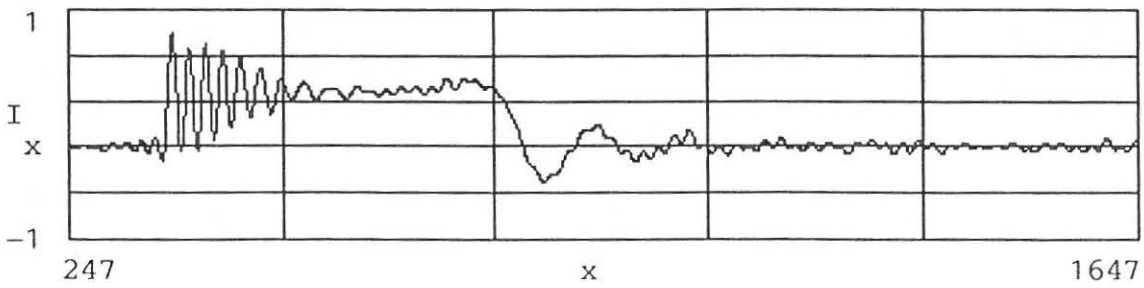

Figure B-1: First starting transient measured with the slot in the top position.

M := READPRN(slot3)

x := 0 ..2047

t := M⟨0⟩

T := M⟨2⟩

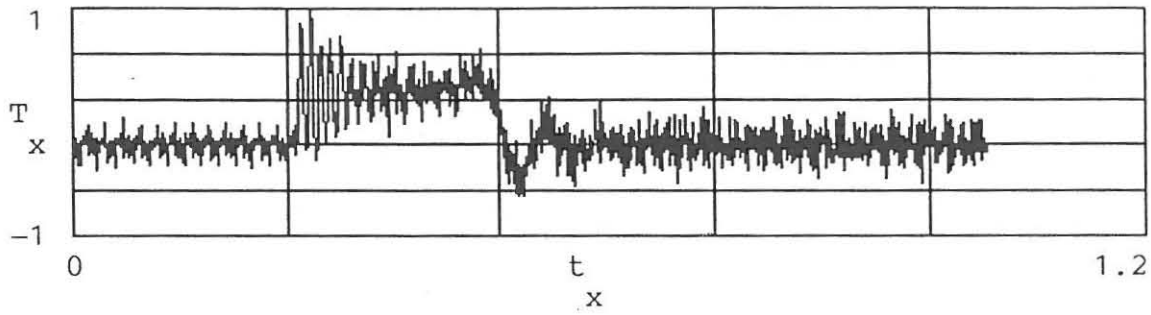

z := fft(T)

y := 0 ..1024

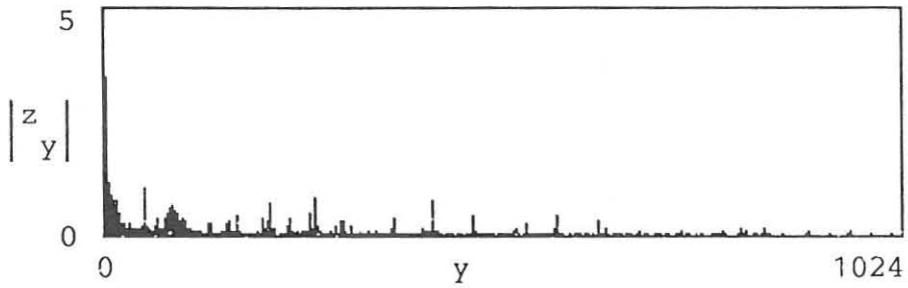

filter := 110 ..1024

z := 0
filter

z := 0
53

z := 0
64

I := ifft(z)

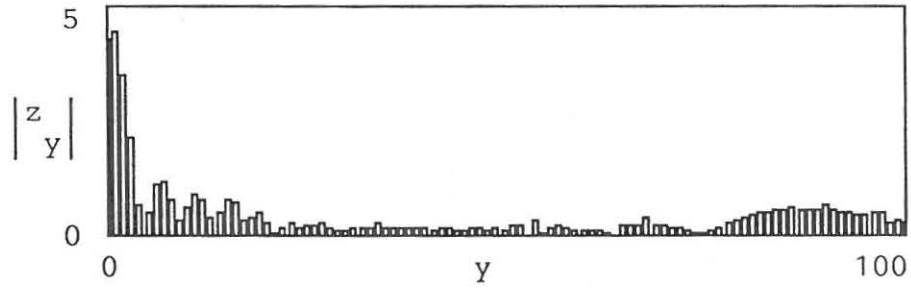

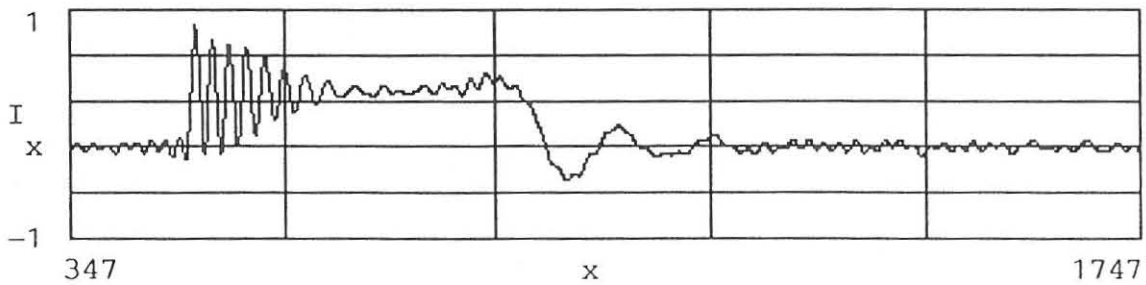

Figure B-2: Second starting transient measured with the slot in the top position.

M := READPRN(slot4)

x := 0 ..2047

⟨0⟩ ⟨2⟩

t := M T := M

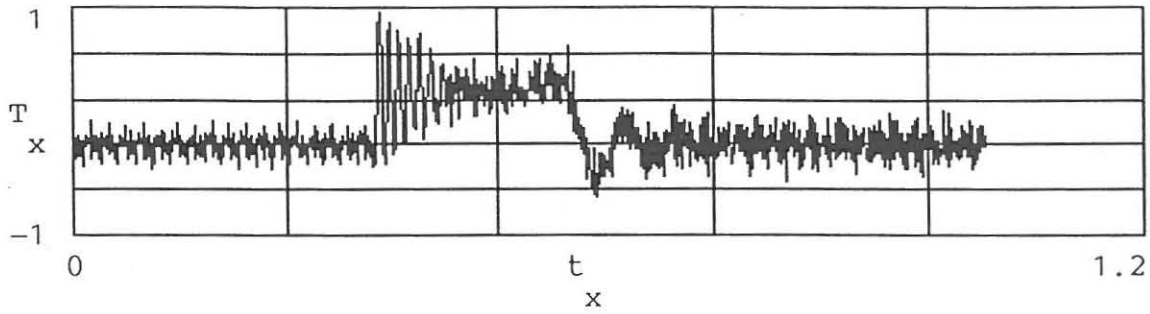

z := fft(T) y := 0 ..1024

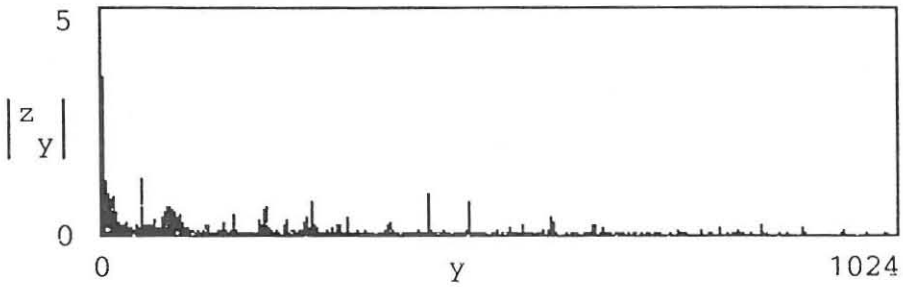

filter := 110 ..1024 z := 0 z := 0 z := 0
filter 53 64

I := ifft(z)

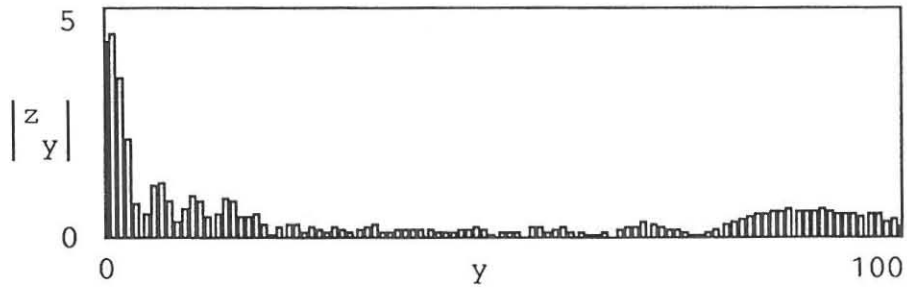

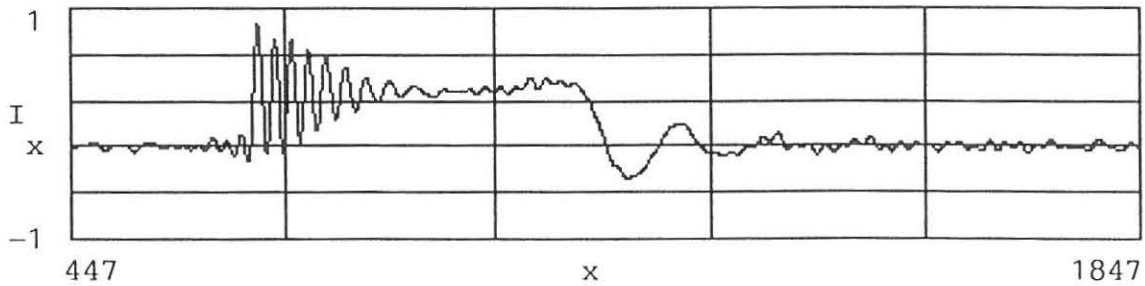

Figure B-3: Third starting transient measured with the slot in the top position.

M := READPRN(slot5)

x := 0 ..2047

<0>

t := M

<2>

T := M

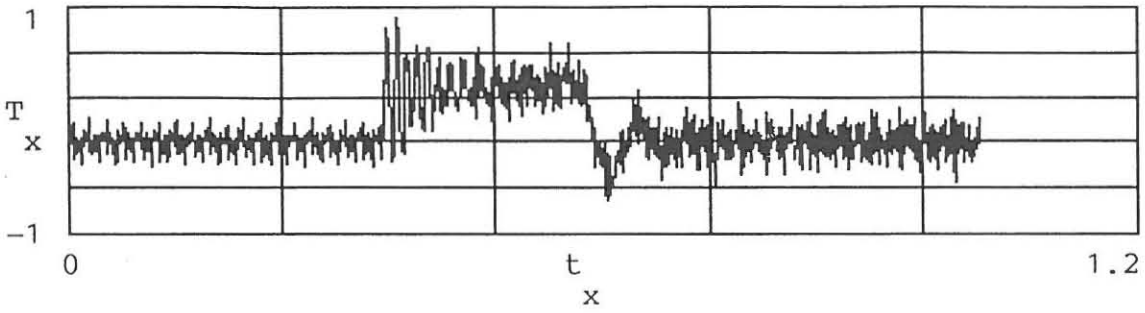

z := fft(T)

y := 0 ..1024

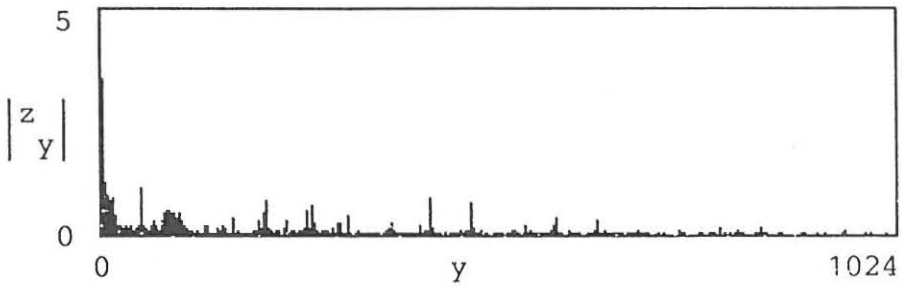

filter := 110 ..1024

z := 0
filter

z := 0
53

z := 0
64

I := ifft(z)

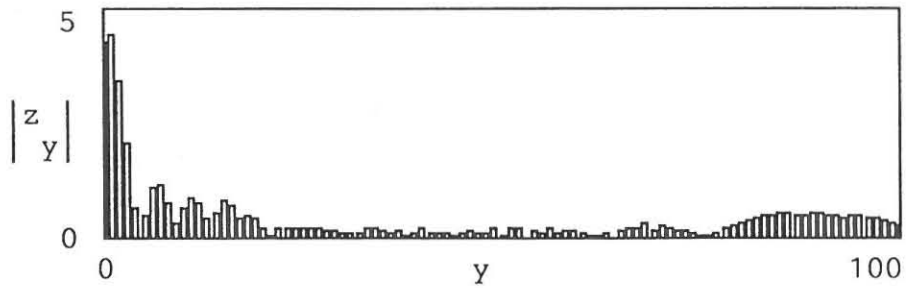

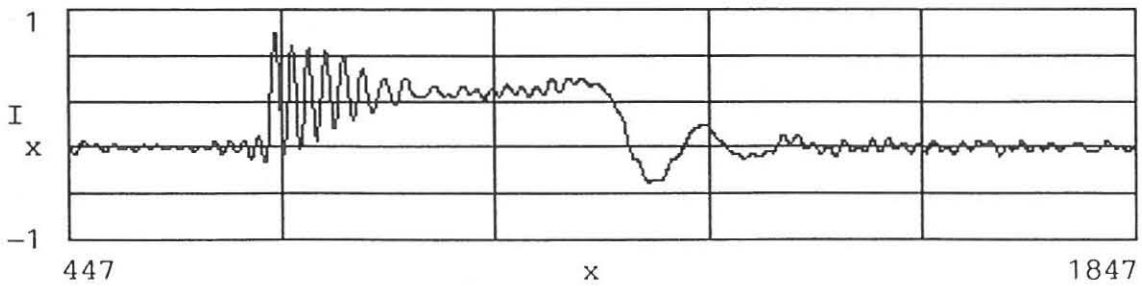

Figure B-4: Fourth starting transient measured with the slot in the top position.

M := READPRN(slot6)

x := 0 ..2047

t := M ⟨0⟩

T := M ⟨2⟩

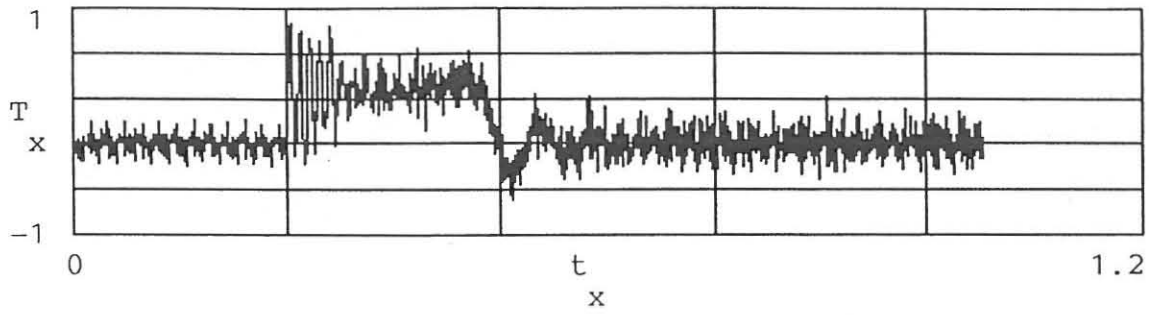

z := fft(T)

y := 0 ..1024

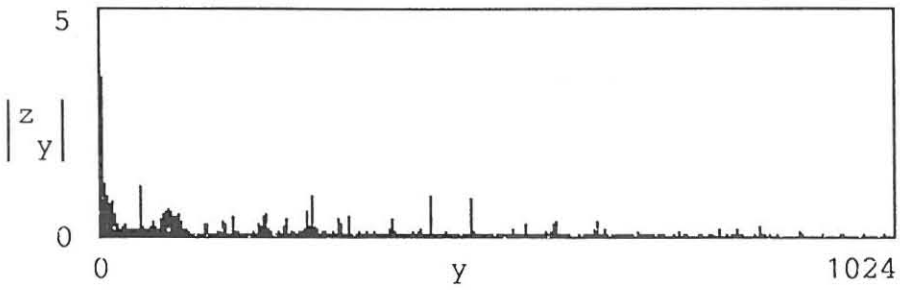

filter := 110 ..1024

z := 0
filter

z := 0
53

z := 0
64

I := ifft(z)

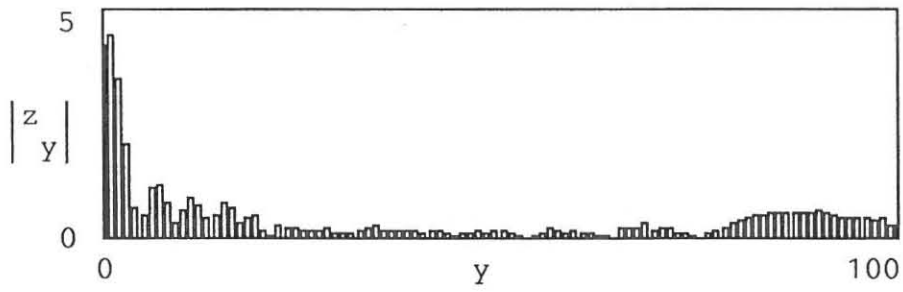

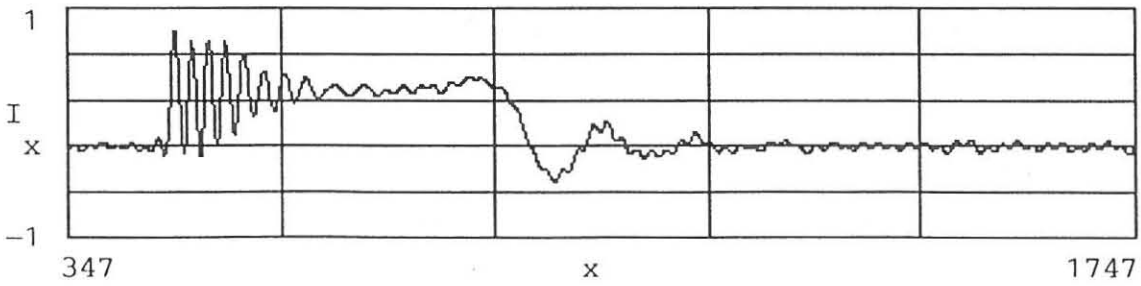

Figure B-5: Fifth starting transient measured with the slot in the top position.

M := READPRN(pos2a)

x := 0 ..2047

t := M⟨0⟩

T := M⟨2⟩

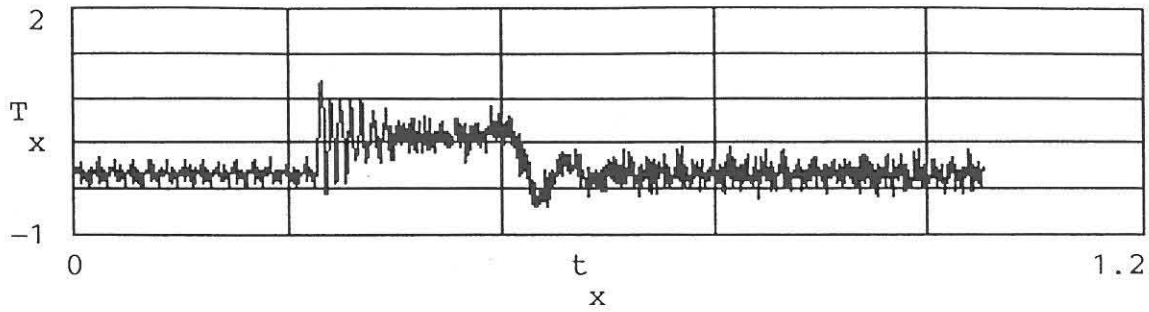

z := fft(T)

y := 0 ..1024

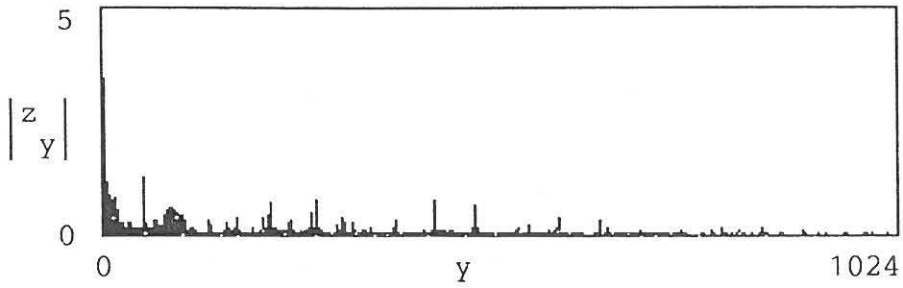

filter := 110 ..1024

z := 0
filter

z := 0
53

z := 0
64

I := ifft(z)

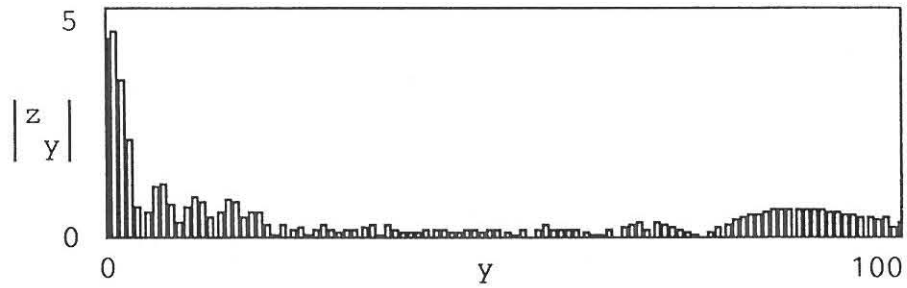

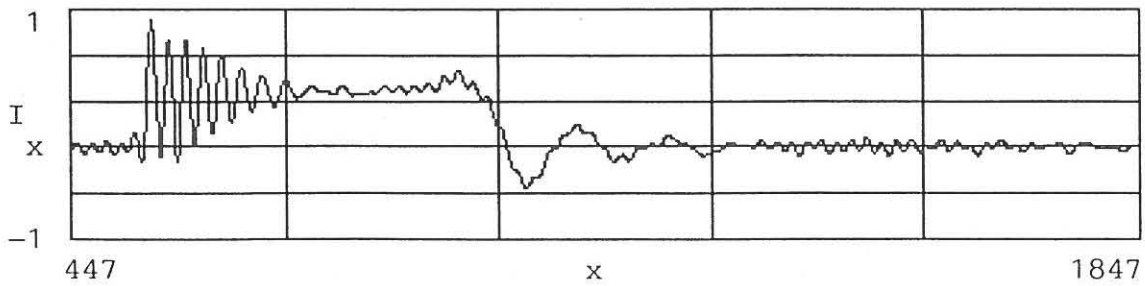

Figure B-6: First starting transient measured with the slot in position 2.

M := READPRN(pos2b)

x := 0 ..2047

t := M⟨0⟩

T := M⟨2⟩

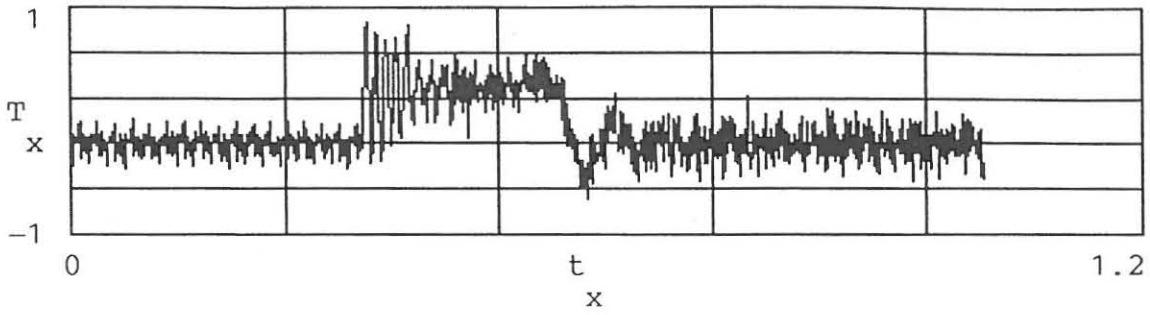

z := fft(T)

y := 0 ..1024

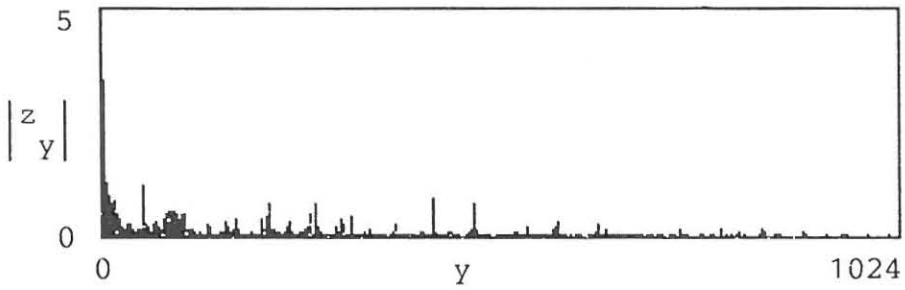

filter := 110 ..1024

z := 0
filter

z := 0
53

z := 0
64

I := ifft(z)

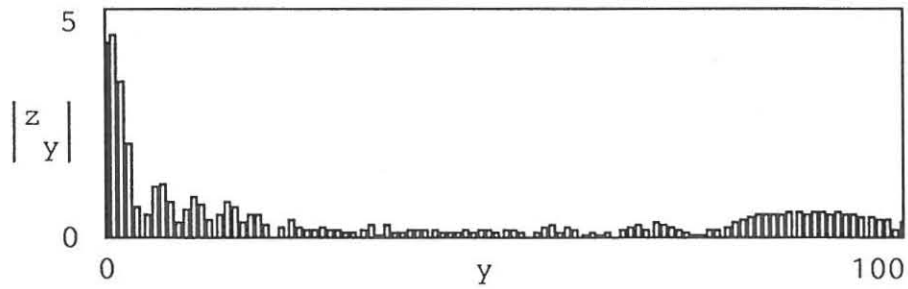

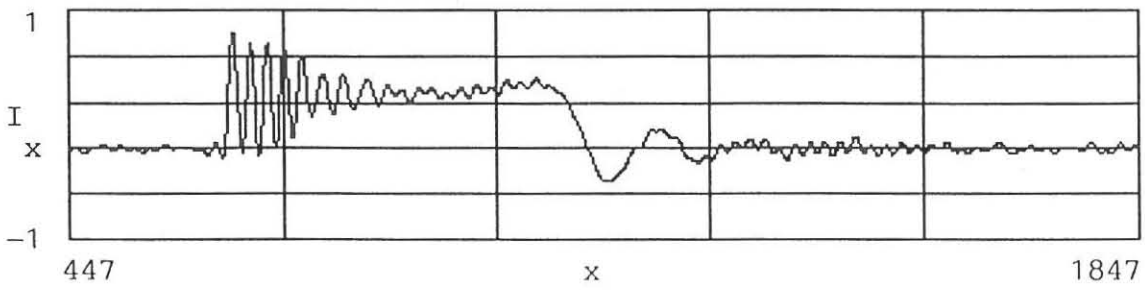

Figure B-7: Second starting transient measured with the slot in position 2.

M := READPRN(pos2c)

x := 0 ..2047

t := M⟨0⟩

T := M⟨2⟩

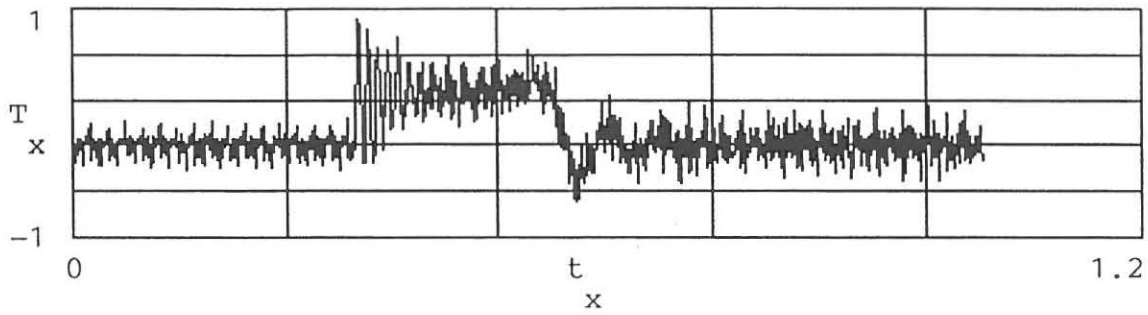

z := fft(T)

y := 0 ..1024

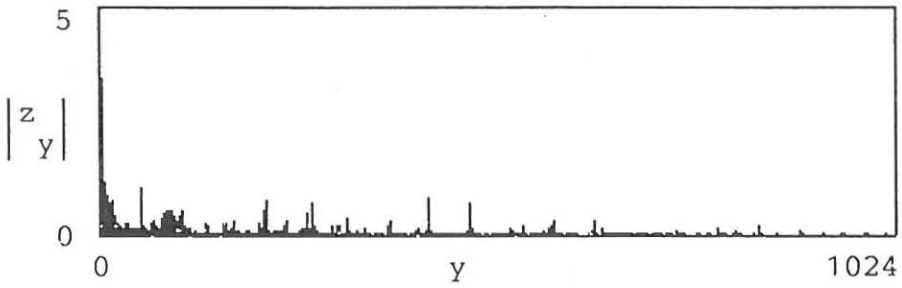

filter := 110 ..1024

z := 0
filter

z := 0
53

z := 0
64

I := ifft(z)

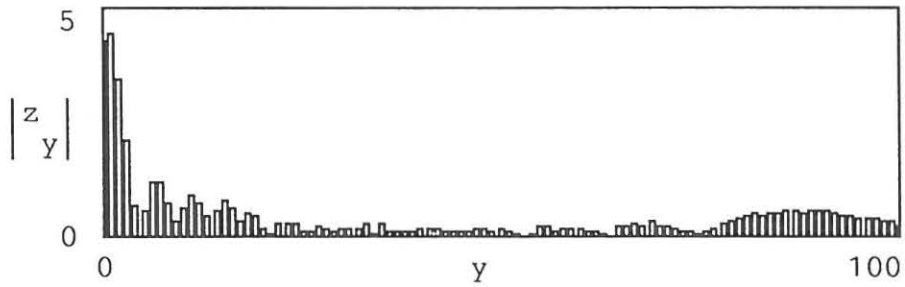

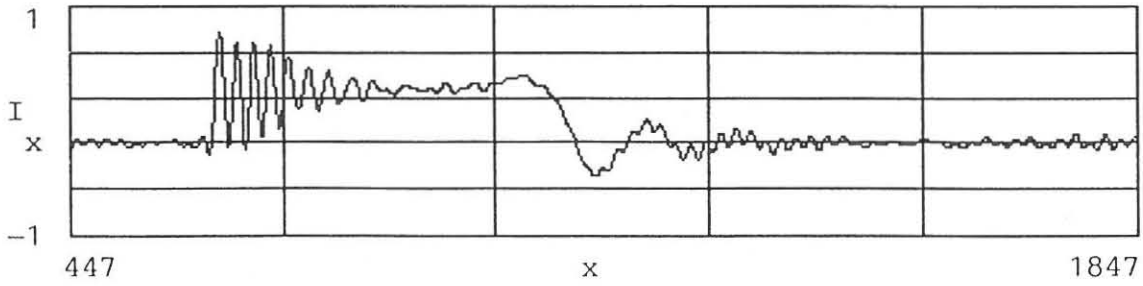

Figure B-8: Third starting transient measured with the slot in position 2.

M := READPRN(pos2d) x := 0 ..2047

t := M⟨0⟩ T := M⟨2⟩

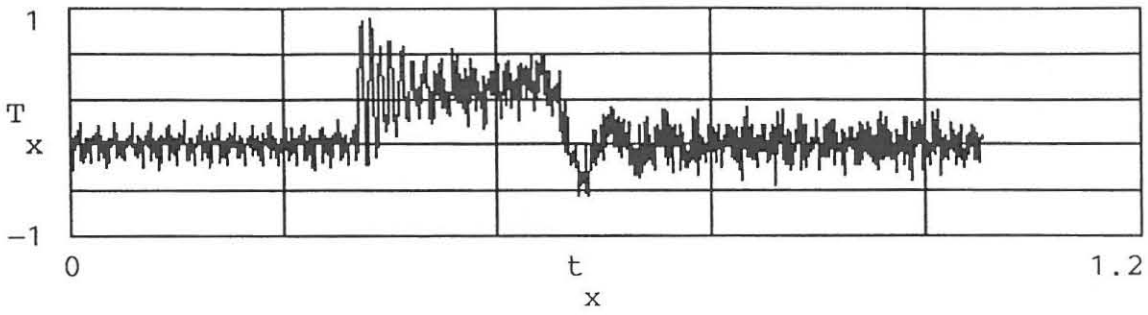

z := fft(T) y := 0 ..1024

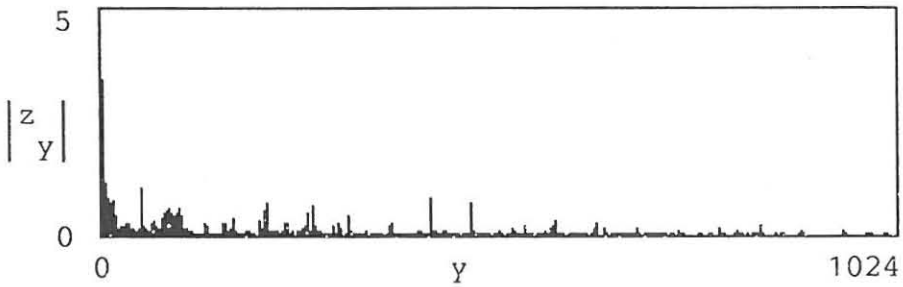

filter := 110 ..1024 z := 0 filter z := 0 53 z := 0 64

I := ifft(z)

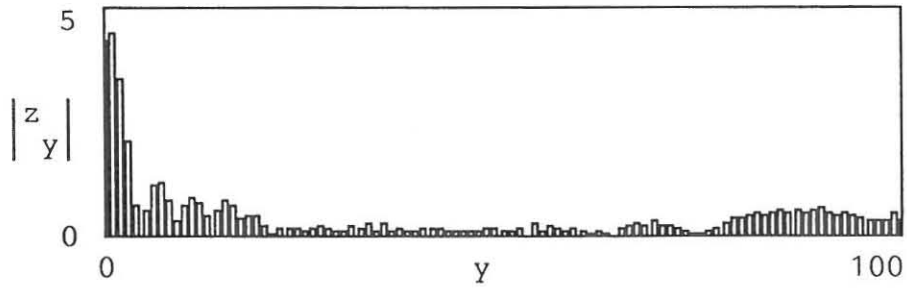

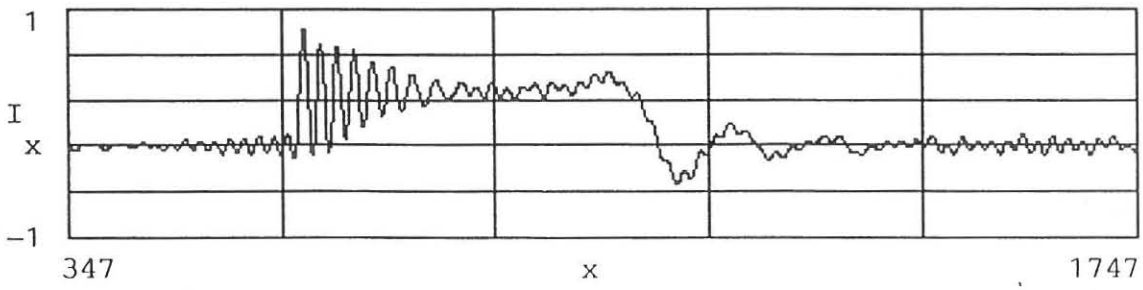

Figure B-9: Fourth starting transient measured with the slot in position 2.

M := READPRN(pos2e)

x := 0 ..2047

t := M⟨0⟩

T := M⟨2⟩

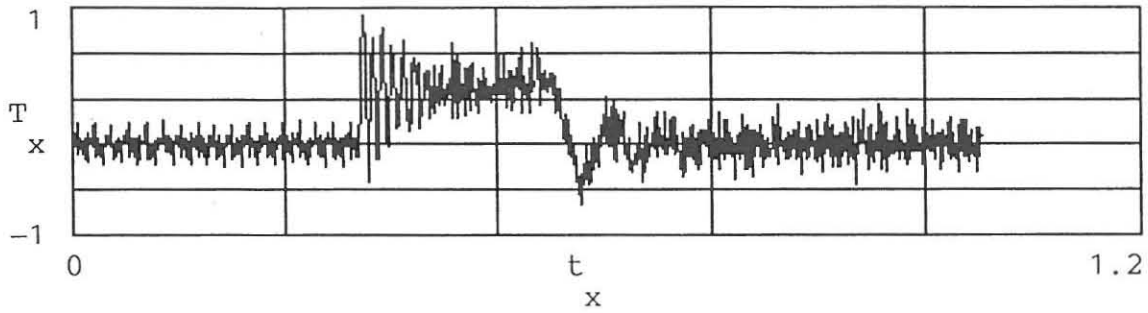

z := fft(T)

y := 0 ..1024

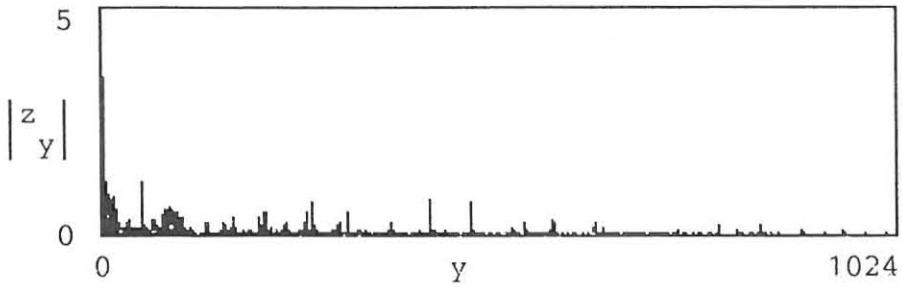

filter := 110 ..1024

z := 0
filter

z := 0
53

z := 0
64

I := ifft(z)

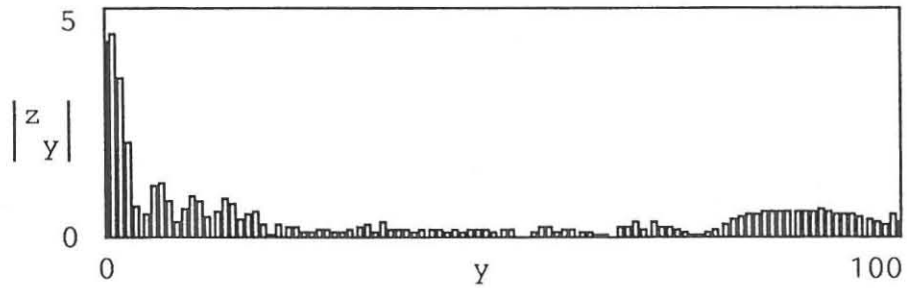

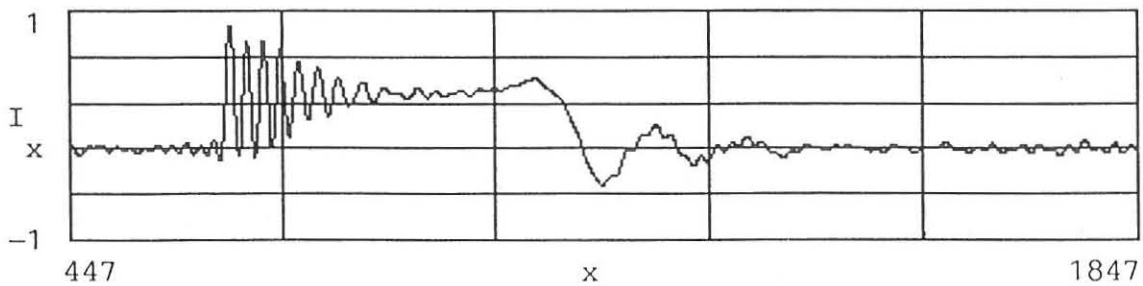

Figure B-10: Fifth starting transient measured with the slot in position 2.

M := READPRN(pos3a)

x := 0 ..2047

t := M⟨0⟩

T := M⟨2⟩

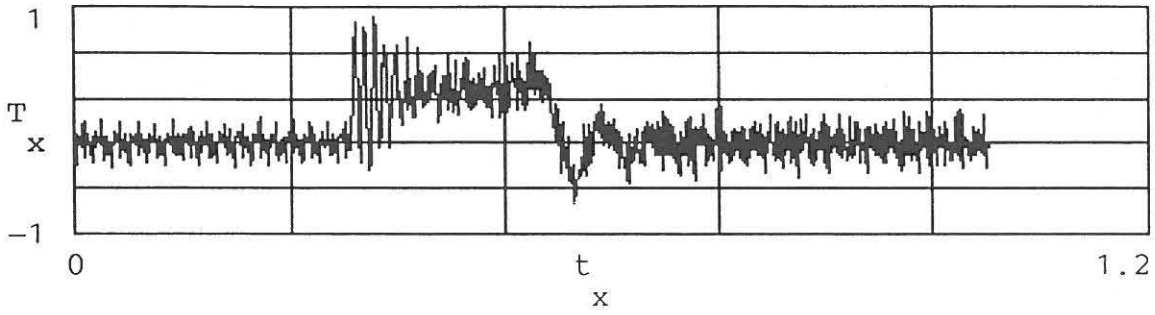

z := fft(T)

y := 0 ..1024

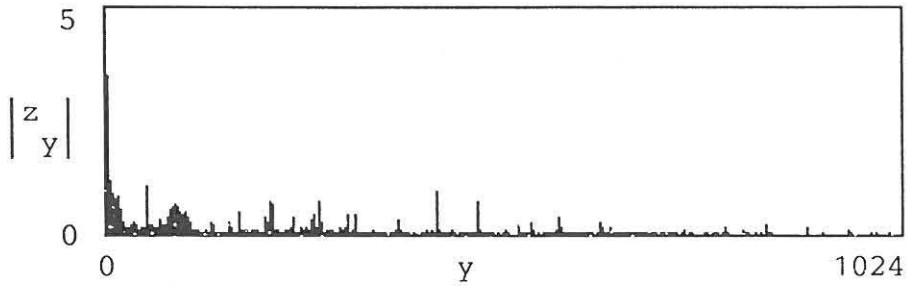

filter := 110 ..1024

z_filter := 0

z_53 := 0

z_64 := 0

I := ifft(z)

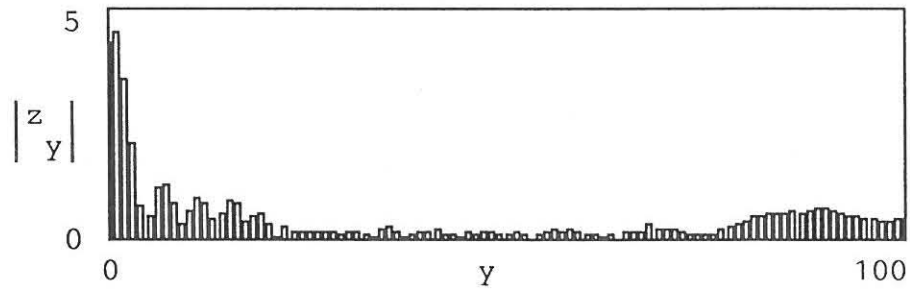

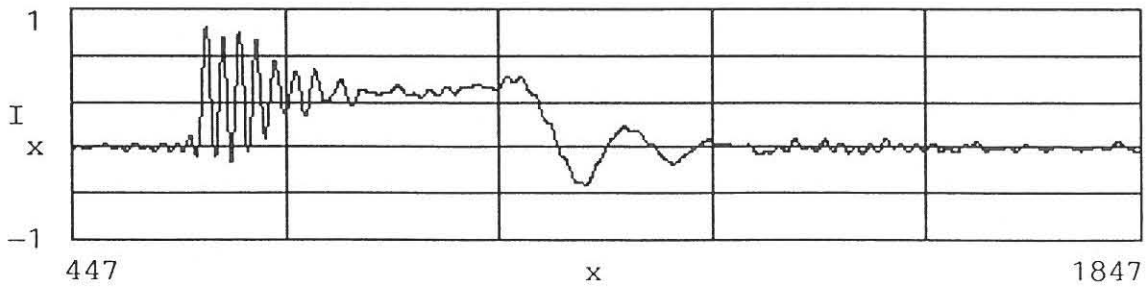

Figure B-11: First starting transient measured with the slot in position 3.

M := READPRN(pos3b) x := 0 ..2047

t := M⟨0⟩ T := M⟨2⟩

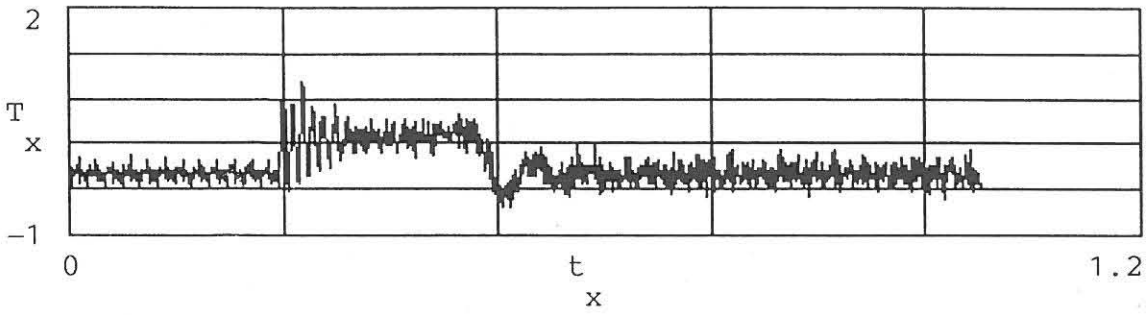

z := fft(T) y := 0 ..1024

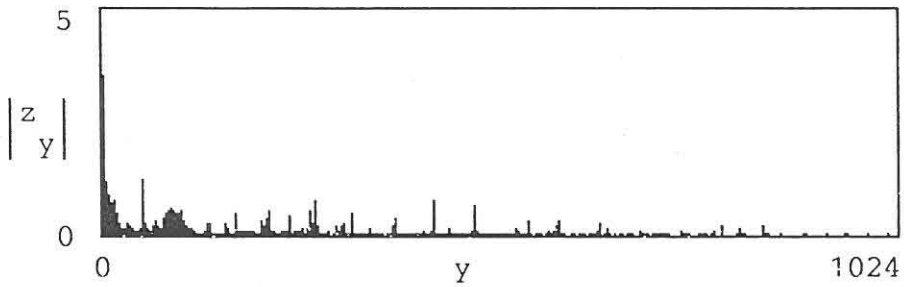

filter := 110 ..1024 z_filter := 0 z_53 := 0 z_64 := 0

I := ifft(z)

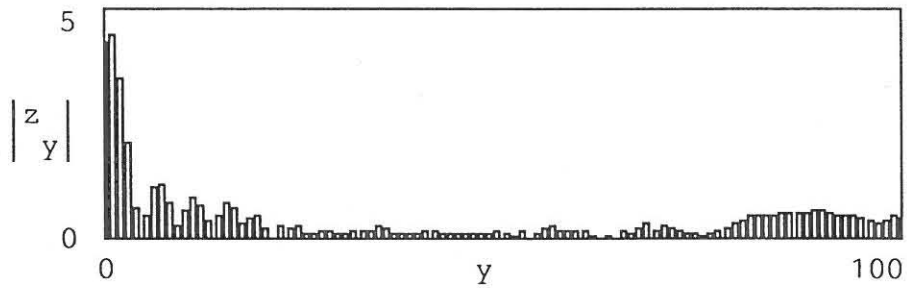

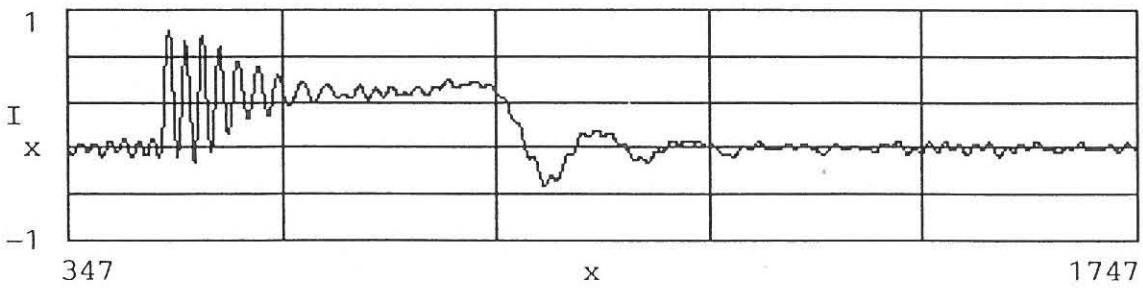

Figure B-12: Second starting transient measured with the slot in position 3.

M := READPRN(pos3c)

x := 0 ..2047

t := M⟨0⟩

T := M⟨2⟩

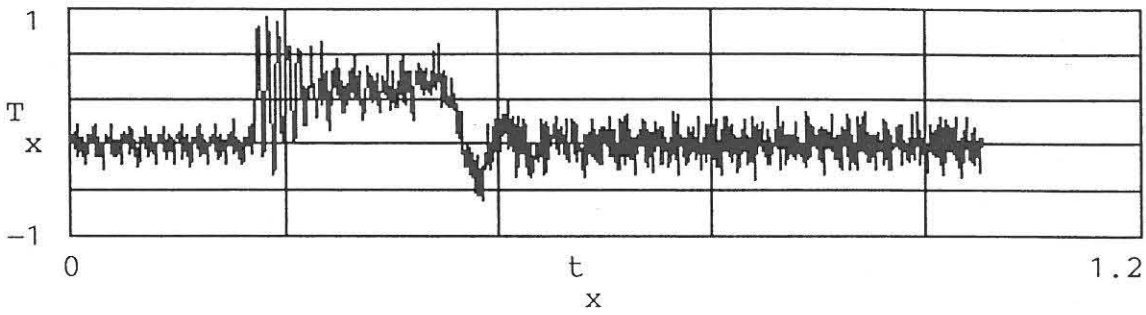

z := fft(T)

y := 0 ..1024

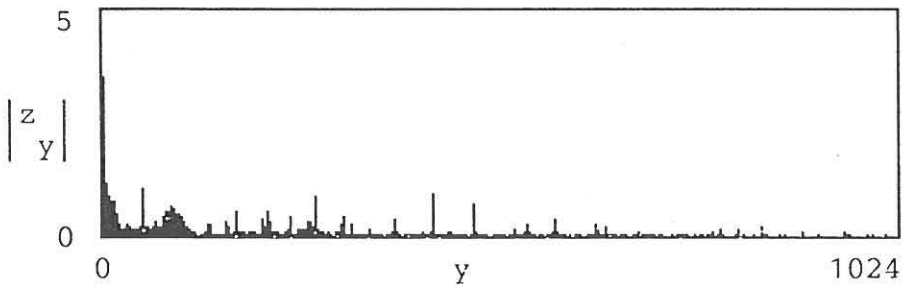

filter := 110 ..1024

z := 0
filter

z := 0
53

z := 0
64

I := ifft(z)

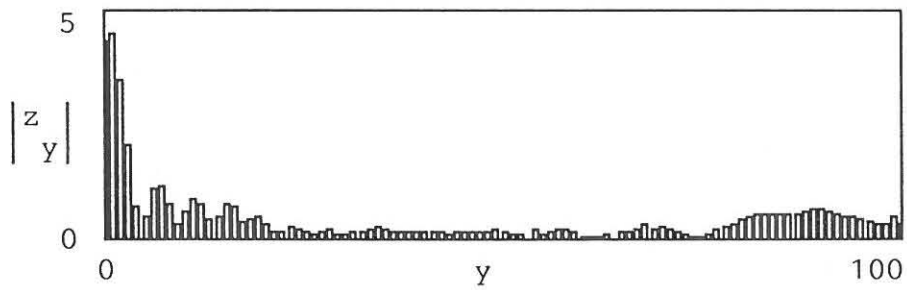

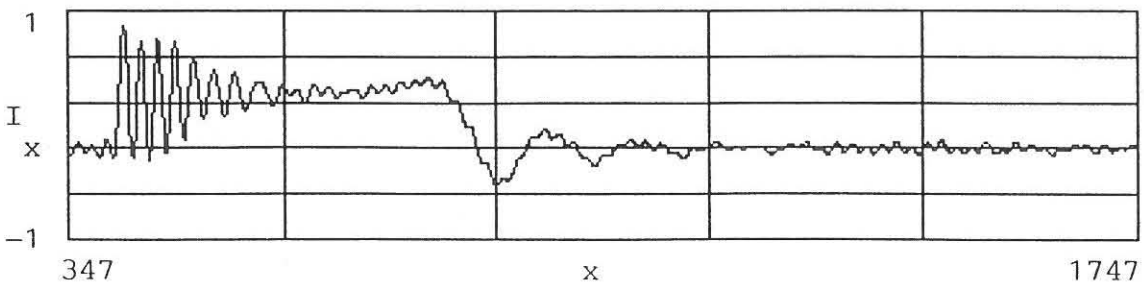

Figure B-13: Third starting transient measured with the slot in position 3.

M := READPRN(pos3d)

x := 0 ..2047

⟨0⟩ ⟨2⟩

t := M T := M

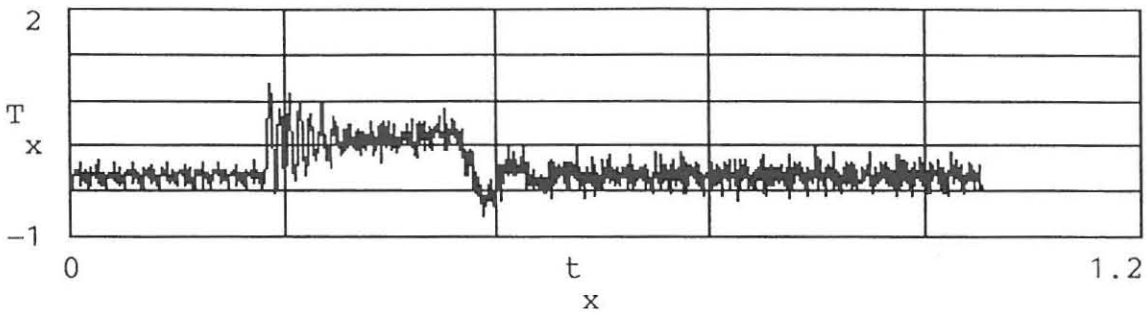

z := fft(T) y := 0 ..1024

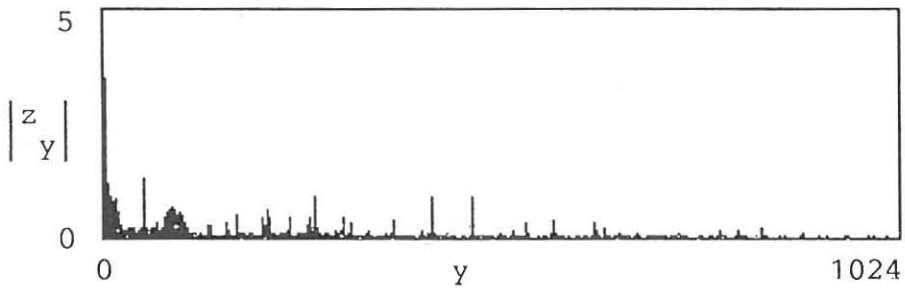

filter := 110 ..1024 z := 0 z := 0 z := 0
filter 53 64

I := ifft(z)

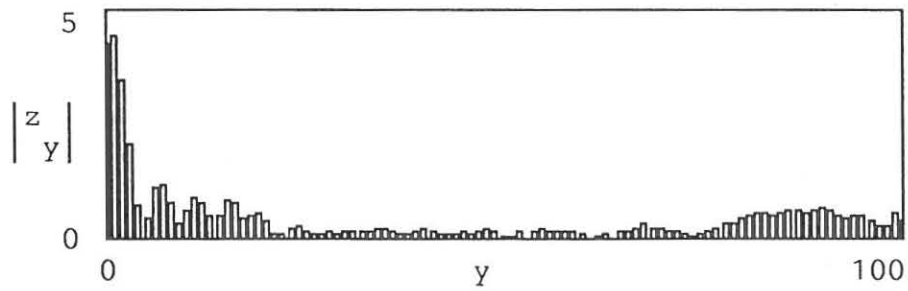

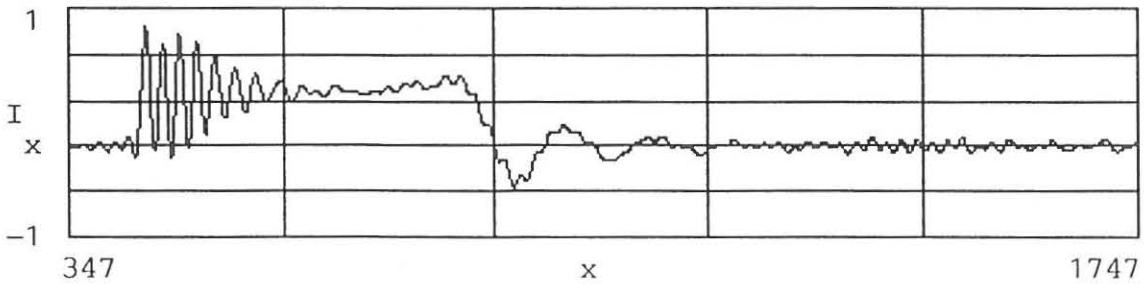

Figure B-14: Fourth starting transient measured with the slot in position 3.

M := READPRN(pos3e) x := 0 ..2047

t := M⟨0⟩ T := M⟨2⟩

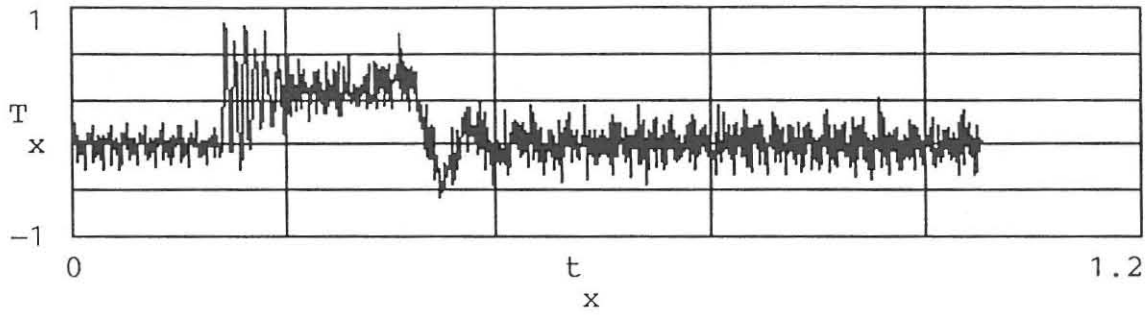

z := fft(T) y := 0 ..1024

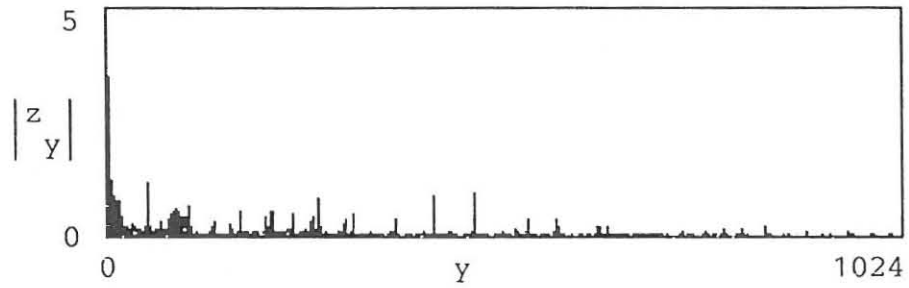

filter := 110 ..1024 z := 0 z := 0 z := 0
filter 53 64

I := ifft(z)

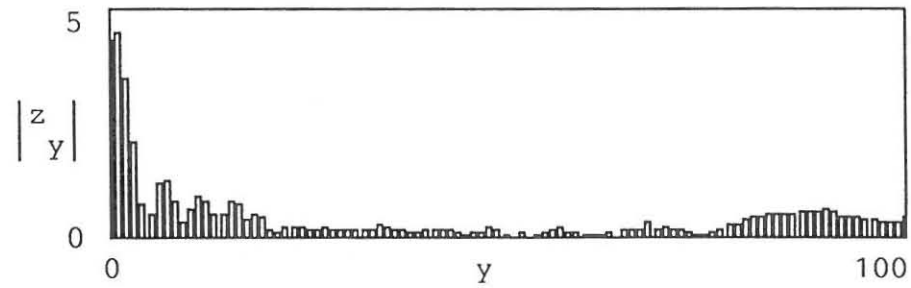

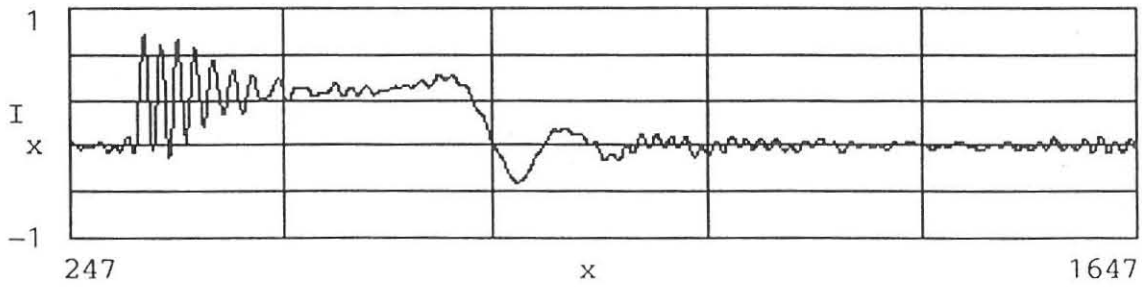

Figure B-15: Fifth starting transient measured with the slot in position 3.

M := READPRN(pos4a) x := 0 ..2047

t := M⟨0⟩ T := M⟨2⟩

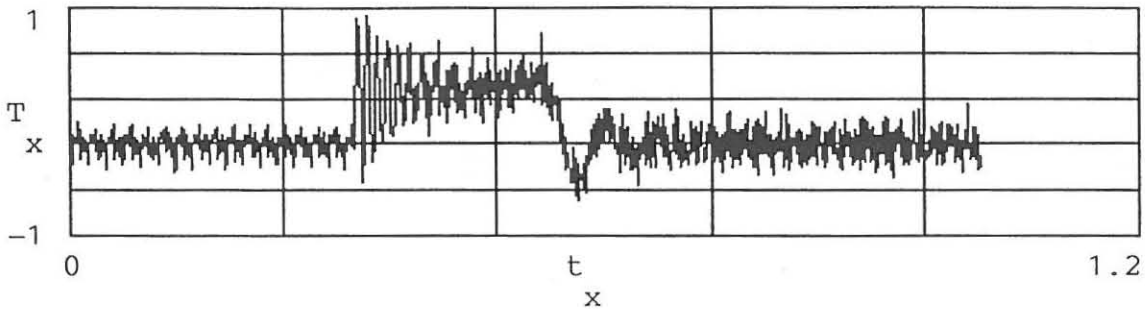

z := fft(T) y := 0 ..1024

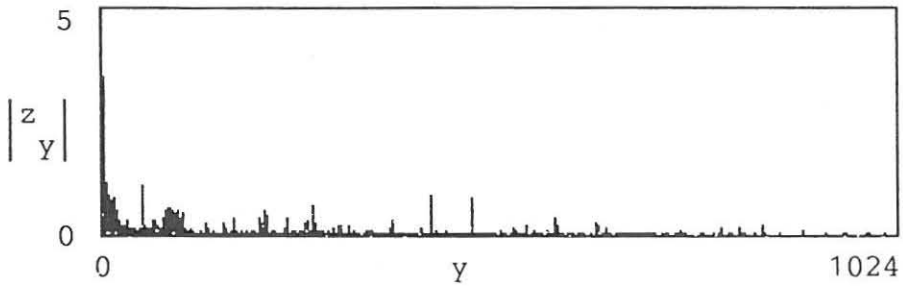

filter := 110 ..1024 z := 0 z := 0 z := 0
filter 53 64

I := ifft(z)

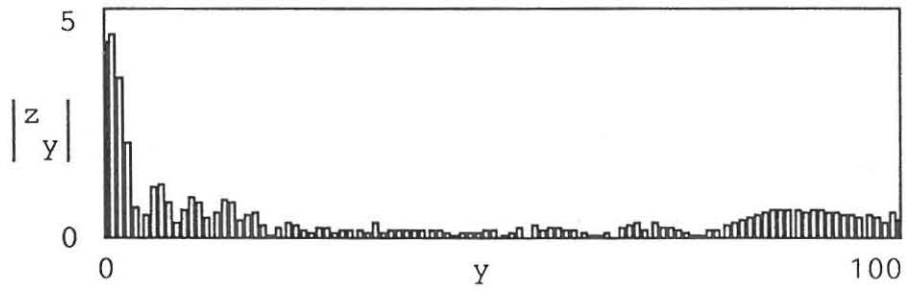

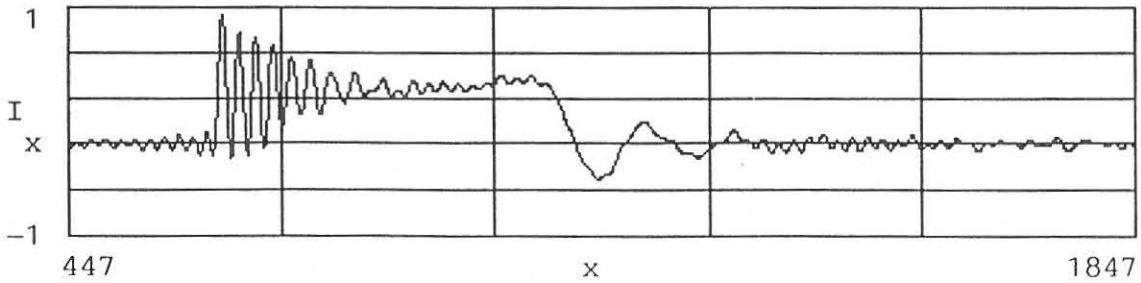

Figure B-16: First starting transient measured with the slot in position 4.

M := READPRN(pos4b)

x := 0 ..2047

t := M⟨0⟩

T := M⟨2⟩

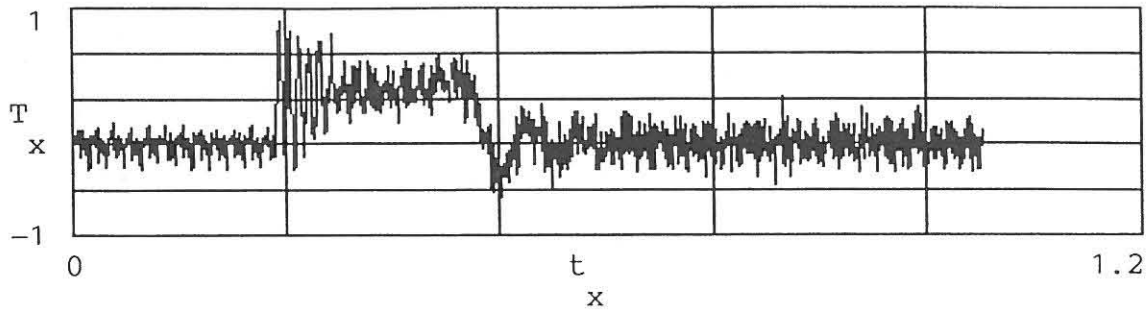

z := fft(T)

y := 0 ..1024

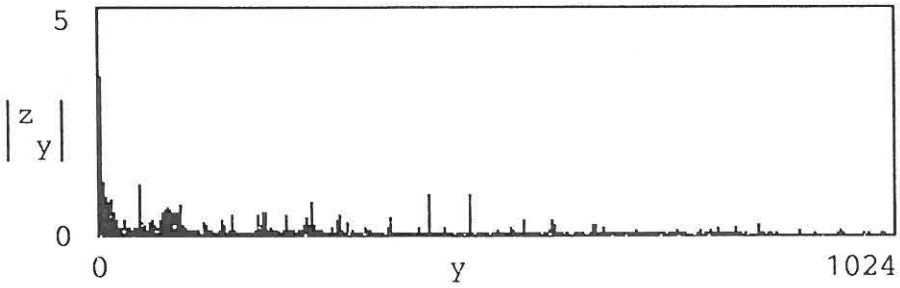

filter := 110 ..1024

z := 0
filter

z := 0
53

z := 0
64

I := ifft(z)

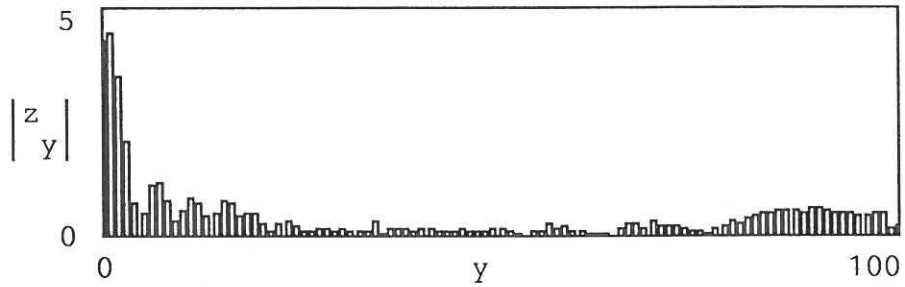

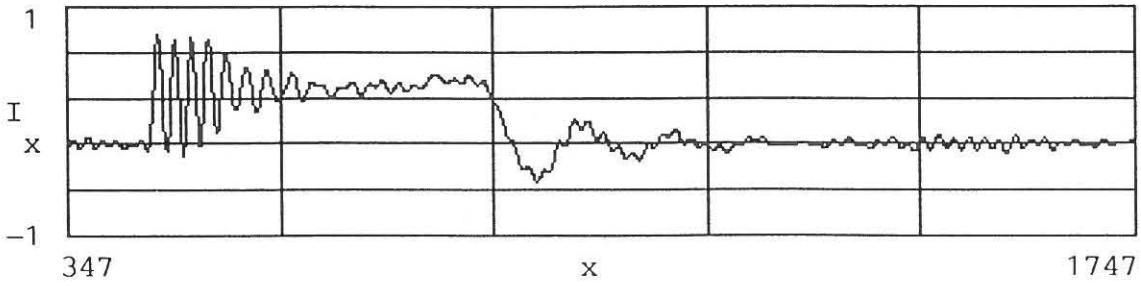

Figure B-17: Second starting transient measured with the slot in position 4.

M := READPRN(pos4c)

x := 0 ..2047

t := M⟨0⟩

T := M⟨2⟩

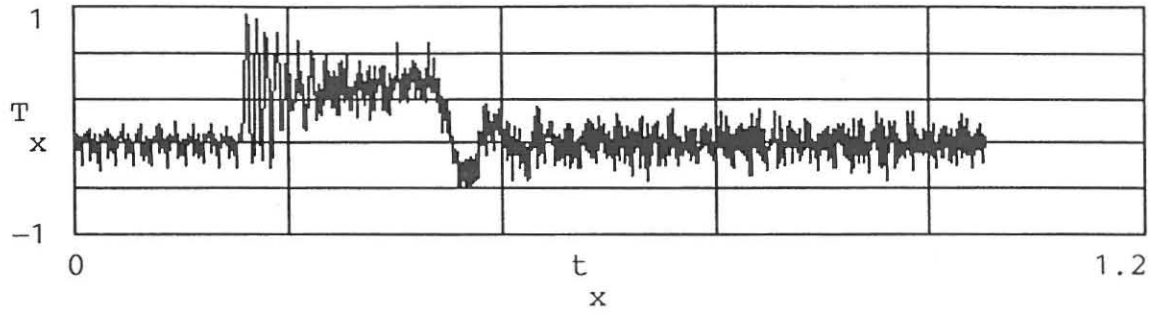

z := fft(T)

y := 0 ..1024

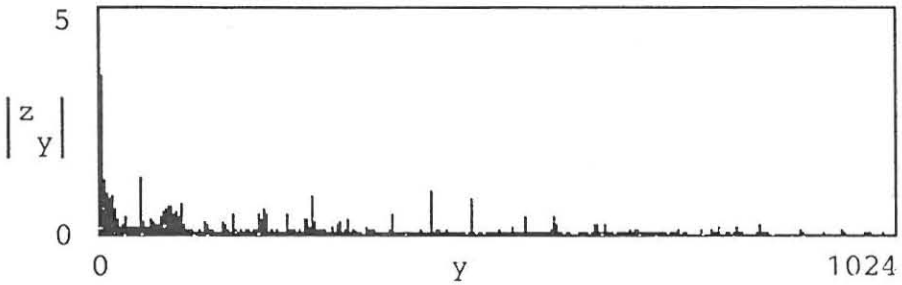

filter := 110 ..1024

z := 0
filter

z := 0
53

z := 0
64

I := ifft(z)

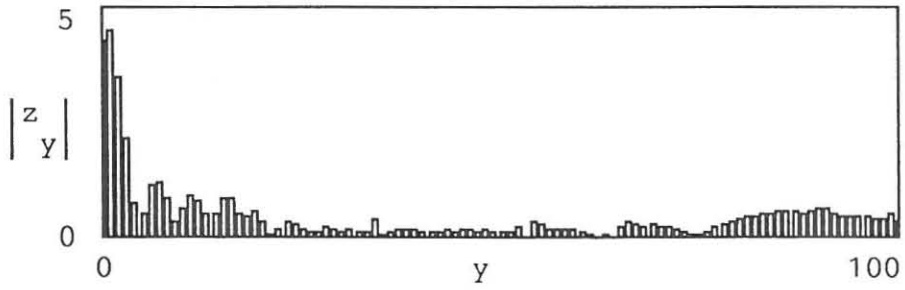

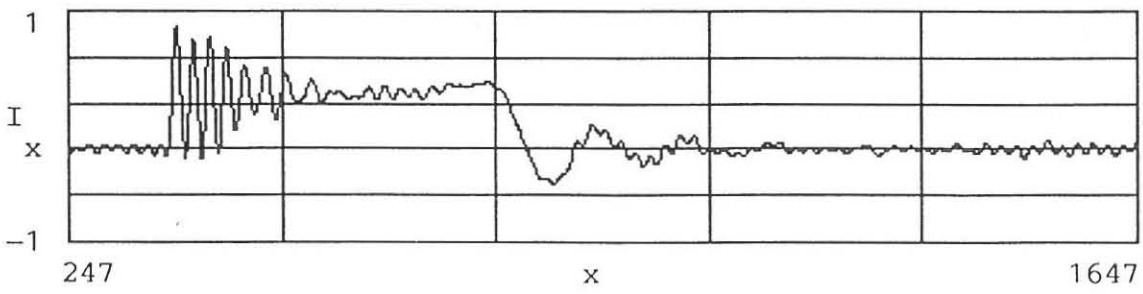

Figure B-18: Third starting transient measured with the slot in position 4.

M := READPRN(pos4d)

x := 0 ..2047

t := M⟨0⟩

T := M⟨2⟩

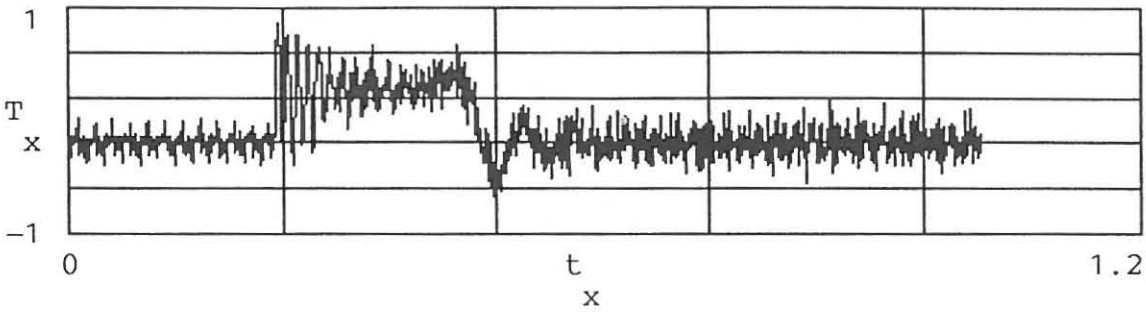

z := fft(T)

y := 0 ..1024

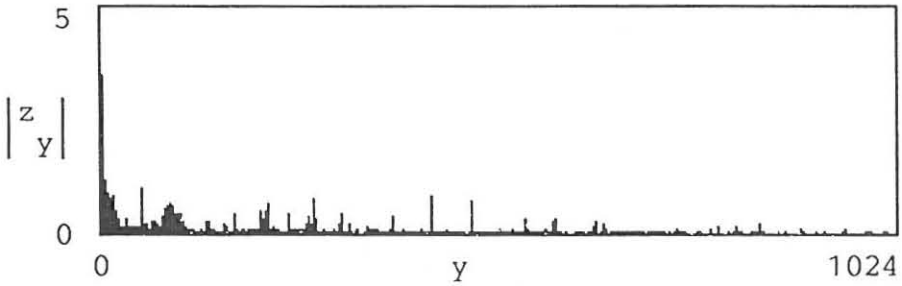

filter := 110 ..1024

z := 0
filter

z := 0
53

z := 0
64

I := ifft(z)

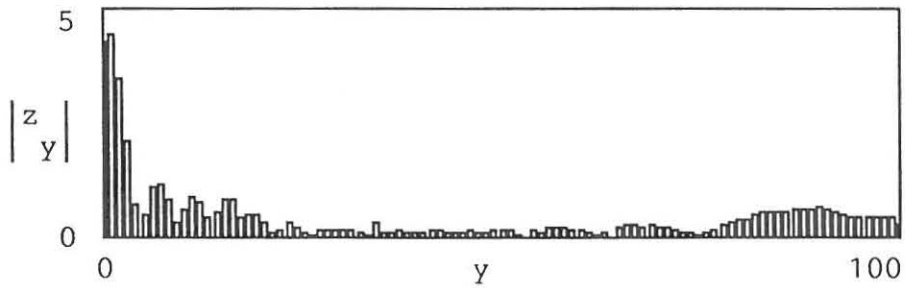

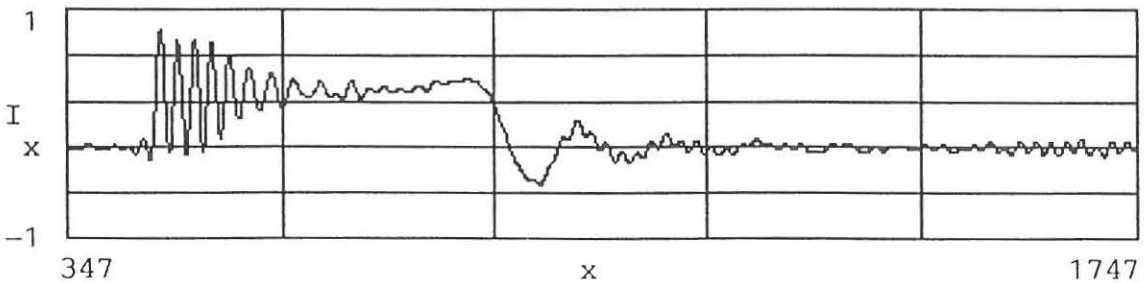

Figure B-19: Fourth starting transient measured with the slot in position 4.

M := READPRN(pos4e) x := 0 ..2047

t := M ⟨0⟩ T := M ⟨2⟩

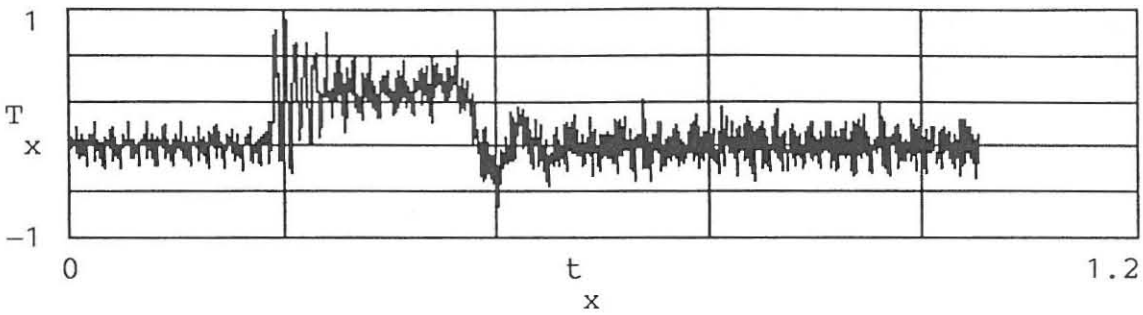

z := fft(T) y := 0 ..1024

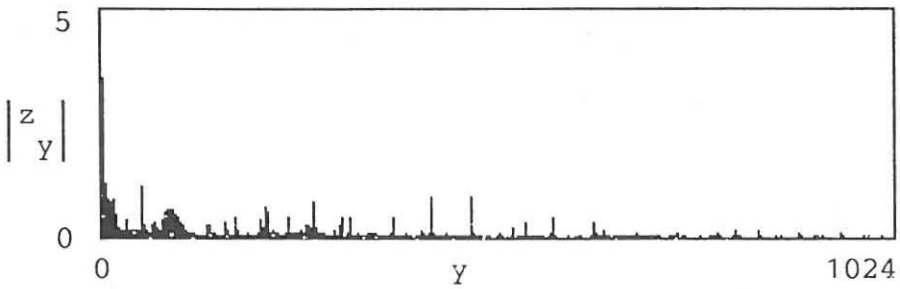

filter := 110 ..1024 z := 0 z := 0 z := 0
filter 53 64

I := ifft(z)

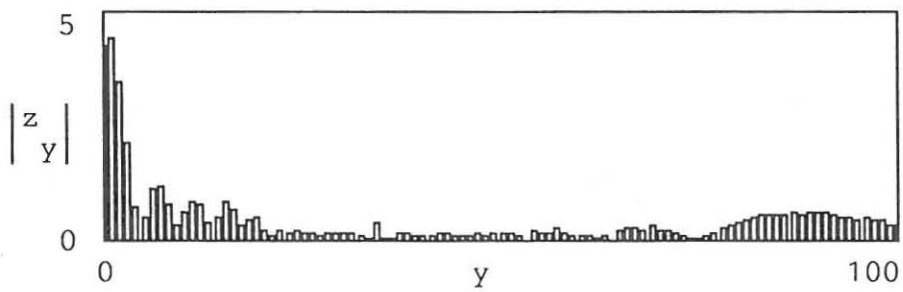

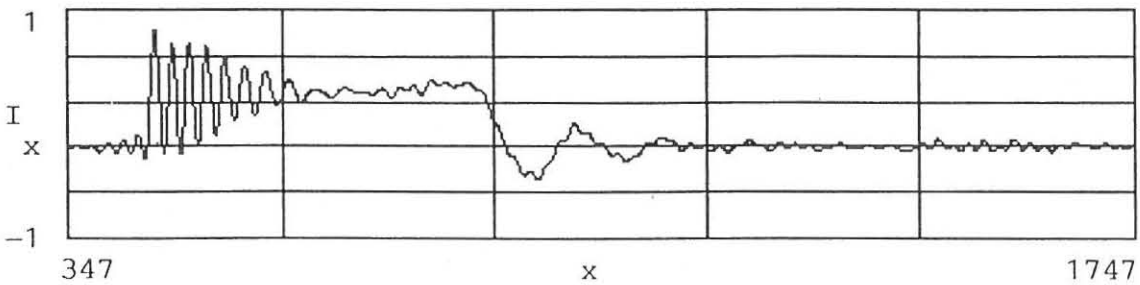

Figure B-20: Fifth starting transient measured with the slot in position 4.

REFERENCES

DE SARKAR, AK. & **BERG, GJ.** 1970. Digital simulation of three-phase induction motors. IEEE Transactions on Power Apparatus and Systems, 6 : 1031-1037.

FITZGERALD, AE., KINGSLEY, C. & **UMANS, SD.** 1985. Electric Machinery. McGraw - Hill Book Co., Singapore.

GHANI, SN. 1988. On simulating dynamic behaviour of three phase induction machines with squirrel cage rotor. SIMULATION, 5 : 182-193.

KLINGSHIRN, EA. & **JORDAN, HE.** 1970. Simulation of polyphase induction machines with deep rotor bars. IEEE Transactions on Power Apparatus and Systems, 6 : 1038-1043.

KRAUSE, PC. 1987. Analysis of electric machinery. McGraw - Hill Book Co., Singapore.

KRAUSE, PC. & **THOMAS, CH.** 1965. Simulation of symmetrical induction machinery. IEEE Transactions on Power Apparatus and Systems, 11 : 1038-1053.

LANDY, CF. 1970. Reswitching transients produced in induction motors. Unpublished MSc. Thesis. University of the Witwatersrand. Johannesburg.

LEVY, W. 1990. Modeling and simulation of induction motors for variable speed drives, with special reference to deep bar and saturation effects. Unpublished Ph.D. Thesis. University of the Witwatersrand. Johannesburg.

LIPO, TA. & **CONSOLI, A.** 1984. Modeling and simulation of induction motors with saturable leakage reactances. IEEE Transactions on Industry Applications , 1 : 180-189.

McCULLOCH, MD., LANDY, CF., LEVY, W. & **MacLEOD IM.** CASED : a Simulation package designed for variable speed drives. Submitted to simulation.

SAY, MG. 1978. Alternating current machines. Pitman Publishing Limited, London.

SLEMON, RS. 1992. Electric machines and drives. Addison-Wesley Publishing Company, Inc, Massachusetts.

SMITH, JR. 1990. Response analysis of AC electrical machines: computer modules and simulation. Research Studies Press Ltd., Hertfordshire.

STEPHENSON, JM. 1969. New low noise tachogenerator. IEE Proc, 11:1982

TAVNER, PJ. and PENMAN J. 1987. Condition Monitoring Of Electrical Machines. Research studies Press Ltd. Hertfordshire, England.

WOOD, WS., FLYNN, F. & **SHANMUGASUNDARAM, A.** 1965. Transient torques in induction motors due to switching of the supply. IEE Proc, 7 : 1348-1354.

Central University of Technology, Free State

EXTRA REFERENCES

BARNETT, S. 1979. Matrix methods for engineers and scientists. McGraw-Hill Book Company (UK) Limited, Berkshire.

CHAPRA, SC. & **CANALE, RP.** 1985. Numerical methods for engineers with personal computer applications. McGraw-Hill Book Co., Singapore.

GHANI, SN. 1988. Digital computer simulation of three-phase induction machine dynamics - a generalized approach. IEEE Transactions on Industry Applications , 1 : 106-113.

GOLUB, GH. & **ORTEGA, JM.** 1992. Scientific computing and differential equations. Academic Press, Inc, San Diego.

GOMES, AADFP. 1984. The effects of supply time-harmonics on the torque of squirrel cage induction motors. Unpublished Ph.D. Thesis. University of the Witwatersrand. Johannesburg.

HO, SC., HONG, CG. & **HWANG, GJ.** 1989. Transient and steady state performance of a squirrel-cage induction motor. IEE Proc, 3 : 136-142.

HTSUI, JSC. 1985. Magnitude, amplitudes and frequencies of induction-motor air-gap transient torque through simultaneous reclosing with or without capacitors. IEEE Transactions on Power Apparatus and Systems, 6 : 1519-1525.

PILLAI, SK. 1989. A First course on electrical drives. Wiley Eastern Limited, India.

SPESCOM, TMS. 1989. MOTOR DIAGNOSTICS : An expert eye on machine health. PULSE, 10 : 4-9.

WIEDER, S. 1992. Introduction to MathCAD® for scientists and engineers. McGraw-Hill, Inc, New York.

MATHEWS, JH. 1987. Numerical methods for computer science, engineering, and mathematics. University Press, Cambridge.